AFIT/GA/ENY/91D-4

INVESTIGATION OF THE INFLUENCE OF ROTARY AERODYNAMICS ON THE STUDY OF HIGH ANGLE OF ATTACK DYNAMICS OF THE F-15B USING BIFURCATION ANALYSIS

THESIS

Ralph D. Fero
Captain, USAF

AFIT/GA/ENY/91D-4

Approved for public release; distribution unlimited

REPORT DOCUMENTATION PAGE

Form Approved
OMB No. 0704-0188

1. AGENCY USE ONLY (Leave blank)	2. REPORT DATE	3. REPORT TYPE AND DATES COVERED
	Dec 1991	Master's Thesis

4. TITLE AND SUBTITLE
Investigation of the Influence of Rotary Aerodynamics on the Study of High Angle of Attack Dynamics of the F-15B Using Bifurcation Analysis

5. FUNDING NUMBERS

6. AUTHOR(S)
Captain Ralph D. Fero

7. PERFORMING ORGANIZATION NAME(S) AND ADDRESS(ES)
Air Force Institute of Technology
WPAFB, OH 45433-6583

8. PERFORMING ORGANIZATION REPORT NUMBER
AFIT/GA/ENY/91D-4

9. SPONSORING/MONITORING AGENCY NAME(S) AND ADDRESS(ES)

10. SPONSORING/MONITORING AGENCY REPORT NUMBER

11. SUPPLEMENTARY NOTES
vs. deflection angles of the rudder, stabilator, and aileron

12a. DISTRIBUTION/AVAILABILITY STATEMENT
Approved for Public Release;
Distribution Unlimited

12b. DISTRIBUTION CODE

13. ABSTRACT *(Maximum 200 words)*

The purpose of this thesis research was to use bifurcation analysis to investigate the effectiveness of rotary balance data in the prediction of aircraft spin behavior as both a stand alone representation of a model's aerodynamic data and in a conventional hybrid model. Using the foundation of a previously developed model of the F-15B, the rotary balance aerodynamic force and moment data were implemented as a function of angle of attack, angle of sideslip, non-dimensional rotation steady state rate and the control surface deflections. Bifurcation diagrams were developed as a function of alpha versus δ_t, δ_r, and δ_a to show highlights of equilibrium and dynamic behavior of the aircraft. For selected configurations, the resulting aircraft state variables showed the rotary balance data model having close correlation to experimental flight test data. Comparison of selected configurations with the hybrid and conventional static and forced oscillation models, showed comparable results. However, the models bifurcation diagrams were very different. Problems were identified with static contributions of the rotary balance data indicating a possible cause. The development of the hybrid model displayed the difficulties in blending of the aerodynamic data in the presence of deficient experimental data or inaccurate data modelling.

14. SUBJECT TERMS	15. NUMBER OF PAGES
Bifurcation, Spin Dynamics, Aerodynamic Stability, Continuation Theory, Equations of Motion, Rotary Balance, Dynamic Models	166
	16. PRICE CODE

17. SECURITY CLASSIFICATION OF REPORT	18. SECURITY CLASSIFICATION OF THIS PAGE	19. SECURITY CLASSIFICATION OF ABSTRACT	20. LIMITATION OF ABSTRACT
Unclassified	Unclassified	Unclassified	UL

AFIT/GA/ENY/91D-4

INVESTIGATION OF THE INFLUENCE OF ROTARY AERODYNAMICS ON THE STUDY OF HIGH ANGLE OF ATTACK DYNAMICS OF THE F-15B USING BIFURCATION ANALYSIS

THESIS

Presented to the Faculty of the School of Engineering

of the Air Force Institute of Technology

Air University

In Partial Fulfillment of the

Requirements of the Degree of

Master of Science in Astronautical Engineering

Ralph D. Fero, B.S.E.

Captain, USAF

December 1991

Approved for public release; distribution unlimited

Acknowledgements

At the foundation of this investigation are the past developments by Dr James Planeaux (Capt), Capt Tom Barth, Capt Daniel Baumann and Capt Robert McDonnell. Without their efforts, this research would not have been possible within the time allotted. The confidence of Dr Planeaux and Dr Shankar Mall to allow this research to occur was essential to its success. The willingness of Dr Brad Liebst to assist in my advisement was greatly appreciated. Discussions with Bill Barnhart and Jack Ralston from the NASA Langley Spin Tunnel were of value in the understanding of rotary balance data and they are thanked for providing the data that was essential for the investigation. I would like to thank Joe Wilson of NASA Dryden, Maj Carl Hawkins and Dr Craig Jahnke in their responsiveness to answering my questions concerning their research efforts. I acknowledge the contributions of my reading committee, Dr Robert Calico and Dr Curtis Spenny, for their helpful comments in preparing this document.

Many times people are deceived by the obstacles that confront them, but through determination, patience and perseverance one eventually overcomes. During this process, one may be perceived as reaching in the wrong direction but in reality are right on course. I thank my parents and my friends for their understanding of the frustrations that occur during research efforts and their patience and vision that the final results would meet their expectations.

Captain Ralph D. Fero Jr.

Table of Contents

List of Figures

Page

List of Tables

List of Symbols

α	angle of attack (degrees)
β	sideslip angle (degrees)
δ_a	aileron deflection angle (degrees)
δ_d	differential elevator deflection angle (degrees)
δ_e	stabilator (elevator) deflection angle (degrees)
δ_r	rudder deflection angle (degrees)
γ	secondary control parameter
λ	control parameter
θ	pitch angle (degrees)
ϕ	bank angle (degrees)
Ω	magnitude of the total rotation vector (radians/seconds)
Ω_{osc}	oscillatory component of the total rotation vector (radians/seconds)
Ω_{ss}	steady state component of the total rotation vector (radians/seconds)
$\bar{\Omega}$	total rotation vector (radians/seconds)
$\bar{\Omega}_{osc}$	oscillatory vector component of the total rotation vector (rad/seconds)
$\bar{\Omega}_{rot}$	rotary vector component of the total rotation vector (rad/seconds)
$\Omega_{ss}b/2V_{tr}$	non-dimensional rotation rate
b	wing span (feet)
$\hat{b}_i$	body axis unit vector, i=1,2,3

C_i	aerodynamic coefficient, i=x,y,z,l,m and n
$C_{i,Hybrid}$	Hybrid model coefficients, i=x,y,z,l,m and n $C_{i,Hybrid}(\alpha,\beta,p,q,r,\Omega_{ss},\delta_a,\delta_e,\delta_r,T_l,T_r,\delta_{pv},\delta_{yv})$
$C_{i,Mc}$	McDonnell model coefficients, i=x,y,z,l,m and n $C_{i,Mc}(\alpha,\beta,p,q,r,\delta_a,\delta_e,\delta_r,T_l,T_r,\delta_{pv},\delta_{yv})$
$C_{i,Mc\ non\text{-}rot}$	non-rotary component of McDonnell coefficients, i=x,y,z,l,m and n $C_{i,Mc\ non\text{-}rot}=C_{i,Mc}(\alpha,\beta,p_{osc},q_{osc},r_{osc},\delta_a,\delta_e,\delta_r,T_l,T_r,\delta_{pv},\delta_{yv})$
$C_{i,Mc\ static}$	static component of McDonnell coefficients, i=x,y,z,l,m and n $C_{i,Mc\ static}=C_{i,Mc}(\alpha,\beta,p=0,q=0,r=0,\delta_a,\delta_r,\delta_e,T_l,T_r,\delta_{pv},\delta_{yv})$
$C_{i,RB}$	rotary balance model coefficients, i=x,y,z,l,m and n $C_{i,RB}(\alpha,\beta,\Omega_{ss},\delta_a,\delta_d,\delta_e,\delta_r,T_l,T_r,\delta_{pv},\delta_{yv})$
$C_{i,RB\ static}$	static component of the rotary balance coefficients, i=x,y,z,l,m and n $C_{i,RB\ Static}=C_{i\ RB}(\alpha,\beta,\Omega_{ss}=0,\delta_a,\delta_d,\delta_e,\delta_r,T_l,T_r,\delta_{pv},\delta_{yv})$
C_l	roll moment coefficient
C_m	pitch moment coefficient
C_n	yaw moment coefficient
C_x	axial force coefficient
C_y	side force coefficient
C_z	normal force coefficient
$\bar{c}$	mean aerodynamic chord (feet)
d_{Ty}	offset of thrust from C.G. in x direction (feet)
d_{Ty}	offset of thrust from C.G. in y direction (feet)
d_{Tz}	offset of thrust from C.G. in z direction (feet)
f	vector function

g	gravitational constant (32.174 ft/sec^2)
I_x	moment of inertia about the x-axis
I_{xz}	cross product of inertia in the x-z plane
I_y	moment of inertia about the y-axis
I_z	moment of inertia about the z-axis
m	aircraft mass (slugs)
p	roll rate (radians/second)
p_{osc}	oscillatory component of roll rate (radians/second)
q	pitch rate (radians/second)
q_{osc}	oscillatory component of pitch rate (radians/second)
$\bar{q}$	dynamic pressure (lbf/ft^2)
r	yaw rate (radians/second)
r_{osc}	oscillatory component of yaw rate (radians/sec)
S	wing planform area (ft^2)
T_l	left engine thrust (lbf)
T_r	right engine thrust (lbf)
T_x	thrust in x direction (lbf)
T_y	thrust in y direction (lbf)
T_z	thrust in z direction (lbf)
T_{Zl}	left engine thrust in z direction (lbf)
T_{Zr}	right engine thrust in z direction (lbf)

t	time (seconds)
u	vector of states
V_{tr}	aircraft true speed (ft/sec)
$\hat{V}_1$	unit vector in the free stream velocity direction
$\bar{V}_{tr}$	true velocity vector
y_n	system states

Abstract

Many studies of aircraft high angle of attack dynamics have argued the need for rotary aerodynamic data to be included in a model in order to effectively model aircraft spin behavior. The purpose of this research paper was to use bifurcation analysis to investigate the effectiveness of rotary balance data in the prediction of aircraft spin behavior as both a stand alone representation of a model's aerodynamic data and in a conventional hybrid model. Equilibrium solutions from both models were compared to previous studies which utilized conventional static and forced oscillation aerodynamic data and to flight test results to analyze the effectiveness of rotary aerodynamic data for the prediction of spin behavior.

Using the foundation of a previously developed model of the F-15B, the rotary balance aerodynamic force and moment data were implemented as a function of angle of attack, angle of sideslip, non-dimensional rotation steady state rate and the control surface deflections (δ_a,δ_d,δ_e,δ_r). Bifurcation diagrams were developed as a function of alpha versus δ_r,δ_e, and δ_a to show highlights of equilibrium and dynamic behavior of the aircraft. For selected configurations, the resulting aircraft state variables showed the rotary balance data model having close correlation to experimental flight test data. Comparison of these selected configurations with the hybrid and conventional static and forced oscillation models, showed comparable results. However, the models bifurcation diagrams were very different. Problems were identified with static contributions of the rotary balance data indicating a

possible cause. Despite the static contribution problem, the overall results indicated the rotary balance data model did provide a reasonable representation of the spin dynamics of the aircraft. The development of the hybrid model dispiayed the difficulties in blending of the aerodynamic coefficient data in the presence of deficient experimental data, inaccurate modelling of aerodynamic coefficients or possible differences in the databases such as Reynolds number effects. Recommendations on continued investigation of the effects of the static contributions of the rotary balance data were made.

INVESTIGATION OF THE INFLUENCE OF ROTARY AERODYNAMICS ON THE STUDY OF HIGH ANGLE OF ATTACK DYNAMICS OF THE F-15B USING BIFURCATION ANALYSIS

I. Introduction

The flat spin is the most dangerous spinning motion exhibited by an airplane where the aircraft's angle of attack (AOA) approaches 90° with a high rate of rotation. Conventional aircraft control surfaces become increasingly ineffective as the AOA approaches 90° and as the spin develops it may become impossible for the pilot to recover. Today's fighter aircraft are also heavier than earlier designs, with weight more concentrated along the fuselage. This design evolution was a factor of the desirability of a more maneuverable aircraft. With this distribution of mass, the yaw moment of inertia of the aircraft has increased as much as 20 times compared to early fighters but the effective control surfaces have remained practically the same (11:1). This combination of high yaw moment of inertia and relatively ineffective control surfaces at high angles of attack warrants analysis of spin characteristics of aircraft because recovery is very difficult if not fatal.

Aircraft high angle-of-attack research has been increasing over the past twenty years. The most recent full scale research effort is the X-31 where one of its areas of investigation is the use of thrust vectoring paddles to improve the agility

and handling qualities of an aircraft while flying at high angles of attack. In February 1991, testing began at AOA up to 70°. The ability of an aircraft to achieve high angle of attack will considerably reduce the time needed to maneuver an aircraft to obtain a good firing position in close-in combat (14:38). Research is ongoing to improve designs of future aircraft and their control systems to have stability and agility during high AOA maneuvers. For developed aircraft, it is desired to design either effective pilot procedures or aircraft control systems that can predict and recover an aircraft from potentially fatal attitudes accompanied with high angle of attack maneuvers. Loss of control of the aircraft can occur through non-linear behavior such as stalls, departures, wing rock, nose slice, spin entry, and full spins. Considering the costs involved in full scale testing, it is desirable for the development of a methodology that could investigate the aircraft dynamics associated with high angle of attack flight, specifically aircraft spin behavior, with the use of scale model aerodynamic data. Investigations of this form have used combinations of static wind tunnel, forced oscillation and rotary aerodynamic data. It is the objective of this paper to investigate the effectiveness of rotary aerodynamic data in modeling high angle of attack dynamics in the regime of α=30° to 90° using the methodology of bifurcation analysis.

Previous Studies

The mathematical modeling of an aircraft's motion during high angle of attack

maneuvering has shown to be an effective tool for the flight dynamicist however it is highly dependent on the results of wind tunnel tests for the required static and dynamic aerodynamic data (27:244). In 1972, Adams (1) used a numerical routine to predict spin modes for various aircraft by searching for steady spin states. His results did not compare well with flight test data. Adams attributed poor results to the deficiencies of the aerodynamic data his model was based on. The discrepancies he found may have been corrected with the inclusion of rotary balance data.

As technology advanced with digital computers in the 1960s many flight dynamic models of aircraft spinning were developed. In most cases these models involved the combination of aerodynamic data from static tests with small disturbance oscillatory data. In these models the aerodynamic data were sometimes inaccurate and spin modes could not be predicted (22:144). Early studies of spins involved numerical simulations using static wind tunnel data to predict spin entry and possible recovery techniques. As indicated above, their results did not compare well with flight test data nor spin tunnel results. Chambers, Bauman and Anglin determined that rotary balance data was necessary to correctly model the aerodynamics during a spin (11). In many investigations utilizing rotary balance data, this conclusion has been substantiated.

During the past forty years many research efforts have been made on the study of aircraft spin behavior utilizing rotary aerodynamic data. Some encountered problems obtaining acceptable results utilizing the rotary balance data. However

most have found significance of including rotary aerodynamic data in their models for prediction of aircraft spin modes. In 1954, Scher (32) applied equations of motion and spin-geometry relationships with rotary balance aerodynamic data to calculate step by step the details of a spin recovery motion for an unswept-wing fighter-airplane configuration. At first, his results did not agree with the assumptions of steady spin. However, as also determined by Stone, Burk and Senger (37), the rotary balance data had to be modified due to inconsistencies in the mounting of the model. The values he obtained were inconsistent with the assumption that the aerodynamic and inertial forces and moments should balance during steady spin. As a result, the spin behavior he obtained were not validated by the test aircraft of the investigation.

With the improvement of the technique of rotary balance wind tunnel testing, the integrity of the data has improved from the tests of over forty years ago. A most recent analysis was performed in 1989 by Martin and Hill (22) where rotary balance data was used in a model of a basic training aircraft using a six-degree of freedom flight dynamics model of aircraft spin. The model was used to predict equilibrium spin conditions and spin recovery techniques. Their results were promising when compared to scale model wind tunnel tests. In 1981, Tischler and Barlow (38) were able to accurately determine spin modes of a low-wing general aviation aircraft using rotary balance data. Studies by Birhle (9) on a fighter aircraft design in 1980, had demonstrated that the spin computed with static aerodynamic data did not match the flight motion whereas the spin computed with

rotational data duplicated the developed spin. This result again emphasized the significance of rotary balance data representing the dynamics during spin motion. Ogburn, Nguyen and Hoffler (27) have done recent research showing that the addition of dynamic terms, including rotary aerodynamics can significantly affect the simulated flight motions. Their efforts also showed a substantial influence of the rotary aerodynamic data on the motions and controls for the aircraft configurations they tested.

High angle of attack maneuvers are very nonlinear and require complex analysis tools to study the behavior. Mehra and Carroll (26) performed fairly extensive analysis of the F-4 Phantom fighter in 1979 demonstrating the use of bifurcation and continuation methodology as an analysis tool for the study of aircraft high AOA behavior. Bifurcation theory was not a new concept however it had not been previously applied to aircraft dynamics. The tool enables an analyst to use more complex (higher order, nonlinear) aircraft models thereby enabling analysis of more demanding flight conditions such as spins, stalls and wing rock. Bifurcation methodology provides insight into the solution of nonlinear equations through development of a mapping of equilibrium and periodic solutions of an aircraft's equations of motion. This results in a global view of the nonlinear behavior of the aircraft. Further discussion of bifurcation theory is presented in Chapter III.

Many recent research efforts have used bifurcation analysis for the study of aircraft dynamics. Hawkins (17), Jahnke (18,19,20), Zagaynov and Goman (39),

and Guicheteau (16) used bifurcation theory to analyze nonlinear behavior associated with high AOA maneuvers of various aircraft configurations including the F-14 and F-15 fighters. Barth (6) and Planeaux and Barth (28) did an investigation of high AOA behavior of the F-15 using bifurcation analysis and were able to identify periodic solutions indicative of aircraft wing rock behavior. Baumann (7), Beck (8) and Planeaux, Beck and Baumann (29) continued the F-15 research with an expanded aerodynamic database allowing analysis up to 90° AOA. With the new model they analyzed the effectiveness of control augmentation. The most recent effort with the F-15 model, performed by McDonnell (24) and Planeaux and McDonnell (30) investigated the effectiveness of thrust vectoring for spin recovery. Many options for spin recovery using thrust vectoring were identified.

Of the efforts mentioned utilizing bifurcation methodology, only three included the contributions of rotary aerodynamic data. Hawkins (17), Jahnke (28) and Mehra and Carroll (26,10) developed hybrid models combining the data from static, forced oscillation and rotary balance testing in attempt, to more accurately model the aircraft dynamics. Mehra and Carroll's analysis included an investigation of different approaches to integrating rotary aerodynamic data into a model. Their effort did provide many methods for consideration some of which were incorporated by Hawkins and Jahnke in their aircraft models.

Overview

There is still a debate over what effective benefit rotary balance data provides in a model. This paper will continue the development of the F-15B model by Barth (6), Beck (8), Baumann (7) and McDonnell (24). The inclusion of rotary balance data will be analyzed in two developments. The rotary balance data will first be used in the model as the principal representation of the static, oscillatory and rotary aerodynamic force and moment coefficients. The results of bifurcation analysis and continuation theory will be used to compare the static and forced oscillation aerodynamic based model and a stand alone rotary aerodynamic based model. The comparison will assist in identification of the strength and weakness of rotary balance data as well as possible deficiencies in the modeling of the coefficient data. The second phase of the investigation will be the development and analysis of a hybrid model utilizing the rotary aerodynamic data through blending with the static and forced oscillation aerodynamic data based model. In addition, based on problems encountered with the rotary balance database, an analysis of static aspects of the rotary balance database and perturbation of two of the rotary balance coefficients will be made.

Chapter II will discuss spin tunnel testing, the rotary balance data used in this analysis and the data processing required. Chapter III will present a brief introduction to bifurcation theory and the continuation methodology. Chapter IV will describe the F-15 model and the modifications required with implementation

of the rotary balance data. Chapter V presents the findings of the analysis. The conclusions will be drawn as well as recommendations for future research in Chapter VI.

II. Rotary Balance Data

It should be rather intuitive that the best method to investigate a particular motion of an aircraft would be to use a technique that most accurately represents that motion. The standard wind tunnel aerodynamic coefficient data consists of two types, static and forced oscillation. Both sets of data have been used as the foundation for dynamicist to study the dynamics of aircraft. For the study of aircraft in spinning or coning motion, the most representative modeling would be to rotate a model with its spin axis parallel to the free stream velocity of the relative wind. This reasoning has been identified for the study of aircraft research since the pioneer days of aviation. In response, rotary balance techniques have been developed providing information on the effects of rotational rates on the overall aerodynamic forces and moments acting on the aircraft.

The fundamental problem of the dynamicist is to properly represent the equations of motion with the aerodynamic reactions and motion variables (control parameters and states) of interest. When analyzing low angle of attack dynamics, adequate dynamic predictions can be made using a linearized small perturbation model with constant aerodynamic derivatives. However, when motions involve large variation in any of the state variables, change in some of the aerodynamic derivatives may vary appreciably with factors of the flight conditions thereby the analysis must involve non-linearities to properly represent the dynamics. It is argued that use of the combination of aerodynamic data of oscillatory and rotary

motion can produce the data required for calculation of flight motions including fairly large excursion motions such as high angle of attack departure and spin entry. The difficulties involved in performing such tests and receiving substantial data concern the correlation between wind-tunnel dynamic test data which are usually available from separate oscillatory and rotary tests, where the model or its motion did not exactly simulate the relevant flight motion of interest (2:209).

For rotary tests, the axis of rotation is parallel to the wind axis. The aerodynamic loads are measured by a strain gauge aligned along the model body axis. The model has a fixed orientation of angle of attack, angle of sideslip and selected control deflections to the wind direction as the model is rotated. The model is seeing a constant rate of motion resulting in a consistent collection of data. In oscillatory tests the motion is not of constant rate thereby the flow is constantly changing and under certain conditions the measurements of the derivative data may be a function of the history of the flow (2:209). At low angles of attack and sideslip the flow is attached to virtually all of the surface of the model and fairly good agreement of the derivative data is found between the rotary and oscillatory test results. However, at high angle of attack, there is increased flow separation and lag effects that may introduce significant differences between the two testing results. As indicated in the AGARD Advisory Report (2:210), tests comparing rotary and oscillatory data have attributed this lag effect for their apparent differences. These effects may influential in the development of the hybrid model. These effects will be considered when comparing the stand alone

rotary balance model with the static and forced oscillation data based model.

The above discussion brings up the issue of the integrity of the F-15 1988 Aerobase which is the source of aircraft aerodynamic force and moment coefficients for the McDonnell (24) and Baumann (7) theses. Part of this investigation involves both the blending and comparing of the dynamics resulting from both the rotary balance and the 1988 Aerobase which represents the oscillatory testing data. The 1988 F-15 Aerobase was obtained from the F-15 System Program Office (SPO) at Wright-Patterson AFB, Ohio and has been used for simulation testing of the aircraft. This database is not well documented on the exact source for its content. However, the McDonnell Douglas Documentation (23) indicates that the stability and control derivatives were derived by analysis of flight test data and where appropriate, superseded relative wind tunnel based estimates. Additionally, in order to provide the maximum amount of range on flight conditions, data from flight test results were utilized to adjust the associated wind tunnel coefficient data (23). Neither the method utilized for blending the flight test data nor a discussion of the methods of data processing used on the raw wind tunnel data were identified in the documentation. It should be noted that inconsistencies may be present for this investigation in the effectiveness of rotary balance data, when the baseline model to be compared and blended consisted of actual flight test data. The 1988 F-15 Aerobase is not a true representation of the limitations of conventional wind tunnel testing results. This factor will be considered when the results are analyzed in Chapter V.

Description of the Rotary Aerodynamic Data

The rotary balance technique measures the 6 aerodynamic force and moment coefficients C_x, C_y, C_z, C_l, C_m and C_n as a function of the 3 state variables: spin rate, angle of attack and angle of sideslip; and the control deflections: δ_e, δ_r, δ_a, δ_d. The rotary balance data obtained for this analysis is documented in NASA Contractor Report 3478 (5) and 3479 (4). The database was obtained from the NASA Langley Spin Tunnel in the form of data files on floppy disk. The data files were arranged by aircraft configuration representative of the data presented in reference (5) and consisted of the six aerodynamic force and moment coefficients tabulated with their associated state variables and control deflections. The spin tunnel data consisted of configurations ranging from the build-up of individual airplane components (body,wings,tail), the basic airplane configured with various control deflections and the airplane configured with conformal fuel tanks. Since this analysis was restricted to a basic F-15B with no stores carriage nor conformal fuel tanks, only 16 configurations were used from the available database. Table I shows the 16 configurations that were used to represent the rotary balance data in this analysis.

The Langley Spin Tunnel tests were conducted at a free stream velocity of 25 ft/sec, which correspond to a Reynolds number of approximately 211,000 based on the model wing cord of 1.33 ft. Studies by G.N. Malcolm at NASA-Ames (2:117) on the sensitivity of the rotational flow fields to Reynolds number variation.

Table I Rotary Balance Database Testing Configurations

Configuration	β	δ_e*	δ_d*	δ_a*	δ_r*
1	0	0	0	0	0
2	0	0	6	0	0
3	0	0	11	0	0
4	0	0	6	20	0
5	0	0	-6	-20	30
6	0	0	6	20	-15
7	0	0	-11	-20	30
8	0	-25	0	0	0
9	-10	0	0	0	0
10	10	0	0	0	0
11	10	0	6	0	0
12	10	0	11	0	0
13	10	0	-6	-20	30
14	10	0	6	20	-15
15	10	0	-11	-20	30
16	10	-25	0	0	0

Each configuration is tested for all combinations of α = 8,10,12,14,16,18,20,25,30,35,40,45,50,55,60,70,80,90 degrees and $|\Omega_{ss}b/2V_{tr}|$ = 0.0,0.1,0.2,0.3,0.4 (some for 0.5,0.6,0.7,0.9) for clockwise and counter clockwise rotations.
* in degrees

have shown that variation in Reynolds number does have a significant effect on the behavior of the aerodynamic derivative coefficients. Aircraft with slender noses or slender forebodies can experience large side forces due to asymmetric separation and vortices on the leeward side of the body. It has been found that the behavior of these vortices and flow separation change as Reynolds number varies. The high Reynolds number effects from the experimental flight test data inherent in the 1988 Aerobase may introduce noticeable differences in the aerodynamic coefficients when compared to the rotary balance data. Since high Reynolds number rotary balance data was unavailable, this investigation was

constrained to blending of the dissimilar Reynolds number data. The Reynolds number effect may account for gross differences when comparing the coefficient data from each model. For all tests, the spin axis passed through the full scale airplane nominal center of gravity (CG) location for AOA above 30°. Testing below 30° AOA required shifting of the spin axis to allow the model a full range of motion. Use of this data would require adjustment of the coefficient data to the nominal cg location. For this analysis only $\alpha > 30°$ was used. The McDonnell (24) analysis was based upon an aircraft at 0.6 Mach and 20,000 ft altitude.

The data was presented for an angle-of-attack range of 8° to 90°, and clockwise and counter-clockwise rotations covering $\Omega_{ss}b/2V_{tr}$ range from 0 to 0.4. Some configurations were presented with an extended $\Omega_{ss}b/2V_{tr}$ range from 0 to 0.9. The data used for this investigation is not the specific data published in reference (5) but a second run collection of the same configurations performed in June-August 1981. The integrity of the axial and side force coefficient data may be questionable (40). Analysis of the data files identified this problem and will be discussed in the next section. A complete description of the testing apparatus and model are in reference (5).

As shown by Table I, the depth of the rotary balance database is limited by the few airplane configurations tested for the basic F-15. This investigation will limit itself to analysis of only configurations that fit within these restrictions. Table II shows the F-15B operational control deflection limitations as compared to the rotary balance database limitations. Unlike the static and oscillatory test data, the

rotary balance data will not be adjusted to the limitations of the operational flight configurations and will thereby provide a better indication of the capabilities of this data as a stand alone representation of the aircraft dynamics.

Table II Control Deflection Limits.

Operational Control Deflection Limits (8:26):

Control Surface	Positive Limit	Negative Limit
Stabilator (δ_e, δ_d)	15°	-29°
Aileron (δ_a)	20°	-20°
Rudder (δ_r)	30°	-30°

Rotary Balance Database limitations:

Control Surface	Positive Limit	Negative Limit
Stabilator (δ_e)	0°	-25°
Differential Stabilator (δ_d)	11°	-11°
Aileron (δ_a)	20°	-20°
Rudder (δ_r)	30°	0°

Data Analysis and Preparation

In examining the raw data, it was identified that the rotary balance data showed problems in the static configurations (i.e. $\Omega = 0$). It is difficult to identify what characteristics of the data is due to poor testing or is inherent in the character of the rotary aerodynamics. To identify possible problems, each data file was compared to the data in reference (5) to identify if any test cases showed very

different results. All coefficients compared fairly well except for a few isolated cases of C_x and C_y. A few cases showed negative signs missing on a series of axial force coefficients and were easily corrected. More severe problems were encountered with particular configuration datasets of C_x and C_y. The magnitudes of the coefficient data for configurations 1 and 4 on Table I for C_x were very different than cases with similar configurations in both reference (5) and the available data on floppy disks. These cases were simply eliminated since no other data was available to replace those configurations. Similarly the test data configurations 1 and 13 for C_y also showed very different results. However, the data for case 1 in reference (5) was satisfactory (compared relative to the 1988 Aerobase coefficient data) and was used as a replacement. In general, the overall estimations of the axial and side force coefficients are questioned.

As the experimental data was collected during the spin tunnel testing, static results were obtained prior to both clockwise and counter clockwise rotations. Therefore, twice as much data was available with static conditions (Ω_{ss}=0) as with any other rotation rate. This provided an opportunity to examine the consistency of the coefficient values for static condition. Many test cases showed reasonably close coefficient values however most cases were inconsistent. Having no available means to decipher which was the best coefficient value from the clockwise and counter clockwise tests, the static condition coefficient data were simply averaged.

In preparation for creating a hybrid model, it needed to be determined whether

the two coefficient databases were reasonably based on the same testing conditions before blending them. The conditions chosen for the 1988 F-15 Aerobase model has been a thrust setting of 8,300 lbs (military power, thrust setting for trim conditions,steady level flight) at 0.6 Mach and 20,000 feet. The testing conditions for the rotary balance coefficients were obtained in a low Reynolds number environment which was not specifically set for variable flight conditions. The CG location as well as the aircraft body fixed coordinate frames were identical for both databases. Both databases are body frame referenced with the (CG) position of 25.65 percent mean aerodynamic chord. Figure 2.1 and 2.2 show comparison of the 1988 F-15 Aerobase as modelled by Baumann (7) and the raw rotary balance force and moment coefficient data for a selected configuration. Of the six coefficients (three force and three moment), the moment coefficients have the better correlation to the 1988 Aerobase. However, given the 1988 Aerobase and rotary balance data base were acquired from different testing facilities, have possible variation in Reynolds number and possible testing errors may be evident in the spin tunnel data, the coefficients would not be expected to match. Some coefficients as with the axial force and roll moment coefficients show large qualitative differences. However, their magnitude differences are everywhere relatively small. Results may not be sensitive to the differences. The effects of variations of the axial and side force coefficient were investigated.

Data analysis is a highly creative venture. Most engineering and research data are assembled in unbalanced sets that provide no attention to the requirements

$\beta=10^\circ, \Omega_{ss}b/2V_{tr}=0, \delta_a=-20^\circ, \delta_d=-6^\circ, \delta_e=0^\circ, \delta_r=30^\circ$

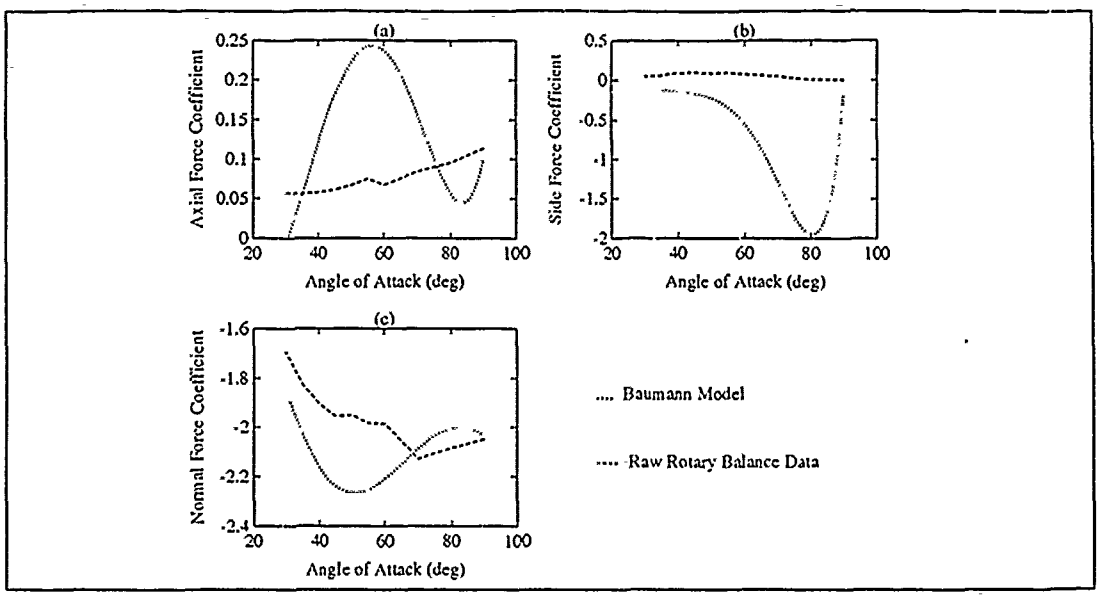

Figure 2.1 Comparison of force coefficients for the raw rotary balance data and the 1988 F-15 Aerobase model by Baumann (7).

$\beta=10^\circ, \Omega_{ss}b/2V_{tr}=0, \delta_a=-20^\circ, \delta_d=-6^\circ, \delta_e=0^\circ, \delta_r=30^\circ$

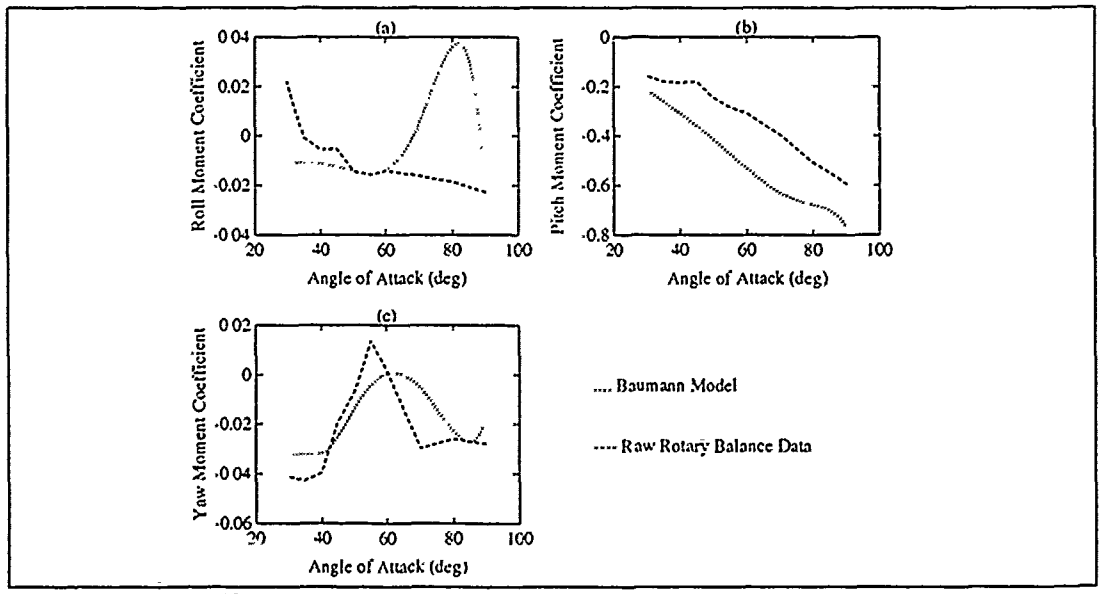

Figure 2.2 Comparison of the moment coefficients for the raw rotary balance data and the 1988 F-15 Aerobase model by Baumann (7).

of statistical analysis of the experimental results. However, because of the limited availability of data, the analyst must work with what he gets. The bifurcation analysis package AUTO (discussed in Chapter III) works best with functions with continuous first partial derivatives. Previous works using AUTO (6),(7),(8),(24) demonstrated problems performing calculations with functions that have discontinuities. It was determined to develop a polynomial as a function of seven variables for each coefficient providing a representation of the coefficients without any discontinuities or sharp changes. This enabled the full character of the database to be modelled in terms of how the coefficients varied with changes of the control surfaces as well as angle-of-attack, angle of sideslip and rotation rate. Representing the data in terms of polynomial equations also provided an efficient means for computation. Table look-ups and cubic spline interpolation between discrete values were considered. However, the high order characteristics of the data and limited depth in configurations led concerns for sudden transitions or discontinuities in the coefficient values resulting in problems with AUTO. As well, there are extreme complexities of implementing a seven variable local fit cubic spline routine. A spline routine used for three dimensional imaging was researched and examined which led to the conclusion that a seven variable effort would be too complex for the intention of this research. Polynomial curve surface fitting of the data will introduce smoothing and possibly invite characteristics into the data that are not discretely present in the raw data. However, the developed characteristics will be driven by the pattern established by the raw data. For the

reader interested in discussion of problems and methods of fitting equations to data, reference (12) is recommended.

Curve fitting is an art. With the size of the database (approximately 2000 experimental cases), the odds of developing the polynomial that perfectly fits are very small. However rewarding results could be obtained even with a moderate fit. Any software used should provide the user with control over the analysis; providing the user with a variety of options. The need for a curve fitting software that could handle a function of seven variables limited the choice to two software packages, SAS (31) and STATISX (36). SAS is a mainframe based package and STATISX is a PC based package. Both software were used for the development of the polynomials. SAS and STATISX were able to provide statistical measures of how accurate the curve fit was. They also provided direct comparison between the raw data and the polynomial function fit.

The raw data consisted of many outliers which were difficult to identify. Plots of various dimensions of the data were made to assist in outlier identification and to identify its complexity for polynomial fitting. Even though most datasets had non-dimensional rotation rates to $\pm$ 0.7, it was determined that the values of the coefficients at rates above $\pm$ 0.5 were inconsistent in sign and magnitude and would contribute more difficulty to the SAS fitting than contribute to the modelling of the database.

The limited configurations available in the rotary balance database determined the maximum order of any of the variables in the polynomial model. Table III

indicates the maximum order of each of the variables based on the available variation of each. It was determined to limit the polynomial dimension to fourth order for any individual or coupled variables. Higher order polynomials were possible however the complexity in determining a quality fit was increased. The increase in data processing depth seemed to outweigh the benefit of a closer fit. A sixth and eighth order model were developed for some of the coefficients. The higher order models did not provide a tremendous improvement to the fit and displayed unwanted behavior with some of the independent variables. The complexity in identifying the cause of the behavior outweighed the improvements.

Table III Maximum Order of Each Polynomial Variable

Variable	Maximum Polynomial Order
α	8
β	2
$\Omega_{ss}b/2V_{tr}$	10
δ_a	2
δ_d	3
δ_e	1
δ_r	2

The curve fitting began by identifying all combinations of the variables to a fourth order multi-variable polynomial. Some combinations should not even be considered. Control surface effects would not be strongly coupled since their positions are mechanically independent and aerodynamic coupled influences are negligible. For example, aileron settings may create aerodynamic influences on rudder derivatives but the distance between the control surfaces result in the

effects being negligible. The only coupled terms involving multiple control deflections are the differential stabilator and aileron since they are inherently coupled in the design of the aircraft by the linear relation, $\delta_d=(0.3)\delta_a$. Six of the sixteen available configurations in Table I varied δ_d independent of the defined linear relationship with δ_a. This allowed the resulting polynomial to have independent terms of δ_d in addition to coupled with δ_a. It was left to SAS to identify terms that had no correlation to the behavior of the data. Indicating the strength of SAS and giving validity to the polynomial "surface" fit, SAS was able to identify those coupled terms that were not needed in the polynomial. The coupled term of aileron and differential stabilator deflection was identified, as predicted.

STATISX was used to prepare the raw data for use in SAS. The SAS routine GLM was used to perform a linear regression to determine the coefficients of the defined polynomial. Using a method of maximizing the standardized residual mean square value towards 1.0 and identifying strong terms using the student's t distribution function, the "best" polynomial was determined. At times, the process involved trial and error in removing and adding terms. However, each SAS run presented evidence of the sensitivity of a coefficient to particular variables or their combination. The student's t distribution function provided "clues" to what the next "guesses" should be. The residuals of each polynomial fit were plotted against the independent variables to identify trends and to assist in determination of the "quality" of the fits.

As an experiment, to test the method used, a fourth order polynomial of four

variables was created and a random database of results was constructed. Knowing the "answer" to the polynomial fit, SAS runs were performed utilizing similar decisions made on the rotary balance database. This was performed to validate the method utilized. The resulting polynomial was very similar to the one created showing validity in the development process used for the rotary balance coefficient polynomials.

The first attempt at fitting the data was to break each coefficient into 6 individual polynomials broken at 20° increments with 10° overlapping in angle of attack. The objective was to reduce the amount of data each fitting needed to use and decrease the residuals for a more accurate representation of the data. The decision to use angle of attack was determined by examining the effects of breaking up the data base into sets based on each of the seven independent variables (i.e. dividing the entire database into three groups defined by angle of sideslip: β=-10°,β=+10°,β=+10°). Seven combinations of the data (22 resulting datasets) were developed representing each of the independent variables. Using the complete fourth order polynomial representation (approximately 200 terms), the standardized residual mean square results were compared to see which combination of datasets provided the "best" fit. This processing also assisted in identifying which variables were most difficult to model. Datasets divided by angle of attack showed the best standardized residual mean square values and those by angle of sideslip the worst. This resulted in the development of 36 equations representing the six coefficients. The resulting polynomials consisted of equations

ranging from 15 to 37 multi-variable terms. Once the 36 equations were developed, 79 distinct monomials in 7 variables were identified. A matrix of the polynomial coefficients was constructed with those terms not required for a particular polynomial term given a null value. Each set of six equations was blended together using a cubic spline relationship similar to Eqn (45) of Chapter IV.

When the 36 equation model was used with AUTO, each of the six coefficients encountered problems in performing parameter sweeps. This indicated difficulties with the transitions between the individual equations. As shown in Figure 2.1, C_x,C_z and C_m show fairly linear behavior which resulted in minimal problems with transitions from individual equations in their modelled polynomials. However, each did experience occasional problems. C_y (see Figure 2.5),C_l and C_n had much more character for the polynomials to represent which resulted in more frequent discontinuous transitions between the equations representing the coefficient. Figure 2.3 shows the C_l and C_n six part polynomial models for two different configurations as compared to the raw rotary balance data. The model obviously was an excellent fit. However, the sharp transitions between the individual equations are evident. Figure 2.3 is not representative of the "worst" case discontinuities. Because each equation of a coefficient polynomial was defined on a limited database, each displayed different behavior to the independent variables. Most often the behavior difference was slight. Occasionally gross differences occurred. It was difficult to examine every dimension of the seven variable

polynomials and identify when difficult transitions occurred. AUTO encountered discontinuity problems on every continuation run, hindering the investigation. Two and one half months of development were invested in the 36 equation model however a different representation of the data had to be pursued. The range of angle of attack for blending the transition between equations was expanded however the results with AUTO were still not successful. It is anticipated that problems with individual polynomials for particular combinations of independent parameters may have undesirable behavior. With further development, the six part polynomials could work and would be the better polynomial representation of the data because of its close fit. However if noise were present in the data, the polynomial would also be amplifying its contribution.

A two piece equation was also developed which encountered similar problems. Figure 2.4 shows the C_l and C_n coefficients for two different configurations. The second case for each coefficient demonstrate how the polynomial can show very different behavior and result in a poor fit while having good correlation on other configurations as shown in the first case. Rather than experience similar problems as with the six part model, it was decided to focus on a single equation fit; eliminating the discontinuity problems, allowing the full database to be used and providing better control over the overall sensitivity of a polynomial to individual parameters.

A single equation representation of each coefficient was developed utilizing the 79 identified terms of the 36 equation development. The standardized residual

(a,d): $\beta=0°,\Omega_{ss}b/2V_{tr}=0,\delta_a=0°,\delta_d=0°,\delta_e=0°,\delta_r=0°$ (b,c): $\beta=10°,\delta_a=-20°,\delta_d=-6°,\delta_r=30°$

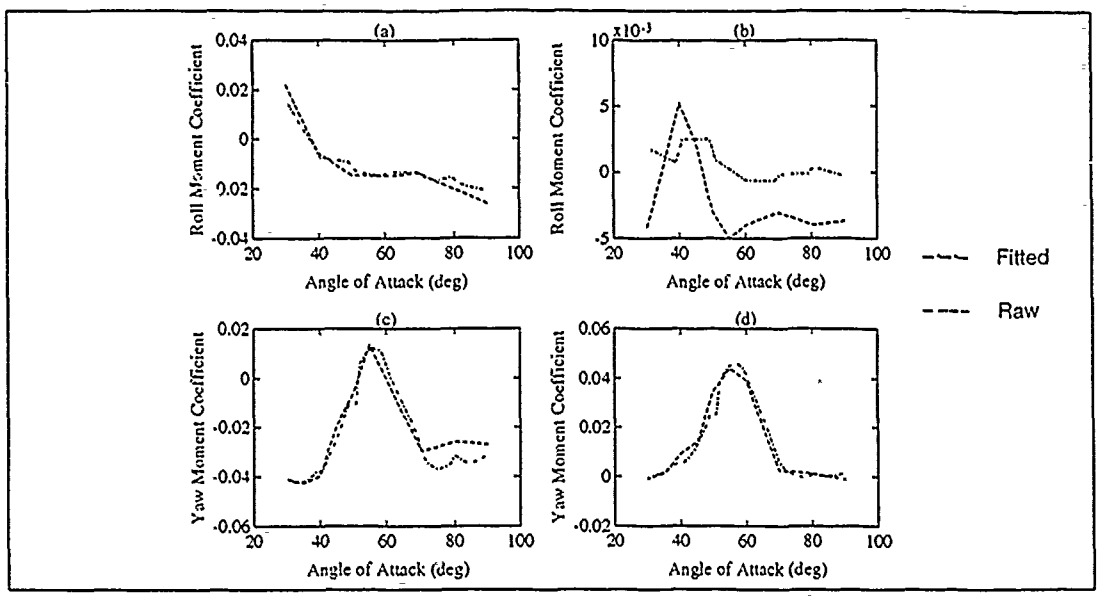

Figure 2.3 Examples of the six equation polynomial representation of the rotary balance data compared with raw data.

(a,d): $\beta=0°,\Omega_{ss}b/2V_{tr}=0,\delta_a=0°,\delta_d=0°,\delta_e=0°,\delta_r=0°$ (b,c): $\beta=10°,\delta_a=-20°,\delta_d=-6°,\delta_r=30°$

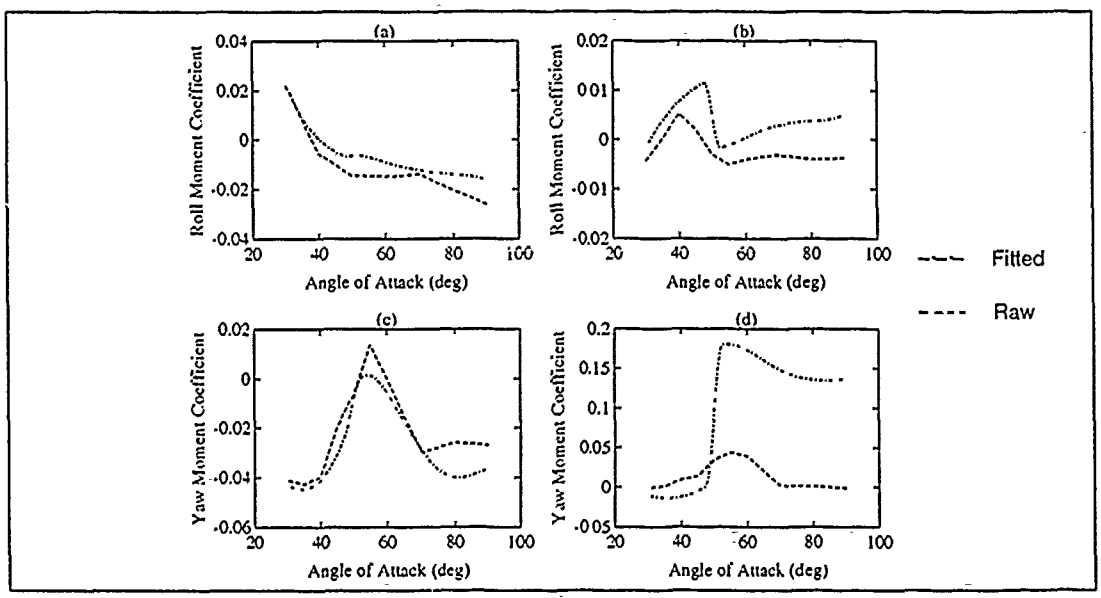

Figure 2.4 Examples of the two equation polynomial representation of the rotary balance data compared with raw data.

square criteria ranged from 0.80 to 0.98 with C_x being the worst and C_m the best coefficient data fit. All coefficients except C_x had a value greater than 0.9. The resulting polynomials were continuous resulting in smooth operation with AUTO.

The coefficient functions were plotted for different sample aircraft configurations and states comparing them to the raw rotary balance data and the 1988 Aerobase to validate the accuracy of the fits. Figures 2.5 and 2.6 are an indication of comparison of the single 79 term polynomial, raw rotary balance data and the Baumann model.

It is evident from Figures 2.5 and 2.6 that the polynomial curve fitting has introduced characteristics that are not evident in the raw data as well as missing some that are evident. What the polynomial fitting has done is to model the database as a whole rather than looking strictly at a snap shot picture of the data that would be found with a table look-up routine. The polynomial fit has basically smoothed the data pacifying outliers and smoothing subtle changes in the data. Comparing the rotary balance coefficient polynomials to the 1988 Aerobase polynomial fitted data shows some similarity in their character but obvious differences. It is apparent that the differential between the rotary balance data polynomial fit and the raw rotary balance data is much smaller than that between the rotary and 1988 Aerobase data. During spin tunnel testing, the problem of aerodynamic interference caused by the aircraft model's wings/fuselage vortices being influenced by the support structure can be significant. In addition, any motion that alters the rotation center location of a test could cause error in the post

$\beta=0°,\Omega_{ss}b/2V_{tr}=0,\delta_a=0°,\delta_d=0°,\delta_e=0°,\delta_r=0°$

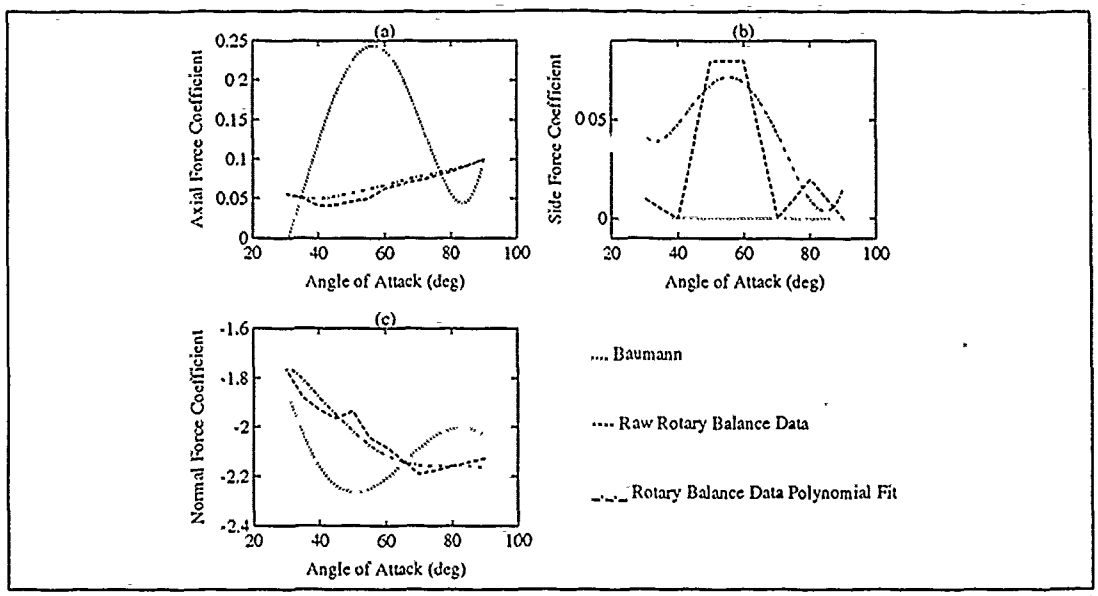

Figure 2.5 Comparison of the force coefficient rotary balance data polynomial fitted data, raw RB data and the Baumann model (7).

$\beta=0°,\Omega_{ss}b/2V_{tr}=0,\delta_a=0°,\delta_d=0°,\delta_e=0°,\delta_r=0°$

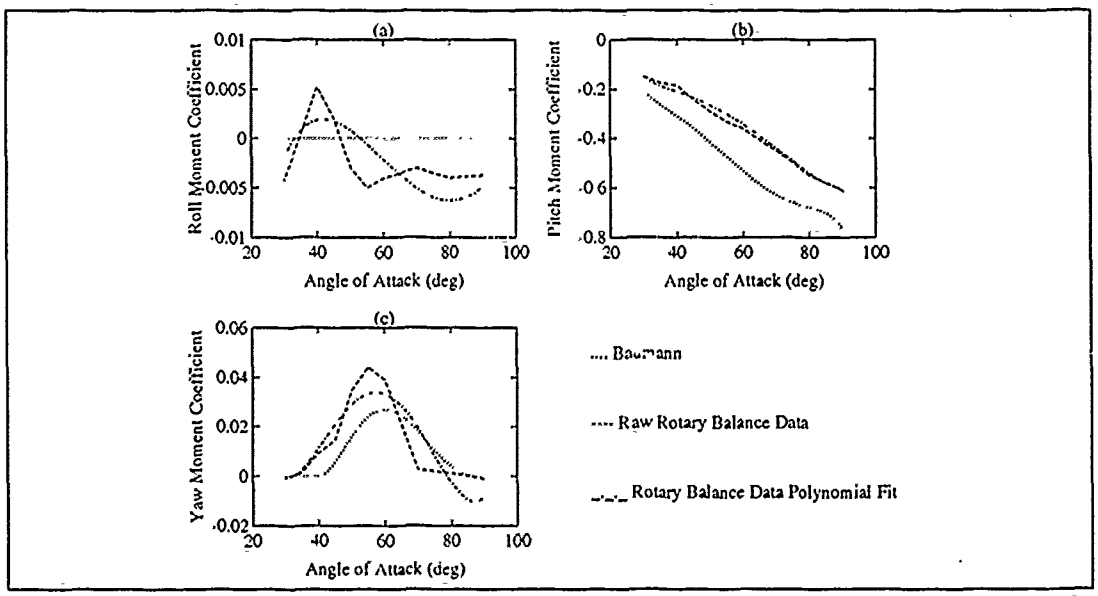

Figure 2.6 Comparison of the moment coefficient rotary balance polynomial fitted data, raw RB data and the Baumann Model (7).

processing which was based on a predetermined rotation center location (2:7-11). The behavior of the rotary balance data in Figures 2.5 (b) and 2.6 (a) could be attributed to these possible inaccuracies in spin tunnel testing. It is anticipated that the results using either database exclusively or combined will provide quite different results. The Baumann (7) 1988 Aerobase coefficient representation and the 79 term rotary balance database polynomial can be referenced on page 119 and 145 respectively in Appendix C.

III. Bifurcation Theory

This chapter will discuss the basic principles of bifurcation theory and its application toward nonlinear systems. The qualitative study of nonlinear differential equations is concerned with how to deduce important characteristics of the solution without actually solving the equations. Through bifurcation theory this study can investigate highly nonlinear motion of aircraft in a spin without the need to basically destroy information contained in the nonlinear equations by linearizing them with small perturbation analysis. There are many types of bifurcations and each type has a different effect on the response of a system. The concepts to be discussed are: equilibrium points, phase space, stability, turning points, bifurcation points, periodic solutions, Hopf points and an example of unfolding of an organized center. Most of the information in this chapter is referenced from Seydel (34). Other useful texts on the subject of bifurcation theory are references (15) and (21). A brief description of the software program AUTO will follow with a short discussion on homotopy, an important application of continuation theory needed for this research.

Equilibrium Points

When a system is in physical equilibrium or in a steady state for bodies in motion (i.e. an aircraft), the states that describe the system are termed the

equilibrium points. Equilibrium points are also referred to as stationary points. In the study of aircraft dynamics, only autonomous systems will be analyzed. For an autonomous system, the differential equations of motion do not explicitly contain time on the right hand side of the equations. An autonomous system can be written as

$$\dot{u} = f(u) \tag{1}$$

where u is an n-dimensional vector of state variables and f is an n-dimensional vector of functions describing the motion of the system. The system is in equilibrium when the states are constant, $\dot{u} = 0$. The states that describe this equilibrium of the system would satisfy the equation

$$f(u) = 0 \tag{2}$$

These states are called the equilibrium points or stationary points.

Phase Space

Suppose the state of a system is described by the state vector u and the nonlinear equation

$$\dot{u} = f(u,\lambda) \tag{3}$$

defining the behavior of the system where λ is a control parameter of the system. Points along the solution of Eqn (3) consist of a time coordinate t, the fixed value

control parameter λ and the n dimensional space coordinates $(y_1,y_2,...,y_n)$. If the vector function f is continuously differentiable, there is a unique trajectory through each point u_0 of Eqn (3).

Consider a three dimensional phase space representing the coordinates (y_1,y_2,λ). At equilibrium, $\dot{\lambda}=0$, for a fixed value of λ the solution will remain in a plane, the phase plane. A stationary solution is represented by a point, Figure 3.1. As the parameter λ is varied, the position of the state solutions change in the phase plane. If the parameter λ is freely variable, the equilibrium solution path forms a curve in the (y_1,y_2,λ) space, Figure 3.2. These curves represent equilibrium solutions as they depend on variable parameters of the system. This is simple to visualize in three dimensions but consider a set of eighth state equations of motion of an aircraft dynamic model and the multiple parameters that can be varied. The parameter λ could represent the control deflections of the aircraft's rudder, stabilator, ailerons or any parameter within an aircraft attitude control system. It becomes evident that the visualization of the equilibrium solution curves can become quite complex. However, qualitative information can be found by viewing the curve projections of a chosen system state as the value of a single control parameter is varied, i.e. viewing the aircraft state α as elevator deflection is varied. The resulting projection is a bifurcation diagram. Applications of a bifurcation diagram utilized for this investigation are the examination of effects on particular states of aircraft dynamics as control surfaces are varied. The resulting

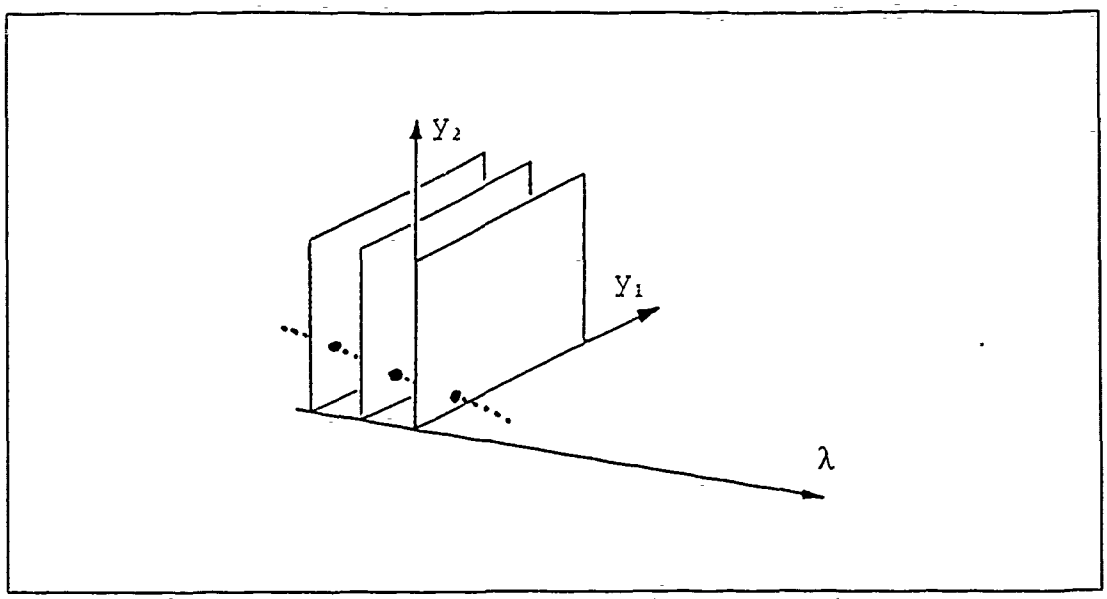

Figure 3.1 A stationary solution in several phase planes (41:3).

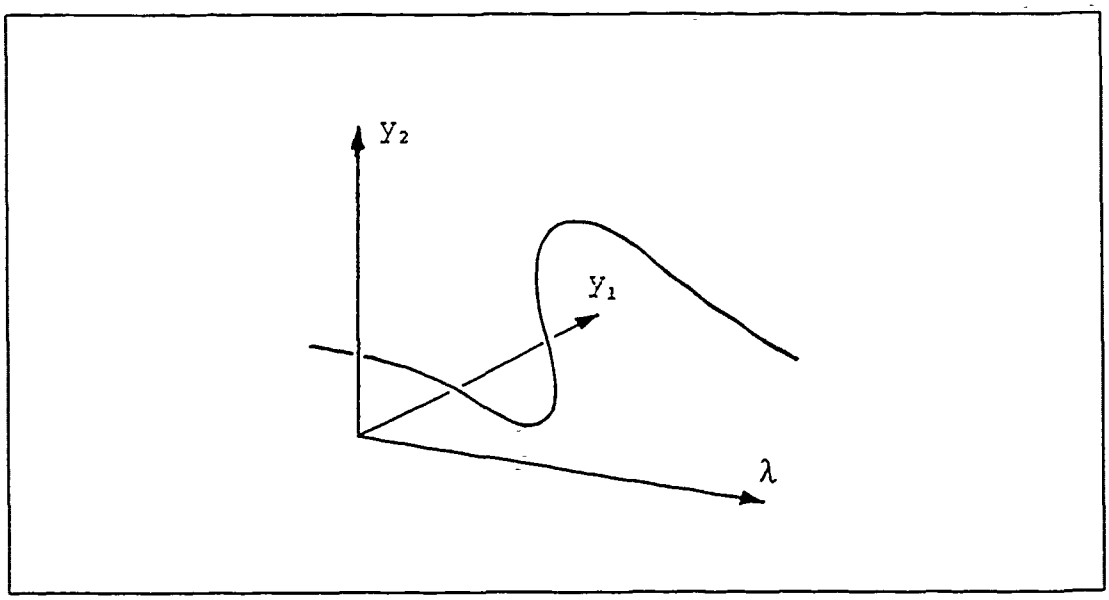

Figure 3.2 Solution curves in (y,λ)- space (41:3).

solution curves provide information for identification of effective controls for aircraft maneuvers or of unusual aircraft states that could occur when the aircraft is configured with particular control surface deflections. Figure 3.3 is an example of a bifurcation diagram. Bifurcation diagrams also allow for the identification of multiple states a system can attain for a given value of a control parameter, λ. It is advantageous to identify configurations that could lead to abrupt changes in the aircraft dynamics as the aircraft states jump to a different solution value.

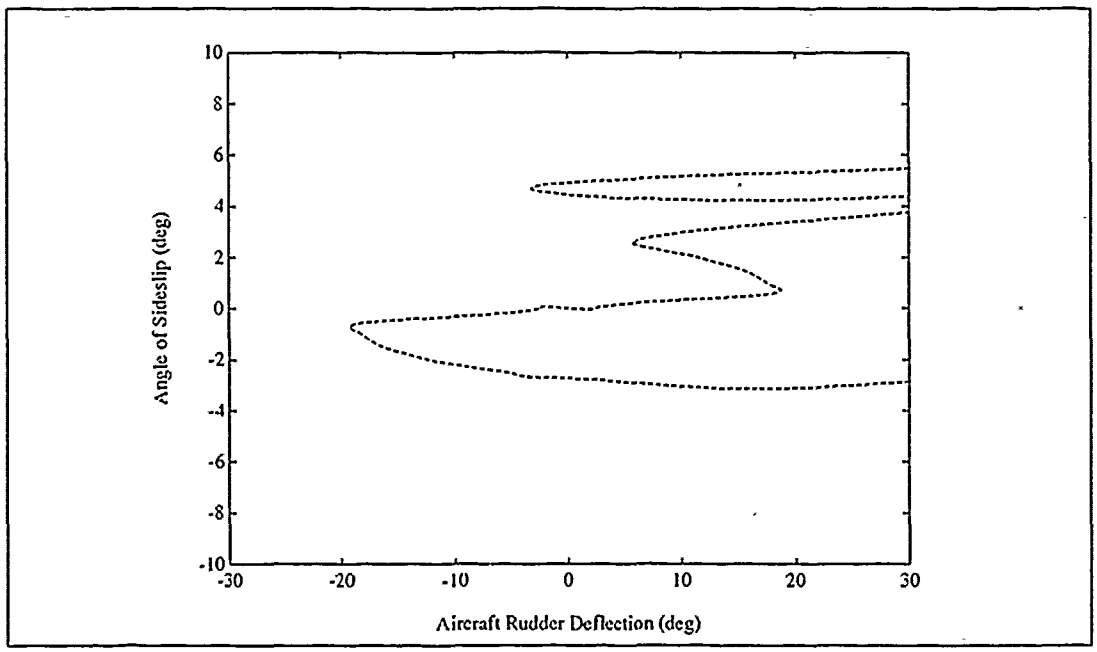

Figure 3.3 Example Bifurcation Diagram.

Stability

Stability is the tendency of a system, when disturbed from a given equilibrium, to return to that equilibrium. An equilibrium may be stable for a small perturbation

but unstable for a large perturbation showing that a system's stability is only valid within the domain of attraction of the solution of interest. Figure 3.4 is a way of looking at the various definitions of stability. A marble placed perfectly balanced on the top of the hill (A) is an unstable equilibrium state. Any disturbance will cause the marble to leave its position and never return. At position (B) the marble is apparently stable for small disturbances however under a strong influence, the marble may leave this location. Equilibrium locations (B) and (C) represent weak stable equilibrium and location (D) represents a strong stable equilibrium. A larger disturbance at location (D) will allow return of the marble to its original stable position.

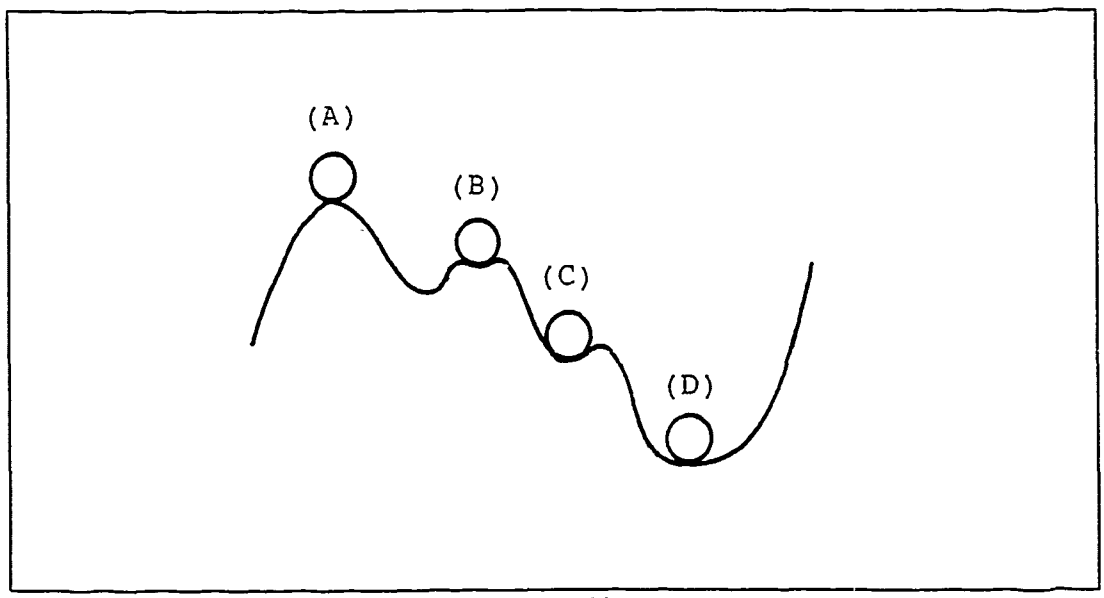

Figure 3.4 Geometrical example of stability.

Stability of a stationary point determines whether the state of the system is attracted to or repelled from the point. Local stability refers to the stability in a

small region around a stationary point. Local stability of a fixed point of a nonlinear system can be calculated by determining the eigenvalues of the equivalent linear system. The eigenvalues are obtained by linearizing the equations of the system about the stationary point of interest. A stationary point is stable if the real parts of all eigenvalues are less than zero and unstable if any eigenvalue has a real part that is greater than zero. In two dimensions, Figure 3.5 shows the various stability types in the phase space. If the eigenvalues are real numbers greater than zero, the stationary point is a source or if less than zero a sink. If the eigenvalues are real numbers with opposite sign, a saddle point is formed. For complex conjugate eigenvalues with nonzero real parts, if Real < 0 a stable spiral is formed else if Real > 0 an unstable spiral. For the condition with complex conjugate eigenvalues with zero real parts a center is formed. With multi-

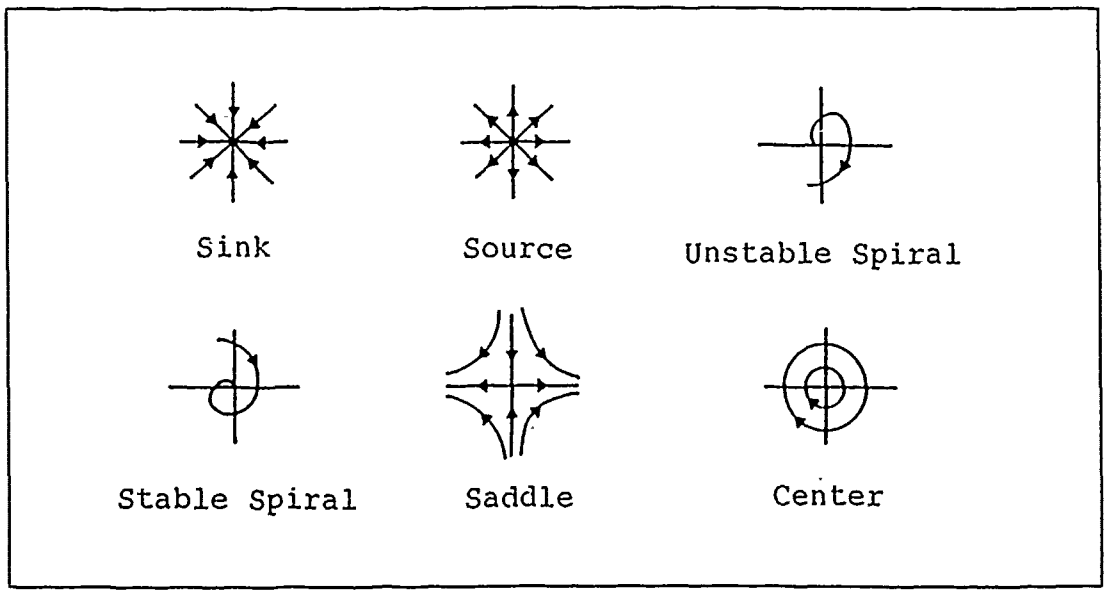

Figure 3.5 Stability types.

dimensional systems, the higher dimensional, analogous phase behavior to Fig 3.5 must be imagined. The behavior are too complex to visualize however do occur.

Turning Point

A simple example of a turning point can be introduced using the scalar equation

$$\dot{y} = \lambda - y^2 \tag{4}$$

The equilibrium solutions can be determined from

$$0 = \lambda - y^2 \tag{5}$$

The solutions $y(\lambda)$ of equation (4) form a parabola that is only defined for $\lambda \geq 0$. At $\lambda=0$ there is only one solution ($y=0$) where as for $\lambda>0$ there are two solutions. The point where a solution begins to exist ($\lambda=0, y=0$) is a turning point or also referred to as a limit point. Figure 3.6 graphically shows a limit point. A solid line depicts a stable solution branch and a dashed line an unstable branch. This convention will be used throughout this report. It should be noted that in n-dimensional systems a turning point does not always separate stable equilibrium from unstable equilibrium. An eigenvalue always changes sign at the turning point but others may already be greater than zero.

Turning points often arise in pairs resulting in hysteresis effects. Figure 3.7 is an example of a hysteresis effect. Characteristic of hysteresis are jump phenomena which take place at λ_1 and λ_2. As λ is increased along the upper

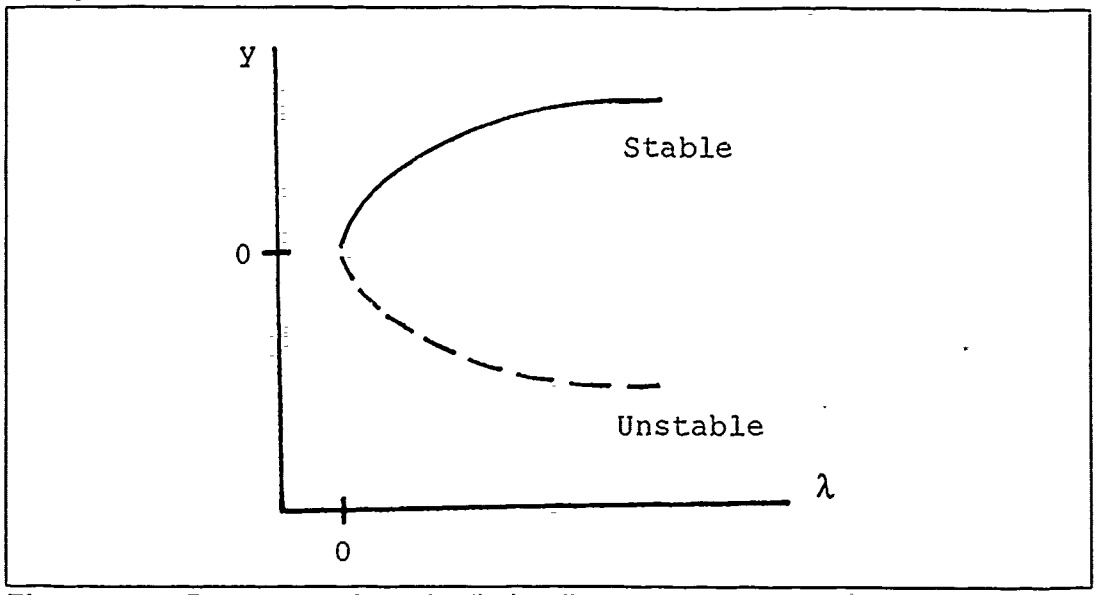

Figure 3.6 Representation of a limit point.

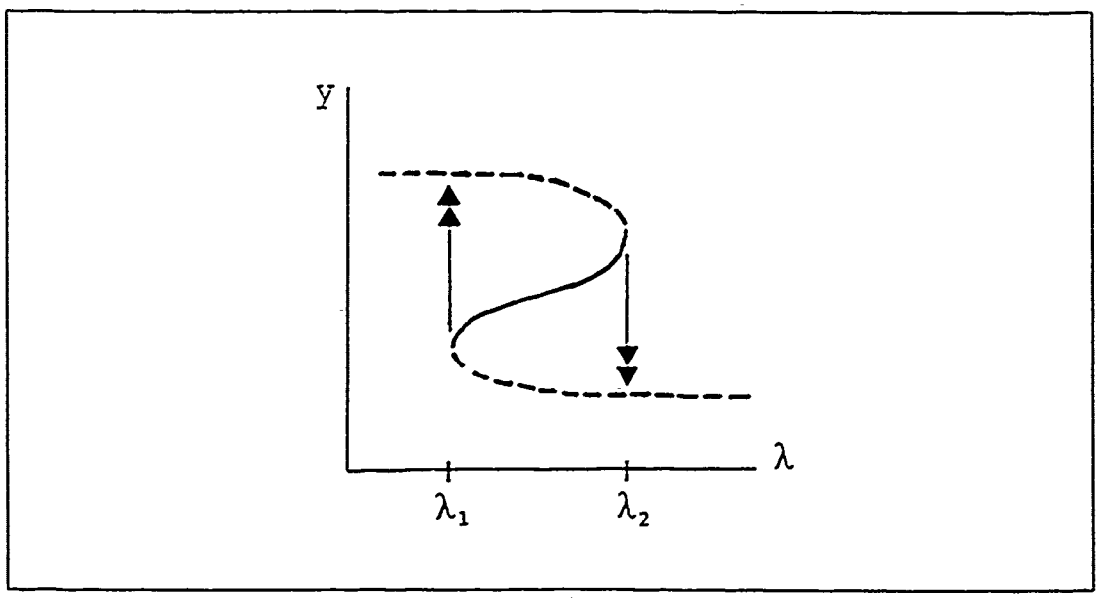

Figure 3.7 Example of a hysteresis or jump phenomenon.

branch approaching the right limit point, increasing the value of λ beyond the value λ_2 will cause a jump to the lower branch. Similar characteristics can be found for the value λ_1. This phenomenon is also referred to as a jump phenomenon Such behavior has been found in aircraft dynamics as discussed in reference (33) by Schy and Hannah.

Bifurcation Points

A bifurcation is a point where something is divided into two parts. A bifurcation occurs in a system when the variation of an independent control parameter creates a point where the behavior of the system can assume one of two different states for the same set of system parameters. Consider a system described by the scalar equation

$$\dot{y} = \lambda y - y^2 \tag{6}$$

For all values of λ there is the trivial solution y=0. If $\lambda \neq 0$ the non-trivial solution is $y=\lambda$. A stability exchange occurs as depicted in Figure 3.8. The point at $\lambda=0$ is referred to as a transcritical bifurcation point. Other qualitative types of simple bifurcations are possible but will not be discussed.

When the branch y=0 loses stability at the bifurcation point and branches into two stable trajectories, the event is referred to as a supercritical pitchfork. If the

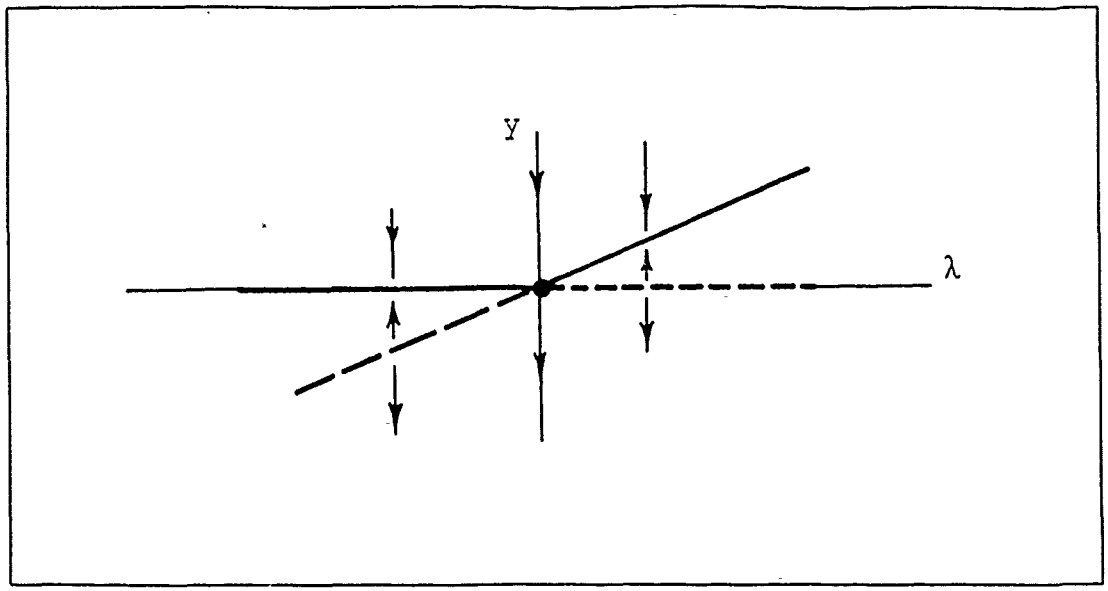

Figure 3.8 Example transcritical bifurcation point.

branch y=0 gains stability at the bifurcation point and the bifurcation of unstable branches occur, the result is called a subcritical pitchfork. Examples of supercritical and subcritical pitchforks are shown in Figure 3.9.

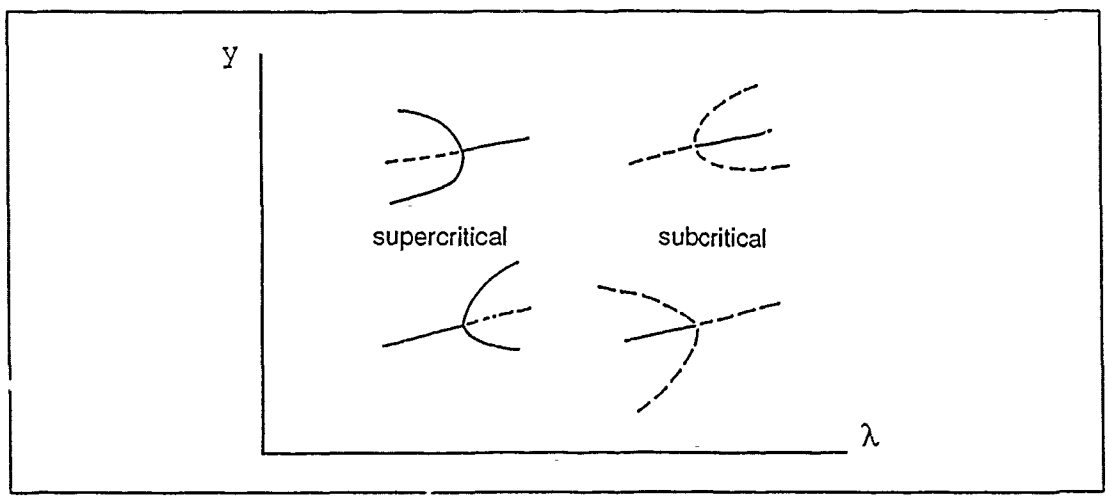

Figure 3.9 Examples of supercritical, subcritical bifurcations.

Limit Cycle

A limit cycle represents regular motion such as the vibration of a string or current flowing through an electrical circuit. A limit cycle is an isolated periodic solution of an autonomous system, represented in the phase plane or phase space for n-dimensional systems by an isolated closed path. Unlike a center, the neighboring paths are not closed but either spiral into or away from the limit cycle. Figure 3.10 is an illustration of a stable limit cycle. For the stable limit cycle, any state of the system near the limit cycle will drift into the periodic motion defined by the limit cycle.

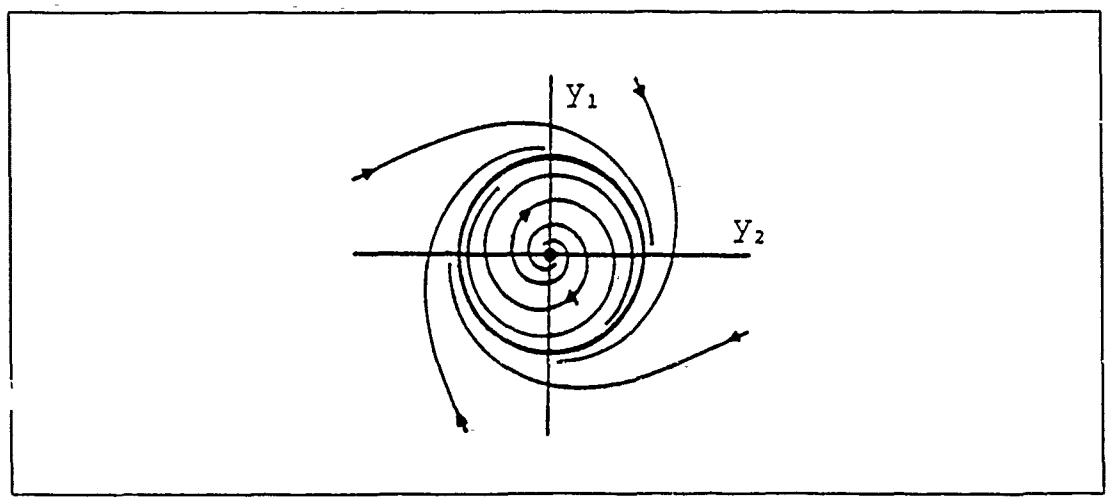

Figure 3.10 Example stable limit cycle.

Hopf Bifurcation

Hopf bifurcation is the door that opens from the small room of equilibria to the large hall of periodic solutions (34:61).

The type of bifurcation that connects equilibria with periodic motion is Hopf bifurcation. Consider the system

$$\begin{aligned} \dot{y}_1 &= \lambda y_1 + y_2 - y_1(y_1^2 + y_2^2) \\ \dot{y}_2 &= -y_1 + \lambda y_2 - y_2(y_1^2 + y_2^2) \end{aligned} \tag{7}$$

$y_1=y_2=0$ are the only equilibrium values for all λ and no stationary bifurcations occur. The Jacobian matrix for this system is

$$\begin{vmatrix} \lambda & -1 \\ 1 & \lambda \end{vmatrix} \tag{8}$$

and has eigenvalues $\lambda=\pm i$. The equilibrium solutions are stable for $\lambda<0$ and unstable for $\lambda>0$ with a loss of stability at $\lambda=0$. Using polar coordinates

$$y_1 = r\cos\theta \ , \ y_2 = r\sin\theta \tag{9}$$

the system of equations can be simply expressed as

$$\begin{aligned} \dot{r} &= r(\lambda - r^2) \\ \textit{and} \quad \dot{\theta} &= 1 \end{aligned} \tag{10}$$

If $\lambda\leq 0$ the entire phase diagram is a stable spiral. If $\lambda>0$ an unstable spiral is formed at the origin surrounded by a stable limit cycle which grows out from the origin as λ increases. The origin changes from being asymptotically stable to being unstable without passing through the stage of a center. Figure 3.11 shows

the phenomenon in two dimensional slices and Figure 3.12 in three dimensions by including λ. On the bifurcation diagram, periodic solutions will be depicted by circles along a branch as shown in Figure 5.2(c) of Chapter V. Closed circles will depict stable limit cycles and open circles unstable limit cycles. It should be understood that a stable periodic orbit is approached by nearby trajectories, whereas trajectories leave a neighborhood of an unstable periodic orbit.

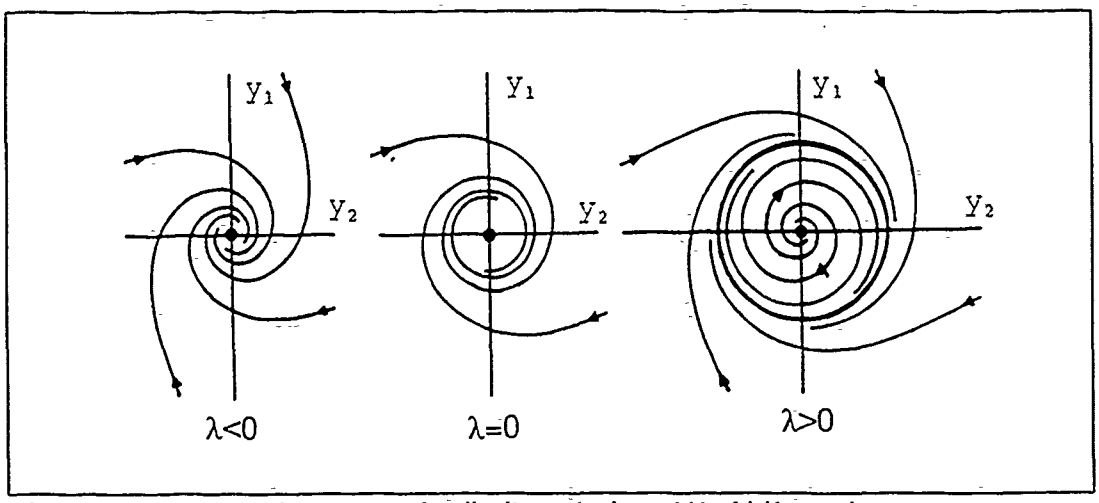

Figure 3.11 Development of a limit cycle in a Hopf bifurcation.

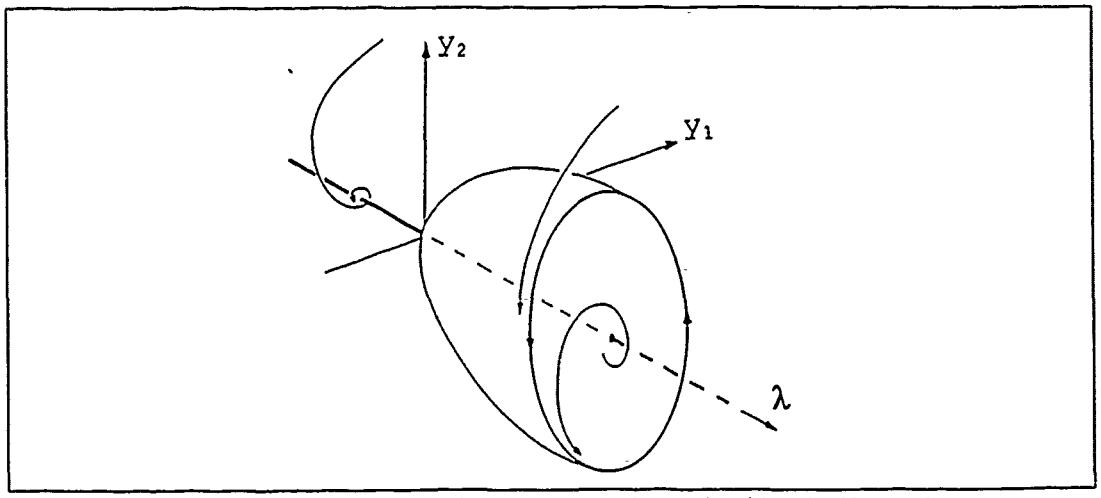

Figure 3.12 Three-dimensional representation of a Hopf bifurcation.

Organized Centers

Locations in solution branches where dynamical behavior changes in the sequence: no multiplicity, then two jumps, then four jumps, then two jumps, is one example of an organized center. This phenomena can best be explained graphically. Figure 3.13 shows various bifurcation diagrams as a second control parameter γ is varied. For this example $\gamma_5>\gamma_4>\gamma_3>\gamma_2>\gamma_1$. For γ_2 two branches are found without connection, the upper branch is an isolated branch, the path A-B is smooth. For γ_3 the situation is the same but the two branches are closer. For γ_4 there is no longer an isolated branch, with the overall branch structure now resembling a mushroom. In this state, the consequences for the path from A to B is severe. There are two hysteresis jumps. There is a transcritical bifurcation that occurs between the values γ_3 and γ_4 that separates a two jump situation to a four jump situation. At some value of γ the branches merge in an isola point. An isola point would be equivalent to the transcritical bifurcation point in Fig 3.8 with two of the like stability branches being a closed path. Increasing γ further can result in a two jump situation. This representative sequence of high-order bifurcations is governed by theory beyond the scope of this investigation. For discussion on understanding why these events occur and further examples of this phenomena, Seydel (34) is referred. This type of phenomena occurs in reality and has been shown during this investigation.

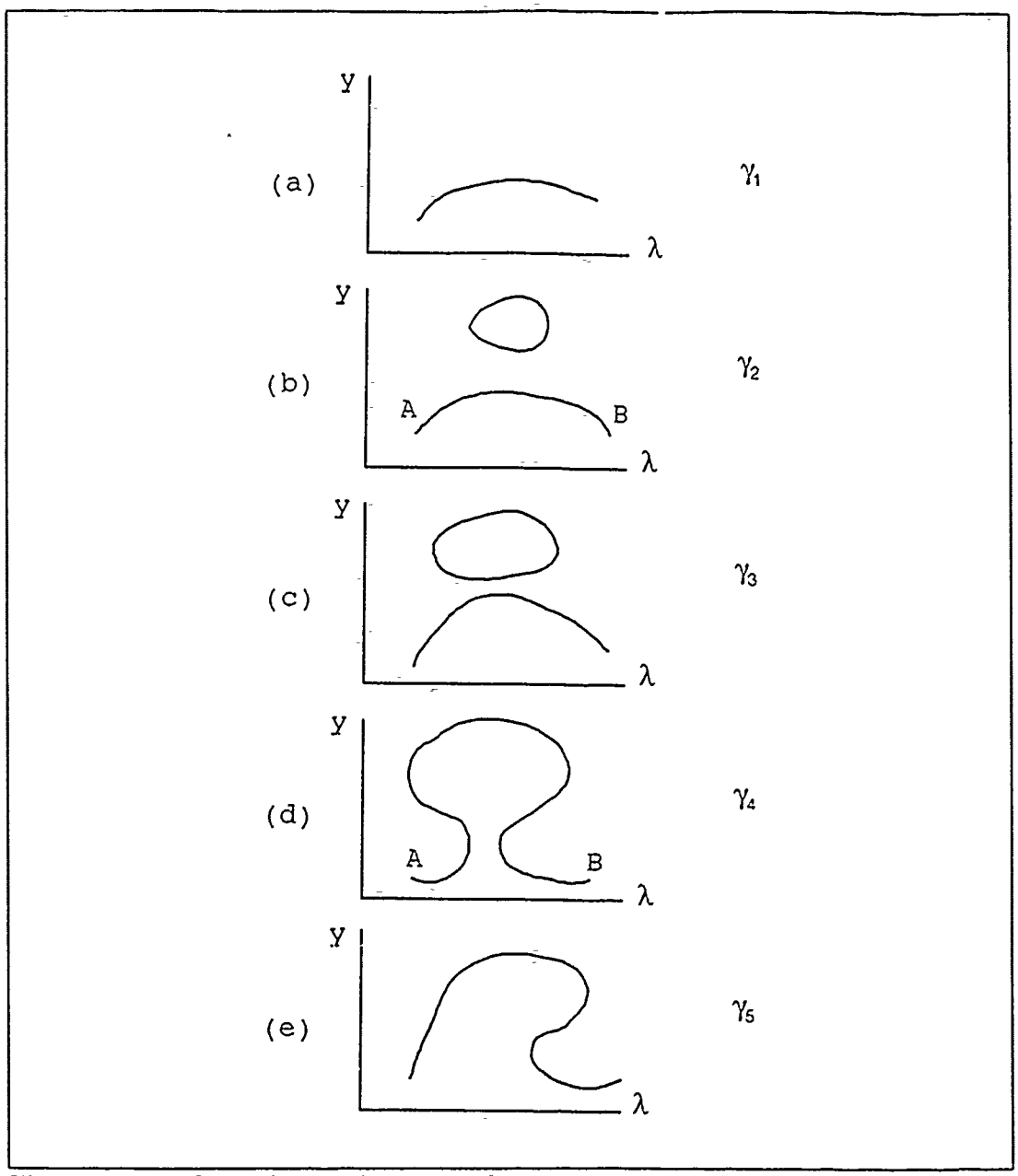

Figure 3.13 Sequences of an organized center.

AUTO Software

The software tool utilized in this investigation for continuation and bifurcation analysis is AUTO. AUTO, written by Eusebius Doedel of Concordia University, is a collection of FORTRAN routines concerning the numerical analysis of nonlinear systems of algebraic and ordinary differential equations. The software's primary purpose is to compute branches of stable or unstable periodic solutions of systems of the form of Eqn (3). Given a function, the Jacobian of the function, the derivative f_λ, a steady state solution for some value λ and a number of control parameters, AUTO can compute steady state branches, accurately determine steady state and Hopf bifurcation points and switch branches at such points. The key to initiating an analysis using AUTO is the identification of a steady state solution of the system of equations to be analyzed. This can be accomplished by considering a simple flight condition or the methods of homotopy could be exercised. Described is only a partial outline of AUTO's capabilities. The reader is encouraged to reference the AUTO User's Manual (13) for additional information on its capabilities and application.

Continuation and Homotopy

Continuation theory is the methodology of answering the question of how solutions of equations vary with a parameter. Continuation methods involve four

basic elements: (1) an initial guess of the solution, (2) choice of the system parameter to vary, (3) a correction iteration of the solution and (4) variation of the iteration step size. Given a set of differential equations describing a dynamical system, a numerical integration routine such as Euler's or Newton's method could be used to integrate the equations. Predictions of the next solutions along a branch are determined as small incremental changes are taken of the chosen system parameter. A corrector iteration is then used improving the guess of the next solution. As the solution branches are identified, variable step lengths are used to allow for small details to be resolved and not skipped, assist in transitioning through turning points and to aid in processing of the numerical iteration methods. The result is a tracing of equilibrium solutions of the system of differential equations.

One important application of continuation is homotopy. Consider an equation f(u)=0 which is difficult to solve for a solution. An initial guess may be even harder to determine. Note that this equation is probably nonlinear and would require iterating to solve . Iterative solution algorithms usually converge very slowly or diverge away from the solution if the initial guess is way off. Assume that an equation g(u)=0 is known that is easily solved with solution u_0 and can be obtained by simplifying f(u)=0. Homotopy is a construction of equations that are linked together and are solved one at a time. The last equation solved is the original equation f(u)=0. The solution of each successive equation is used as an initial guess for the next equation. This describes a discrete homotopy with finite

number of equations. A continuous homotopy is where a parameter λ is introduced that varies on the interval $0 \leq \lambda \leq 1$. This leads to

$$f(u,\lambda) = 0 \ , \ 0 \leq \lambda \leq 1$$
$$f(u,0) = g(u) \qquad f(u,1) = f(u) \tag{11}$$

An example of such a process is with

$$f(u,\lambda) = \lambda f(u) + (1 - \lambda)g(u) \tag{12}$$

At $\lambda=0$, u_0 is the solution. As λ is varied to 1.0, the solution set transitions to that of the equation of interest $f(u)=0$. The method of homotopy will be applied in chapter IV to acquire equilibrium solutions required by AUTO for the rotary balance data model using the known solutions of the McDonnell model (24). For the reader interested in a short tutorial on the methods of continuation, the article "Tutorial on Continuation" by Seydel (35) is highly recommended.

IV. Aircraft Model

The aircraft for this investigation is the McDonnell Douglas Corporation F-15B, a two place high performance fighter developed for the United States Air Force. The F-15 was designed with a cockpit sized for two crew members requiring the only major change of a larger canopy to form the two seat (F-15B) from a single seat version (F-15A). This design feature allowed for application of the F-15 in a multitude of roles in training, air-to-air combat, air-to-ground combat and reconnaissance. The flight characteristics of the F-15A and F-15B are very similar even with the added weight of the second crew member configuration. This will enable some flight test data of the F-15A to be considered in the analysis of the F-15B. One design feature sought for in the F-15 was an aircraft capable of high-energy maneuverability in turning, accelerating and climbing in order to gain a tactical advantage in combat. The low wing loading, very high thrust design of the aircraft adds to its air superiority capability. This air superiority was demonstrated in the F-15's multiple roles in Operation Desert Storm. A figure of the aircraft with control surface sign conventions is located in Appendix B along with aircraft physical dimensions and specifications in Appendix A.

The F-15B has multiple independent control surfaces, left and right aileron, left and right rudder, left and right stabilator, speed brake and variable inlet ramps. The ailerons and stabilator were set by the manufacturer to act differentially with the linear relationship $\delta_d=(0.3)\delta_a$. The speedbrake was not modeled because it

is not a nominal control surface used during high angle of attack maneuvers and is designed for retraction at angles of attack above 15°. The aircraft is an inherently stable design without the use of the Control Augmentation System (CAS). This stability characteristic enabled this analysis to be performed without CAS engaged. The aircraft was modeled for gear up, retracted flaps and stores carriage. The Baumann/McDonnell Model aerodynamic coefficients were modeled for a flight condition of 20,000 feet and a Mach number $M \leq 0.6$ (7). The testing conditions for the rotary aerodynamic coefficients fall within this criterion.

Model Development

The development of the aerodynamic force and moment coefficients for the F-15 model used by McDonnell (24) are documented in the thesis by Baumann (7:20-21). Baumann curve fitted the 1988 F-15 Aerobase which represents the F-15 aerodynamic coefficients for static and forced oscillation testing as well as the inclusion of some actual flight test data. Results of those curve fits are documented in the AUTO Driver program presented in Appendix C. The thrust contributions to the force and moment coefficients used in this research are those developed by McDonnell (24:24). The feature of thrust vectoring will be included in the rotary aerodynamic model however its effectiveness will not be pursued in this investigation. The rotary aerodynamic coefficients obtained by the NASA

Langley Spin Tunnel are represented as

$$C_x = Axial\ Force/(\bar{q}\ S) \quad (13)$$

$$C_y = Side\ Force/(\bar{q}\ S) \quad (14)$$

$$C_z = Normal\ Force/(\bar{q}\ S) \quad (15)$$

$$C_l = Rolling\ Moment/(\bar{q}\ S\ b) \quad (16)$$

$$C_m = Pitching\ Moment/(\bar{q}\ S\ \bar{c}) \quad (17)$$

$$C_n = Yawing\ moment/(\bar{q}\ S\ b) \quad (18)$$

These coefficients are used to represent the rotary contributions for the development of a hybrid model. The coefficients are calculated using the measured forces and moments generated on the test model during rotary balance testing. To include thrust contributions for the stand alone rotary balance data model, the thrust terms developed by McDonnell (24) are combined with the rotary balance coefficient terms. The resulting equations are:

$$C_x = (Axial\ force + T_x)/(\bar{q}\ S) \quad (19)$$

$$C_y = (Side\ Force + T_y)/(\bar{q}\ S) \quad (20)$$

$$C_z = (Normal\ force + T_z)/(\bar{q}\ S) \quad (21)$$

$$C_l = (Rolling\ moment + T_{zr}d_{Ty} - T_{zl}d_{Ty})/(\bar{q}\ S\ b) \quad (22)$$

$$C_m = (Pitching\ moment + T_x d_{Tz} - T_z d_{Tx})/(\bar{q}\ S\ \bar{c}) \quad (23)$$

$$C_n = (Yawing\ moment + T_y d_{Tx} - T_{xr} d_{Ty} - T_{xl} d_{Ty})/(\bar{q}\ S\ b) \quad (24)$$

Equations of Motion

The development of the equations of motion for an airplane are outlined by McRuer, et al (25) which represent a conventional set of differential equations defining the dynamics of an aircraft. With the assumptions of a rigid airframe, inertial earth fixed reference, constant mass and mass distribution of the aircraft and constant gravity, the resulting equations of motion are a ninth order set of differential equations for a body fixed frame of reference. The aircraft's state of motion can be described by the nine state variables (α, β, p, q, r, θ, ϕ, ψ, V_{tr}) and the deflections of any control surfaces defining the moments and forces acting on the aircraft. Following the development by McRuer, et al (30) the following equations are formed.

Translational acceleration equations:

$$\dot{\alpha} = q + \left[-\left[\frac{\bar{q}\ S}{m V_{tr}} C_x - \frac{g}{V_{tr}} \sin\theta + r \sin\beta \right] \sin\alpha + \left[\frac{\bar{q}\ S}{m V_{tr}} C_x + \frac{g}{V_{tr}} \cos\theta \cos\phi - p \sin\beta \right] \cos\alpha \right] \sec\beta \quad (25)$$

$$\dot{\beta} = -\left[\left[\frac{\bar{q}\,S}{mV_{tr}}C_x - \frac{g}{V_{tr}}\cos\theta\right]\sin\beta + r\right]\cos\alpha + \left[\frac{\bar{q}\,S}{mV_{tr}}C_y + \frac{g}{V_{tr}}\cos\theta\sin\phi\right]\cos\beta - \left[\left[\frac{\bar{q}\,S}{mV_{tr}}C_z + \frac{g}{V_{tr}}\cos\theta\cos\phi\right]\sin\beta - p\right]\sin\alpha \tag{26}$$

$$\dot{V}_{tr} = V_{tr}\left[\left[\frac{\bar{q}\,S}{mV_{tr}}C_x - \frac{g}{V_{tr}}\sin\theta\right]\cos\alpha\cos\beta + \left[\frac{\bar{q}\,S}{mV_{tr}}C_y + \frac{g}{V_{tr}}\cos\theta\sin\phi\right]\sin\beta + \left[\frac{\bar{q}\,S}{mV_{tr}}C_x + \frac{g}{V_{tr}}\cos\theta\cos\phi\right]\sin\alpha\cos\beta\right] \tag{27}$$

Rotational acceleration equations:

$$\dot{p} = \left[-\left[\frac{I_z - I_y}{I_x} + \frac{I^2_{xz}}{I_x I_z}\right]qr + \left[1 - \frac{I_y - I_x}{I_z}\right]\frac{I_{xz}}{I_x}pq + \frac{\bar{q}\,S\,b}{I_x}\left[C_l + \frac{I_{xz}}{I_z}C_n\right]\right]\cdot\left[1 - \frac{I^2_{xz}}{I_x I_z}\right]^{-1} \tag{28}$$

$$\dot{q} = \frac{\bar{q}\, S\, \bar{c}}{I_y} C_m + \frac{I_z - I_x}{I_y} pr + \frac{I_{xz}}{I_y} (r^2 - p^2) \tag{29}$$

$$r = \left[\left[\frac{I^2_{xz}}{I_x I_z} - \frac{I_y - I_x}{I_z} \right] pq - \left[1 + \frac{I_z - I_y}{I_x} \right] \frac{I_{xz}}{I_z} qr + \frac{\bar{q}\, S\, b}{I_z} \left[\frac{I_{xz}}{I_x} C_l + C_n \right] \right] \cdot \left[1 - \frac{I^2_{xz}}{I_x I_z} \right]^{-1} \tag{30}$$

Aircraft orientation relative to the earth inertial reference frame (Euler angles):

$$\dot{\theta} = q \cos\phi - r \sin\phi \tag{31}$$

$$\dot{\phi} = p + (q \sin\phi + r \cos\phi) \tan\theta \tag{32}$$

$$\dot{\psi} = (q \sin\phi + r \cos\phi) \sec\theta \tag{33}$$

By the definition of the Euler angles, the yaw angle ψ, is decoupled from the rest of the equations of motion. For application to aircraft dynamics, the usual convention for Euler angle rotations is the sequence: yaw, pitch, roll. Because the yaw rotation does not change the gravity vector relation to the body frame z axis, the aircraft can be modeled without the $\dot{\psi}$ orientation equation resulting in an eighth order model.

A more accurate model of the dynamics of an aircraft would be to include variation in thrust due to the motion of the aircraft. As an aircraft enters high-

energy dynamic attitudes the state of the flow conditions about the air intakes of the engines change resulting in the effective thrust varying. The current model has the aircraft thrust set at a fixed setting of 8300 lbf for an altitude of 20,000 ft. The effects of variable thrust are evident in Figures (5-8) and (5-9) of reference (29) showing changes in the equilibrium solution branches and the effects are further discussed in reference (30). This inaccuracy in the current model is noted however for comparison to previous studies, this modification will not be pursued for this investigation.

Total Rotation Vector

When incorporating rotary balance data into a model it should be referenced under the same conditions upon which it was collected. During rotary balance spin tunnel testing, the model is rotated at a constant rate about an axis parallel to the free stream velocity vector of the tunnel. The test model sees a constant configuration of α, β and free stream velocity. Therefore, the rotary balance data should be referenced using the component of the total rotational rate that is along the free stream velocity vector. The total rotational rate is defined in terms of the body axes rates as

$$\bar{\Omega} = p\,\hat{b}_1 + q\,\hat{b}_2 + r\,\hat{b}_3$$
$$\text{and} \quad |\,\Omega\,| = \sqrt{p^2 + q^2 + r^2} \qquad (34)$$

For spin analysis, the total rotational vector $\bar{\Omega}$ is projected into four rotation rates, Ω_{ss} the steady state component of the rotation vector along the free stream velocity vector and p_{osc},q_{osc},r_{osc} which represent the body frame components of the residual rotational vector. Referring to Figure 4.1, these components are defined as

$$\bar{\Omega}_{rot} = (\bar{\Omega} \cdot \hat{V}_1) \hat{V}_1 = \Omega_{ss} \hat{V}_1 \tag{35}$$

$$\bar{\Omega}_{osc} = \bar{\Omega} - \bar{\Omega}_{rot} = p_{osc} \hat{b}_1 + q_{osc} \hat{b}_2 + r_{osc} \hat{b}_3 \tag{36}$$

$\bar{\Omega}_{rot}$ is the projection of the total rotation vector onto the velocity vector and represents the rotary aspects of the total rotation vector. $\bar{\Omega}_{osc}$ is the orthogonal component of the total rotation vector and is representative of the oscillatory dynamics inherent in the total rotation vector. By the process of vector projections the oscillatory components are defined as

$$p_{osc} = p - \Omega_{ss}\cos\alpha\cos\beta \tag{37}$$

$$q_{osc} = q - \Omega_{ss}\sin\beta \tag{38}$$

$$r_{osc} = r - \Omega_{ss}\sin\alpha\cos\beta \tag{39}$$

Since the rotary balance data was experimentally obtained as function of α, β and $\Omega_{ss}b/2V_{tr}$ and additionally through development of the polynomials as a

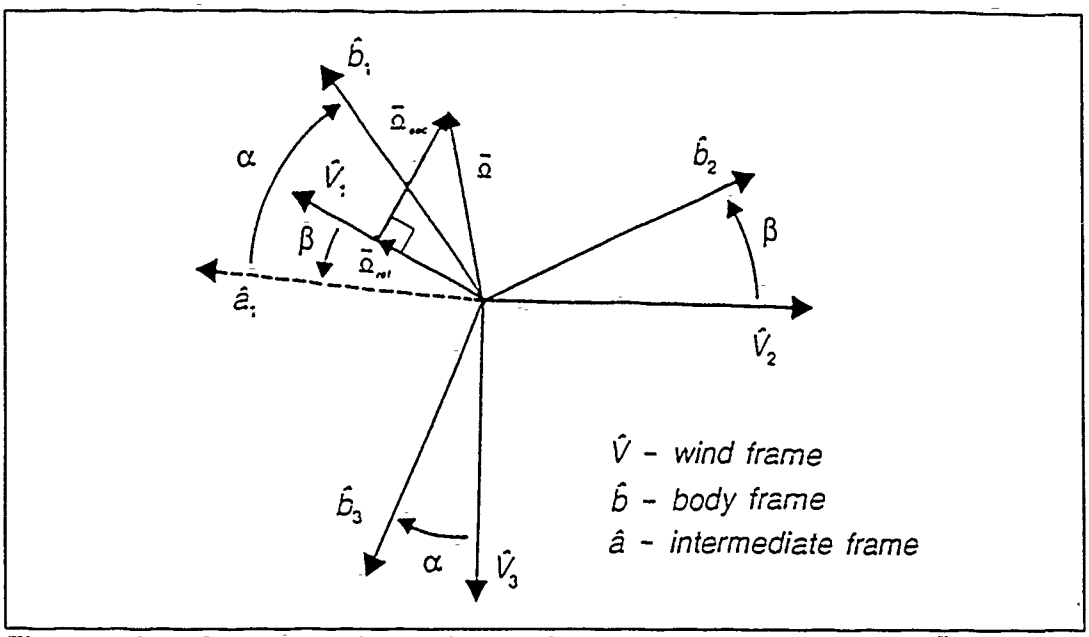

Figure 4.1 Representation of the rotation vector in the aircraft body frame and wind frame.

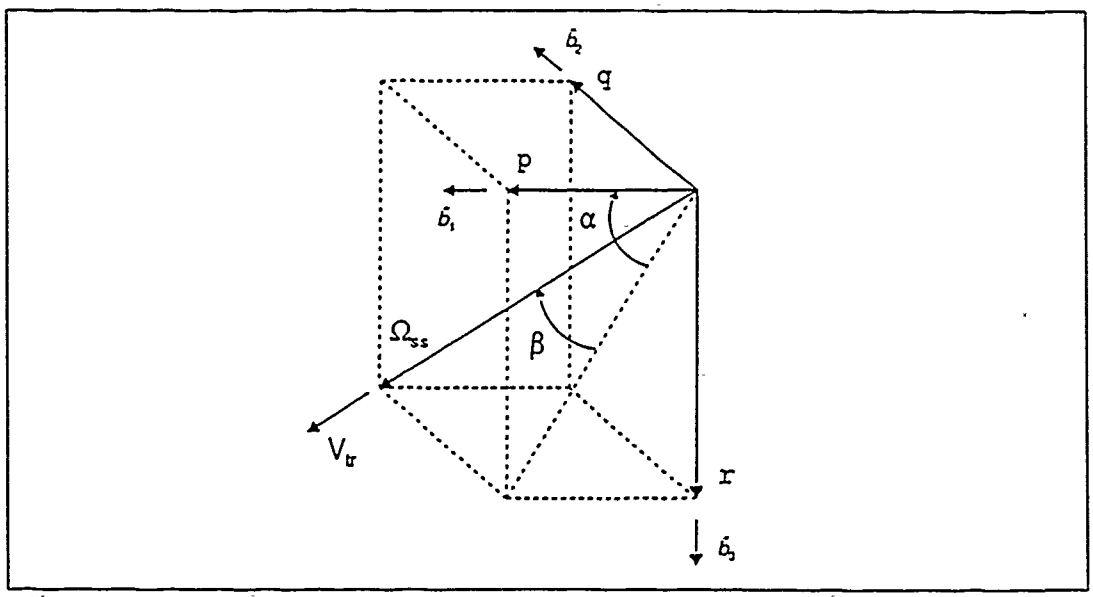

Figure 4.2 Orientation of the rotation vector when oscillatory contributions are negligible.

function of δ_a,δ_d,δ_e and δ_r, the key to the proper use of rotary aerodynamic data rely on the appropriate definition of the steady state rotation rate Ω_{ss}. Hawkins (17:184) used $\Omega_{ss} = (p\cos\alpha + r\sin\alpha)$ which restricted his analysis to zero sideslip angles or the assumption of very small perturbations in sideslip. A more robust representation is

$$\Omega_{ss} = (p\cos\alpha + r\sin\alpha)\cos\beta + q\sin\beta \qquad (40)$$

which is found from $\Omega_{ss} = \bar{\Omega} \bullet \frac{\bar{V}_{tr}}{V_{tr}}$.

It is evident that when a stand alone rotary aerodynamic model is used it is assumed that the oscillatory components of $\bar{\Omega}$ are relatively small (p_{osc},q_{osc},$r_{osc} \approx 0$) compared to Ω_{ss} ($=\Omega_{rot}$) indicating that the rotation vector is closely aligned with the free stream velocity vector (Figure (4.2)). If the orientation of the total rotation vector were grossly misaligned with the free stream velocity vector, the oscillatory terms would play a larger role in the representation of the dynamics of the aircraft. This would support the argument for the need of both forced oscillation and rotary aerodynamic data to properly represent the aircraft's motion. However, for spins which are the basis for this investigation, it is reasonable to assume the steady state rotation and free stream velocity vector are closely aligned.

Rotary Balance Model

For the stand alone rotary balance model, Eqn (40) is used to determine the aerodynamic coefficients as a function of the body rates of the aircraft, angle of attack and sideslip angle. The method of homotopy was incorporated to determine a starting equilibrium solution. A rudder sweep was performed with the McDonnell model using the equilibrium solution $(\alpha,\theta,\delta_e) = (5.0,12.02,-1.39)$ identified by Baumann (7:34). Because of the dissimilarities between the two coefficient databases, the equilibrium solution used for the homotopy application needed to be located at high angle of attack, $\alpha > 60°$ and with zero control deflections. Using the method of homotopy and the known solution from the McDonnell model the path of the equilibrium solution was transitioned to a stand alone rotary balance model using

$$C_i = \lambda C_{i,RB} + (1 - \lambda) C_{i,Mc} \tag{41}$$

where i=x,y,z,l,m and n. The $C_{i,RB}$ coefficients are representative of Eqns (19) to (24). The parameter λ was used as the control parameter in AUTO to trace the path of equilibrium solutions until λ=1 where the model was completely defined by the rotary balance coefficient data. This model will be referred to as the Rotary Balance (RB) Model.

Because of the questionable quality of the axial and side force rotary balance coefficients, a second stand alone rotary balance model was created which used

the Baumann model C_x and C_y coefficients in lieu of the associated RB coefficients. Again using the method of homotopy for the remaining four coefficients a starting equilibrium solution was determined. This model will be referred to as the Modified Rotary Balance (RB) Model. The Modified RB Model will assist in the determination of the impact to the investigation of the undesirable coefficients. The validity of combining the two databases may be of some concern due to the different testing conditions however results should provide information on the impact of a perturbed coefficient database and specifically the contributions of the axial and side force contribution to the equilibrium solution paths.

Hybrid Model

When combining the two coefficient databases it is important not to duplicate information. The rotary aerodynamic data contains static information. The forced oscillation coefficient contributions of the 1988 Aerobase contain dynamic information which is at least partially duplicated by rotary data. To eliminate the duplicate information, the rotary balance data will be biased to eliminate static contribution. The rate components p_{osc},q_{osc},and r_{osc} are used to isolate the and eliminate the duplicate rotary contributions of the 1988 Aerobase. The new coefficients are now represented by

$$C_{i,Hybrid} = C_{i,RB} - C_{i,RB\ Static} + C_{i,Mc\ non\text{-}rot} \qquad (42)$$

where i=x,y,z,l,m and n. The static rotary aerodynamic coefficients are determined for a given configuration by setting $\Omega_{ss} = 0$. The static and dynamic terms from the 1988 Aerobase coefficients with the rotary contribution eliminated are represented by

$$C_{i,Mc\ non\text{-}rot} = C_{i,Mc}(\alpha,\beta,p_{osc},q_{osc},r_{osc},\delta_e,\delta_r,\delta_a,T_l,T_r,\delta_{pv},\delta_{yv}) \tag{43}$$

Since the integrity of static configurations of the rotary aerodynamic data is questionable, a Modified Hybrid model has also been developed. The Modified Hybrid Model replaces the static contribution of the 1988 Aerobase with the static contribution inherent in the rotary balance data. This will investigate the strength and weakness of the static aspect of the rotary balance data. The Modified Hybrid Model coefficients are defined by the relation

$$C_{i,Modified\ Hybrid} = C_{i,Mc\ non\text{-}rot} - C_{i,Mc\ Static} + C_{i,RB} \tag{44}$$

where i=x,y,z,l,m, and n. The static contributions of the 1988 Aerobase, $C_{i,Mc\ Static}$, are determined for a given configuration by setting the body rates equal to zero.

Once the databases are combined, the transition from the stand alone 1988 Aerobase and the Hybrid Models across $\alpha = 30°$ needed to be smoothed. Figure 5.4 of chapter V show the large difference that could occur in coefficient values.

The high and low α databases are blended together with the relation

$$C_i = C_{i,Mc} + (C_{i,Hybrid} - C_{i,Mc})(3 - 2Blend)(Blend)^2$$

$$Where \quad Blend = \frac{\alpha - 30}{5} \tag{45}$$

for angles of attack from 30° to 35°. Due to the limitation of the rotary balance database the comparison of the models for the analysis will be limited to angles of attack above 30°. Unlike previous studies mentioned in Chapter I utilizing RB data in bifurcation analysis models, the span of angle of attack was not restricted by spin tunnel testing limitations of $\alpha > 55°$. Eqn (45) was utilized as a method of homotopy for transition from known McDonnell Model solutions in low α to the Hybrid Model equilibrium solutions in high α.

V. Results

The objective of this investigation was to determine the effectiveness of using rotary balance data for modeling of high AOA aircraft dynamics. The best indication of the capability of a model is to compare its output to experimental flight test data. For asymmetric configurations, flight tests of the F-15 showed highly oscillatory spinning motion at α=50° to 65° with yaw rates of 40 to 90 °/sec. These results can vary as much as ± 20° in AOA and ± 20 in degrees/sec in yaw rate for a given configuration. Smooth spin modes with symmetric loadings exhibited average AOAs from 65° to 75° with average yaw rates of 75 to 133°/sec. Spins of higher rates are possible. However, because of the pilot's physical limitations, flight testing does not pursue determination of the maximum spin rate capability (3:27-28). A typical full-scale aircraft flight test showed a right spin of α = 75° with a spin rate of 3 sec/turn (4:12). During spin tunnel testing, to investigate free spin modes, the scale model was allowed to rotate freely when subjected to the free stream air. The tests with pro-spin controls, recovery controls and symmetric stabilator deflection gave results comparable to the full scale flight test results (4:12). To investigate the effectiveness of RB data, bifurcation diagrams comparable to full scale flight test results were developed and then used to compare the aircraft models developed.

Utilizing equilibrium solutions acquired from the McDonnell model and methods of homotopy, control surface variations were made on each of the five models: RB,

Modified RB, Modified Hybrid, Hybrid and the McDonnell. AUTO was used to acquire equilibrium starting points for high α rudder deflections, elevator deflections and aileron deflections representative of pro-spin and recovery control configurations. To acquire specific configurations, alternating variations of different control surfaces occasionally had to be exercised to acquire equilibrium solutions on a desired solution branches in the high α regime. All bifurcation diagrams were developed with a fixed thrust level of 8300 lbf. The results of the investigation will be discussed in the order of the control surface deflections indicated with numerical and graphical results presented at the conclusion of the chapter. The bifurcation diagrams presented do not always contain all possible equilibrium branches due to the difficulty in obtaining starting equilibria for unknown solution branches.

Rudder Sweep

As an initial comparison of the rotary balance and Hybrid models a rudder sweep was performed at high AOA to determine how different the equilibrium solution paths were. During full scale flight tests it was found that a rudder roll entry technique was the easiest method to intentionally enter a spin. A rudder roll would be initiated after the aircraft was positioned above 20° AOA (3:26). Similarly it was identified by Baumann (6:47) and McDonnell (24:30), an effective method for obtaining an initial high AOA attitude was through an elevator deflection

followed by a rudder sweep (i.e. continuation) to obtain high AOA spin conditions. To further investigate the development of the equilibrium solutions, rudder continuations were made at elevator deflections of -5°, -19° and -25°. The equilibrium solution paths of the rudder continuations are shown in Figure 5.1 for the five models.

Comparison of the RB Model and Modified RB Model (Figure 5.1a,b) show minor changes due to variation in the axial and side force coefficients. The RB model is exhibiting an expanding center phenomenon in the range of α = 30° to 40°. Cause of such behavior has not been determined however it may be reflective of the polynomial behavior inherent in the RB coefficient model.

The Hybrid model (Figure 5.1c) shows similarity to the McDonnell Model (Figure 5.1e) in the upper branch for $\alpha \approx 85°$ with rudder deflections from -20° to 10°. Otherwise the results are rather different. The Modified Hybrid Model (Figure 5.1d) shows indication that the static contributions of the 1988 Aerobase are a major contributor to the character of the equilibrium solutions. The Modified Hybrid Model with RB static contributions shows results closer to the isola of the RB Model as well as the upper branch. Examining the development of the solution paths of the Hybrid model shows a closed path for δ_e=-5° indicating possible formation of an isola center. This is indicative of the RB model however the event is occurring across high α.

Full scale flight test results showed rudder deflection, either pro-spin or anti-spin had no apparent effect on spin recovery (3:28). Comparing the behavior of the

solution branches to full scale flight tests shows the RB model (Figure 5.1a) having the best correlation. The ineffectiveness of rudder in a pro-spin configuration at high AOA with elevator stick aft is reflected in the RB Model results with a continuous branch for full $\pm \delta_r$ with no bifurcation branches to lower AOA. The RB model indicates large jumps in state would need to occur for transition to the solution branches in lower α. The McDonnell model (Figure 5.1e) exhibits effective rudder deflection spin recovery solution paths from high to low α. Small jumps in states could occur as the aircraft states transition between continuation branches. McDonnell investigated the effectiveness of rudder in his model for spin recovery. He found the rudder effectiveness was caused by the curve fitting of the stability derivative $C_{n\delta r}$ resulting in twice the effectiveness of the rudder at larger negative values of δ_e. He made the conclusion that the model was somewhat inaccurate in the effects of rudder at high AOA (29:39). This could explain the many differences found in Figure 5.1.

The blending of the rotary balance data with the McDonnell model in the Hybrid model may not be indicative of the capabilities of the Hybrid model because of the identified problem with the McDonnell/Baumann coefficient database. However, it would be expected for the Hybrid model to exhibit behavior that lie between the two contributing parts. Figure 5.1(c) is exhibiting unique behavior especially along the high α right spin branch. There may be a detached branch that was not acquired that accounts for the solutions above 70° AOA.

Elevator Sweep

The rudder deflection parameter sweeps with fixed elevator and aileron deflections represented asymmetric configurations. A second set of bifurcation diagrams were developed for comparison of a symmetric configuration. Aileron and rudder were held fixed at zero deflection while the elevator was varied from -25° to 25°. Even though the RB coefficient data was not defined for elevator deflections greater than zero, it was felt the symmetry of the configuration could support meaningful results above $\delta_e = 0°$.

Again comparison of the results from the Modified RB model (Figure 5.2b) exhibited minor variation in state variables and equilibrium solutions of the RB model (Figure 5.2a). It was found for each configuration analyzed during this investigation the Modified RB Model exhibited minor variations in state variables and equilibrium solution branches. The results indicated that perturbations in axial and side force coefficients had a minor impact on the equilibrium solutions.

Again the results of the RB model (Figure 5.2a) and McDonnell model (Figure 5.2e) are very different. They both have a branch of right flat spin modes across high α but the RB model exhibits very linear behavior. The RB model was also unable to identify stable solutions. Mehra and Carroll (26:76) found it was usually not possible to obtain flat spin equilibria when only static and forced oscillation data are used. The Baumann and McDonnell model were able to identify flat spin equilibria leading one to believe that the blended flight test data may have been

a major contributor to the character of the equilibrium solutions. The stable regions identified by the McDonnell model are small however. The results of the RB model follow the findings of Mehra and Carroll for no stable equilibria. The RB model did exhibit unstable branches in similar location of the periodic wing rock behavior of the McDonnell model however at a much higher α and non-periodic.

Figures 5.2c and 5.2e show the Hybrid model is very similar in appearance to the McDonnell model. The Hybrid model result shows a more drastic hysteresis with jump phenomena very likely for positive and negative elevator deflections in the range 8° to 15°. Considering the concept of expanding centers, the Hybrid solution appears to be at a different stage of development compared to the McDonnell model. Again another parameter influence appears evident to reflect the stages of isola development between models. Between $\delta_e = \pm 5°$ the α - δ_e bifurcation diagrams appear approximately the same. Table IV compares the aircraft states for $\delta_e = 0°$ to determine how different the models are. The Hybrid Model is indicating slower rates resulting in a much slower spin. To investigate the possible cause of the differences of the models, the force and moment coefficients and states of the aircraft in the region $-25° < \delta_e < -5°$ on the high α branch of Figure 5.2 were examined.

Figure 5.3 shows the comparison of each of the remaining seven states. In each diagram the states have similar behavior in each model until the turning point at $\delta_e = -15°$; i.e. the Hybrid and McDonnell branches have similar states for $\delta_e > -15°$, until the turning point on the Hybrid model at $\delta_e = -15°$ after which the

Table IV Comparison of right spin states of the Hybrid and McDonnell model at high AOA with $\delta_a=0^\circ, \delta_d=0^\circ, \delta_e=0^\circ$ and $\delta_r=0^\circ$.

	Hybrid Model	McDonnell Model
α	66.35°	64.29°
β	-11.48°	-6.71°
p	0.4728 rad/sec	0.7629 rad/sec
q	-0.1261 rad/sec	-0.0901 rad/sec
r	1.072 rad/sec	1.593 rad/sec
θ	-23.65°	-25.56°
ϕ	-6.71°	-3.236°
V_{tr}	238 ft/sec	238 ft/sec
Spin Rate	6.36 sec/turn	3.56 sec/turn

model's exhibit quite different behavior.

As discussed in Chapter III, a jump event could occur within the hysteresis. The jumps in states would be evident of abrupt changes in the aircraft attitude and rates. If the Hybrid model were a prediction of actual F-15B flight behavior, the aircraft would experience sudden changes in attitude if the elevator were held between a -8° and -15° elevator deflection during a spin.

The examination of the states has given additional views of the differences between the models however the coefficients are now examined to assist in identifying the cause of the difference. Figure 5.4 are plots of the three force and three moment coefficients values as the elevator is swept between -5° and -25°. It should be noted that the coefficients for each model were determined following the locus of equilibrium states from Figure 5.3. The hysteresis event is very evident in each of the coefficients. With such strong differences in coefficient

values it would be expected to have very different equilibrium solutions. The bifurcation diagrams of Figures 5.2(c) and (e) may have visual similarity, but the underlying state of the aircraft dynamics does not.

It would be best to compare the coefficients at a single set of state values. The force and moment coefficients were determined for a fixed aircraft state with varied elevator deflections of -5° to -25°. The fixed state chosen was the flat right spin exhibited by the McDonnell model along the upper branch of Figure 5.2e at an elevator deflection of -15°. The aircraft state is exhibited in Table V.

Table V Representative aircraft state for comparison of the Hybrid and McDonnell model coefficient behavior.

α	β	p	q	r	θ	ϕ	V_{tr}
68	-5.44	0.69	-0.079	1.714	-21.92	-2.65	236.5

It should be noted that for bifurcation analysis the diagrams are traces of the equilibrium solutions of the system. The state in Table V from the McDonnell model is only an equilibrium solution for that model and does not represent an equilibrium solution for the Hybrid model. Therefore it should not be compared relative to the behavior exhibited in Figures 5.2 and 5.3.

Figure 5.5 shows the comparison of the coefficients for the aircraft state defined in Table V. Except for the axial force coefficient (Figure 5.5a) , which is practically the same, all the coefficients appear to be offset by a "static" bias. There are

slight changes in slope along some of the coefficients however the bias is the most predominate effect. It is most probable that the questioned static aspects of the modeled rotary balance data has introduced an error bias in the Hybrid coefficients. The Modified Hybrid model (Figure 5.2d) shows very different behavior when the static contributions are representative of only the rotary balance data. The dramatic change in the equilibrium surface is most likely caused by the erroneous static data. If there are errors in the static data, as it is either added or subtracted from a model it may be removing essential information leaving noise vice relevant information.

Table VI is a comparison of each of the five models to the spin tunnel spin mode predictions and the full scale flight test spin mode of 75° AOA and 3 sec/spin rate all at common control settings. Comparing the Hybrid model to the spin tunnel predictions, the inclusion of RB data has not modeled the aircraft states better than the McDonnell model. The Hybrid model results did not lie between the RB and McDonnell model as would be expected. There appears to be an additional factor influencing its results. The RB, Modified RB and Modified Hybrid models showed very good correlation to full scale flight test results and the spin tunnel predictions.

Aileron Sweep

Various sweeps of different control surfaces were performed with AUTO to set

up the conditions for the spin modes identified in Tables VII and VIII. Once a solution for a specific configuration was acquired, an aileron continuation was made. By fixing all controls except aileron, the aircraft behavior was examined as aileron was deflected through the desired pro-spin or spin recovery configuration. Only right spins were identified.

Pro-spin controls are acquired by obtaining full cross-controlled lateral-directional inputs (i.e full positive aileron and full negative rudder) during an abrupt full negative elevator deflection (full aft stick position). Immediately after high α attitude is obtained, the elevator is returned to a neutral position as the aircraft settles into the spin (3:27). Analogous, using AUTO, alternating rudder and elevator sweeps were made to acquire high α solutions and then an aileron sweep was made to acquire a cross-control configuration. A final elevator sweep was made to obtain a neutral elevator deflection. Using the resulting equilibrium solution an aileron continuation was performed resulting in Figure 5.6.

Full scale flight tests showed satisfactory spin recovery can be accomplished with near full aileron/differential stabilator deflection into the spin direction (3:28). For recovery from the right spin identified in Figure 5.6, full negative aileron/differential elevator deflection was made. Since rudder deflection has already been determined earlier to be ineffective for spin recovery, its position is not critical. Figure 5.6 also showed recovery control effectiveness as the aileron was deflected into the right spin direction (negative deflection). Figure 5.7 was similarly developed for comparison of the specific data in Table VIII.

The RB model showed good correlation to the spin tunnel predictions and full scale flight test predictions for the behavior in a pro-spin and recovery control configuration. The conditions identified in Table VII are for pro-spin controls. The RB model (Figure 5.6a) identifies the equilibrium solution along a near horizontal branch showing no immediate spin recovery to lower α with moderate perturbations about $\delta_a = 20°$. The conditions in Table VIII are for recovery controls. The RB model (Figure 5.7a) identifies the equilibrium solution along a vertical branch indicating spin recovery to lower α, i.e. recovery will occur as δ_a decreases towards -20°.

Comparing the RB model between Figures 5.6 and 5.7 does provide evidence of some effects of rudder on recovery controls. Figure 5.6 with negative rudder deflection shows recovery with less aileron deflection positioned into the spin direction than with full positive rudder deflection as shown in Figure 5.7.

In contrast to the RB model results, the McDonnell model (Figures 5.6e and 5.7e) did not exhibit pro-spin nor recovery solutions for the same configurations. McDonnell noted the ineffectiveness of aileron deflection for spin recovery in his model however did not pursue investigating its cause other than noting it was a cause of the spin characteristics of the aircraft and not a problem with the model (24:40).

Discussion

The states extracted for a specific aircraft configuration presented in Tables VI,VII and VIII may be deceiving as to the similarity between models. The discrete examples present similar results however the qualitative structure of the bifurcation diagrams indicate very different behavior.

Considering that nearly all solutions obtained were unstable, it was difficult to justify that a particular behavior may occur. Unfortunately, with the gross differences between models, it was hard to draw any conclusions to the "influence" of rotary balance data. Conclusions could be drawn however to what information it could and could not provide when examined by itself. It was identified by the results of the Hybrid and Modified Hybrid model that the static rotary balance data contributions had a major influence on the proper blending rotary aerodynamic information into the Hybrid model. If large errors were evident in the static data they could cause meaningful rotary information to be "erroneously removed" leaving noise perturbations. This may account for the seemingly independent character of the Hybrid model with the exception of elevator deflection bifurcation diagrams. The rotary balance data apparently has less sensitivity to the elevator control surface than the McDonnell model. The model conflicts that occurred as rudder and aileron deflections were made provided additional difficulty for the Hybrid model to provide meaningful information.

Table VI Clockwise spin state. $\delta_a=0^\circ, \delta_d=0^\circ, \delta_e=-25^\circ, \delta_r=0^\circ$

	α (deg)	Spin Rate (sec/turn)	$\Omega_{ss}b/2V_{tr}$	Ω_{ss} (rad/sec)	V_{tr} (ft/sec)
RB Model	75.3	3.2	0.16	1.973	260
Modified RB Model	75.4	3.2	0.16	1.972	261
Hybrid	84.9	1.7	0.30	3.657	257
Modified Hybrid	76.5	5.1	0.11	1.220	245
McDonnell/ Baumann	82.2	2.1	0.29	3.013	226
Spin Tunnel Predict	65.0	5.1	0.10	1.271	272
Flight Tests	75.0	3.0	----	2.0	---

Table VII Pro-spin controls model comparisons. $\delta_a=20^\circ, \delta_d=6^\circ, \delta_e=0^\circ, \delta_r=-15^\circ$

	α (deg)	Spin Rate (sec/turn)	$\Omega_{ss}b/2V_{tr}$	Ω_{ss} (rad/sec)	V_{tr} (ft/sec)
RB Model	84.4	1.98	0.25	3.177	263
Modified RB Model	83.6	2.04	0.26	3.080	255
Hybrid	63.2	5.28	0.11	1.189	236
Modified Hybrid	85.9	1.31	0.34	4.794	301
McDonnell/ Baumann	60.3	3.79	0.15	1.658	241
Spin Tunnel Predict	80.0	2.70	0.21	2.390	244
Flight Tests	70-85	2-6	---	1-3	---

Table VIII Recovery controls model comparisons.
δ_a=-20°, δ_d=-6°, δ_e=0°, δ_r=30°

	α (deg)	Spin Rate (sec/turn)	$\Omega_{ss}b/2V_{tr}$	Ω_{ss} (rad/sec)	V_{tr} (ft/sec)
RB Model	62.2	4.60	0.12	1.363	250
Modified RB Model	62.2	4.78	0.11	1.313	257
Hybrid	66.0	5.17	0.11	1.2158	244
Modified Hybrid	52.1	7.02	0.08	0.895	252
McDonnell/ Baumann	64.8	3.50	0.16	1.790	240
Spin Tunnel Predict	56.0	6.10	0.08	1.039	278
Flight Tests	50-65	4-6	----	0.7-1.6	---

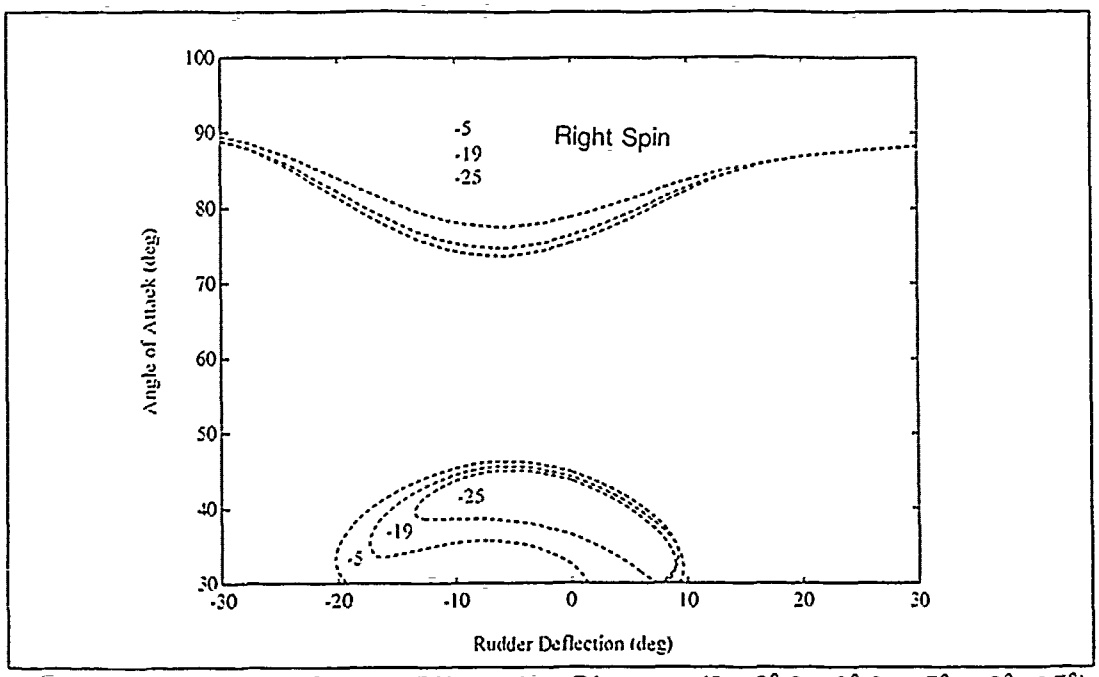

Figure 5.1 Rudder Sweep Bifurcation Diagram (δ_a=0°,δ_d=0°,δ_e=-5°,-19°,-25°) (a) Rotary Balance Model.

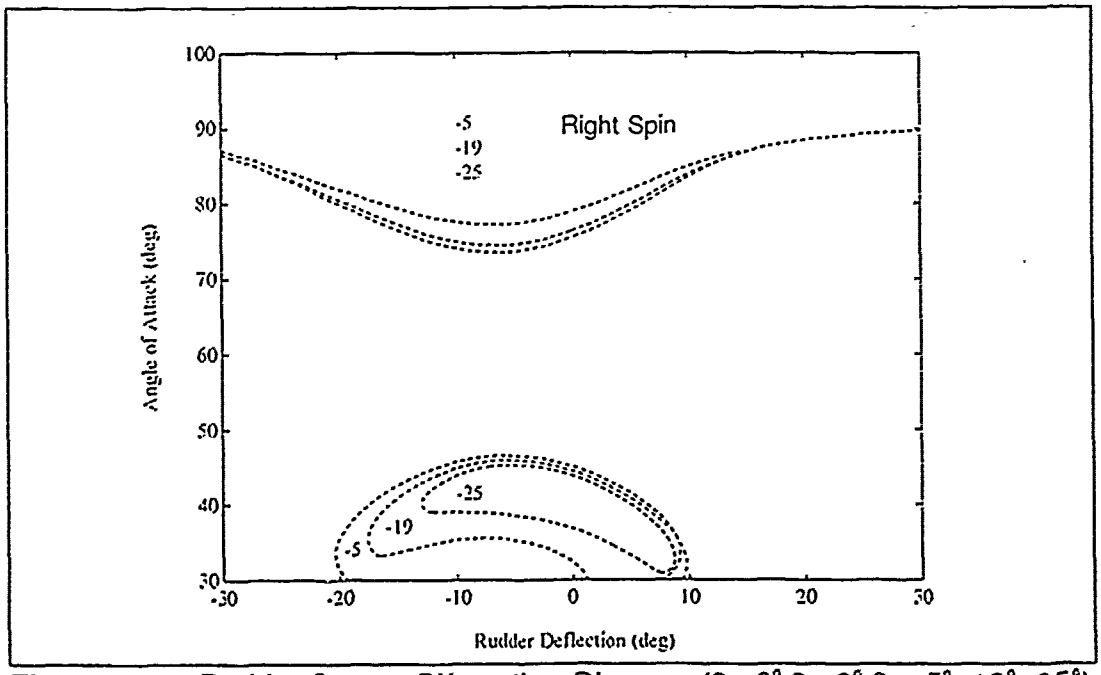

Figure 5.1 Rudder Sweep Bifurcation Diagram (δ_a=0°,δ_d=0°,δ_e=-5°,-19°,-25°) (b) Modified Rotary Balance Model.

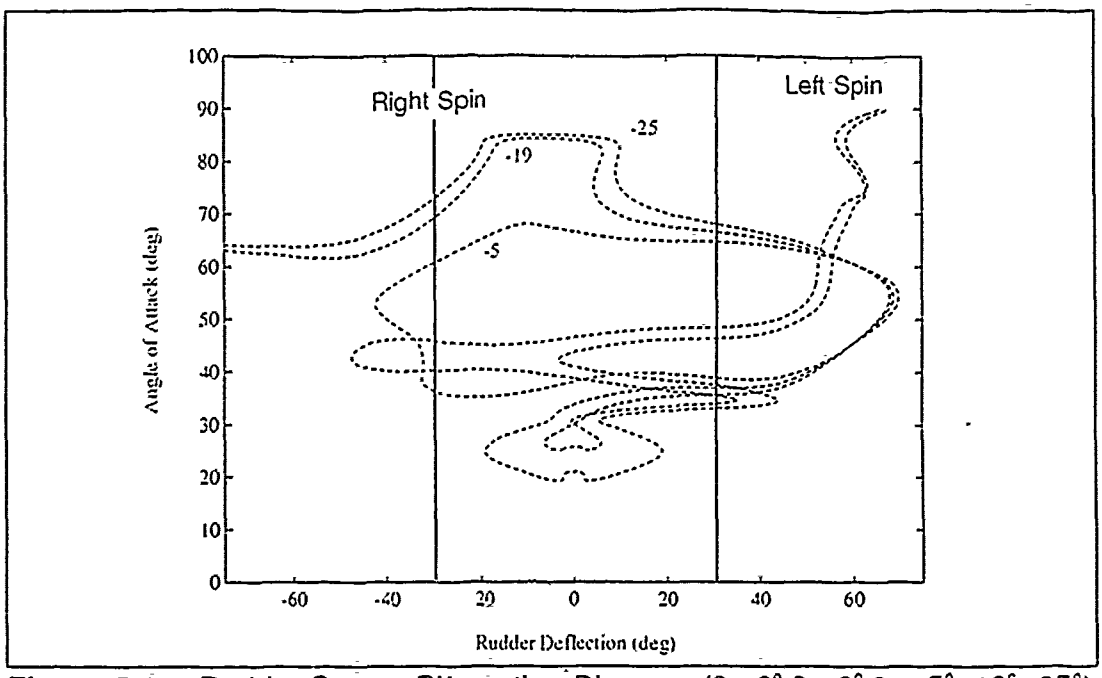

Figure 5.1 Rudder Sweep Bifurcation Diagram (δ_a=0°,δ_d=0°,δ_e=-5°,-19°,-25°) (c) Hybrid Model.

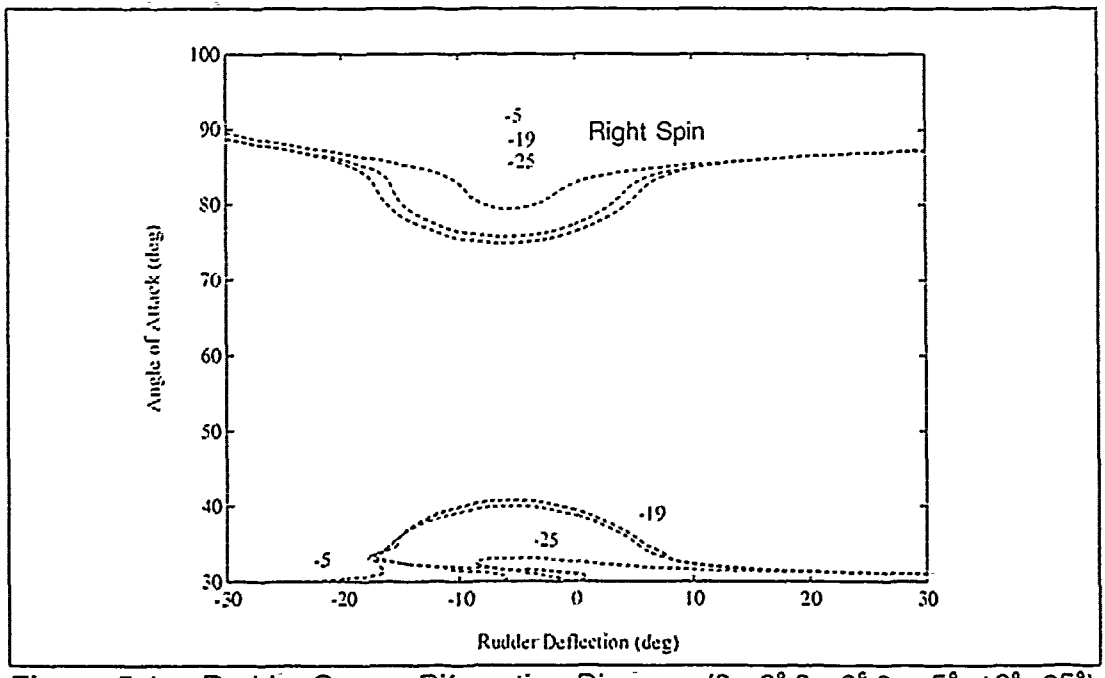

Figure 5.1 Rudder Sweep Bifurcation Diagram (δ_a=0°,δ_d=0°,δ_e=-5°,-19°,-25°) (d) Modified Hybrid Model.

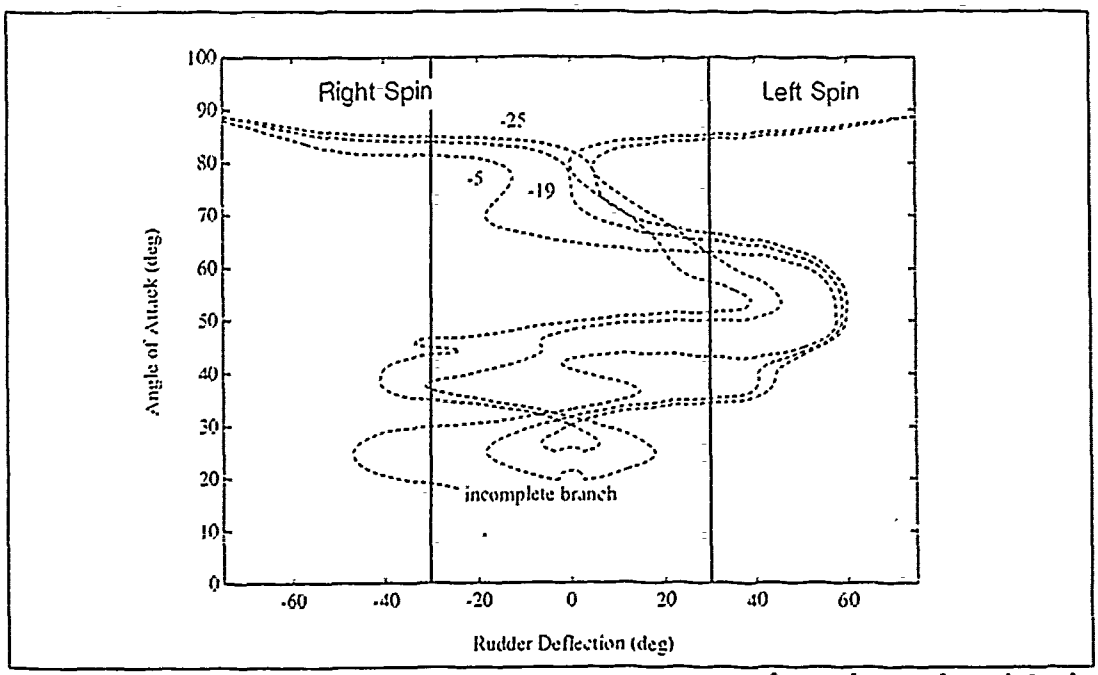

Figure 5.1 Rudder Sweep Bifurcation Diagram (δ_a=0°,δ_d=0°,δ_e=-5°,-19°,-25°) (e) McDonnell Model.

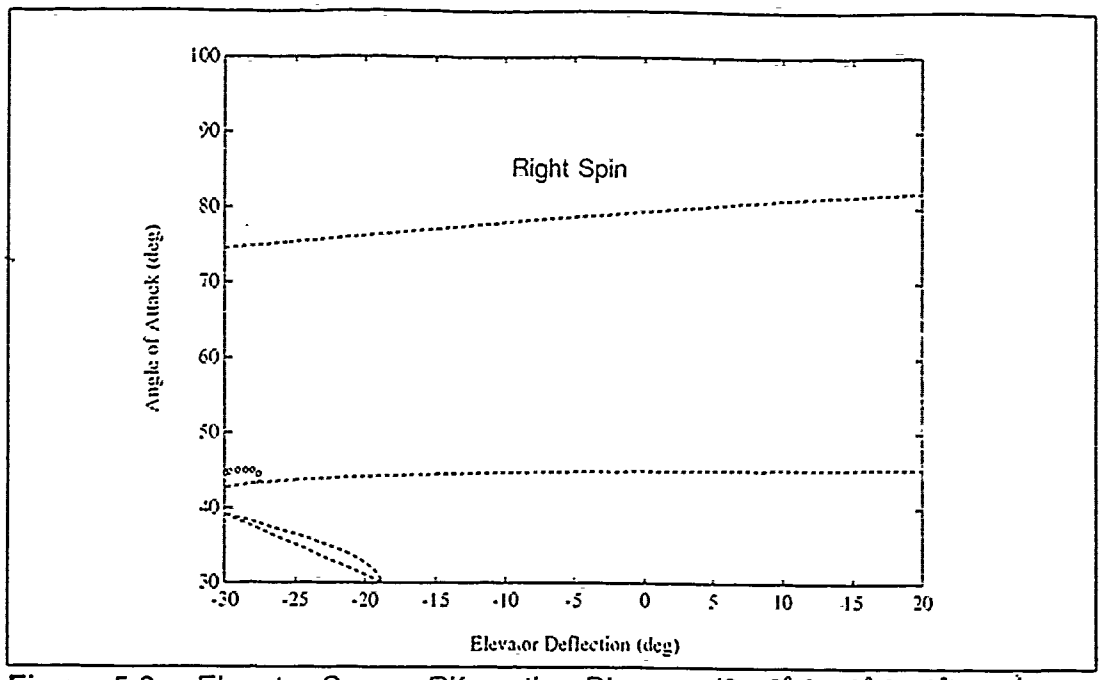

Figure 5.2 Elevator Sweep Bifurcation Diagram (δ_a=0°,δ_c=0°,δ_r=0°)
(a) Rotary Balance Model.

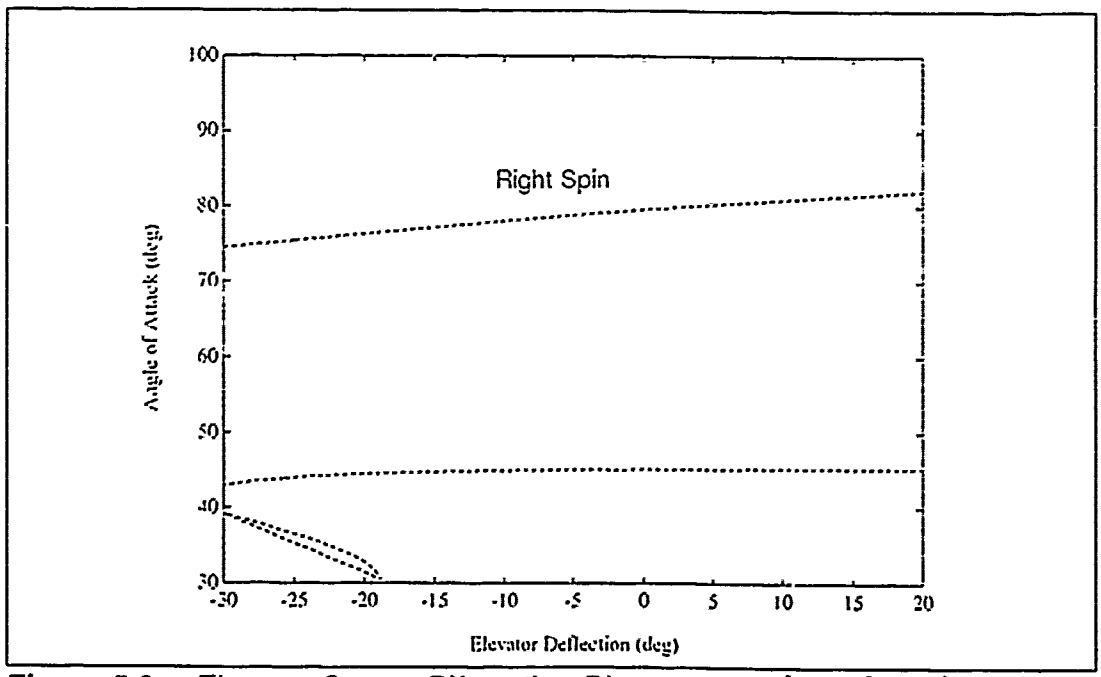

Figure 5.2 Elevator Sweep Bifurcation Diagram (δ_a=0°,δ_c=0°,δ_r=0°)
(b) Modified Rotary Balance Model.

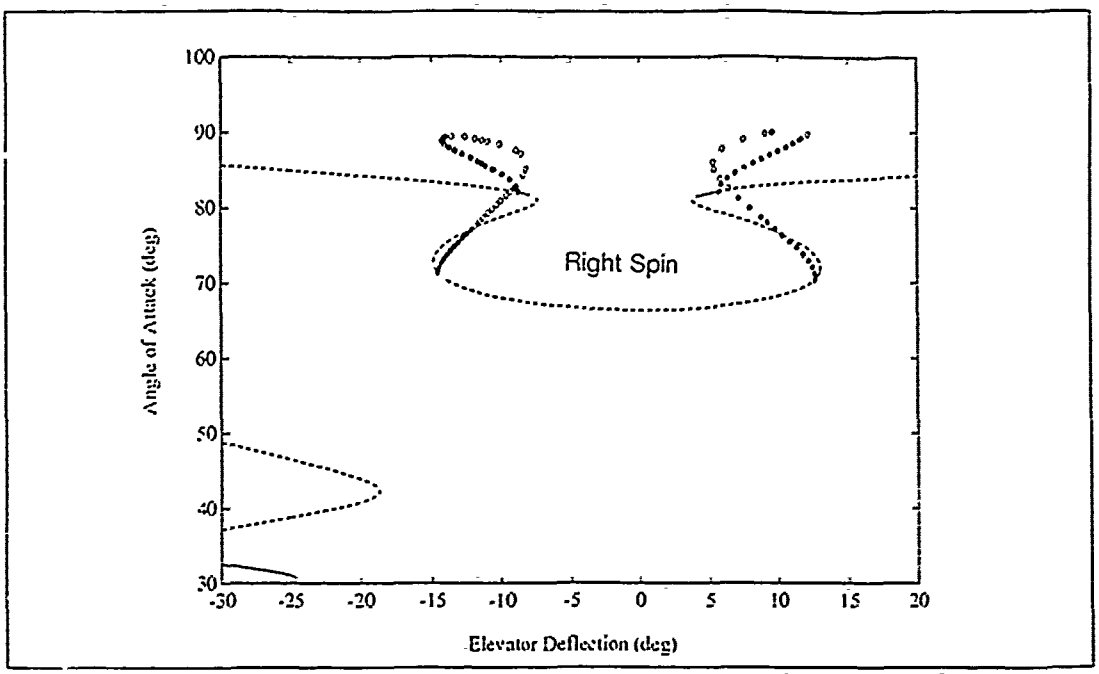

Figure 5.2 Elevator Sweep Bifurcation Diagram (δ_a=0°,δ_e=0°,δ_r=0°)
(c) Hybrid Balance Model.

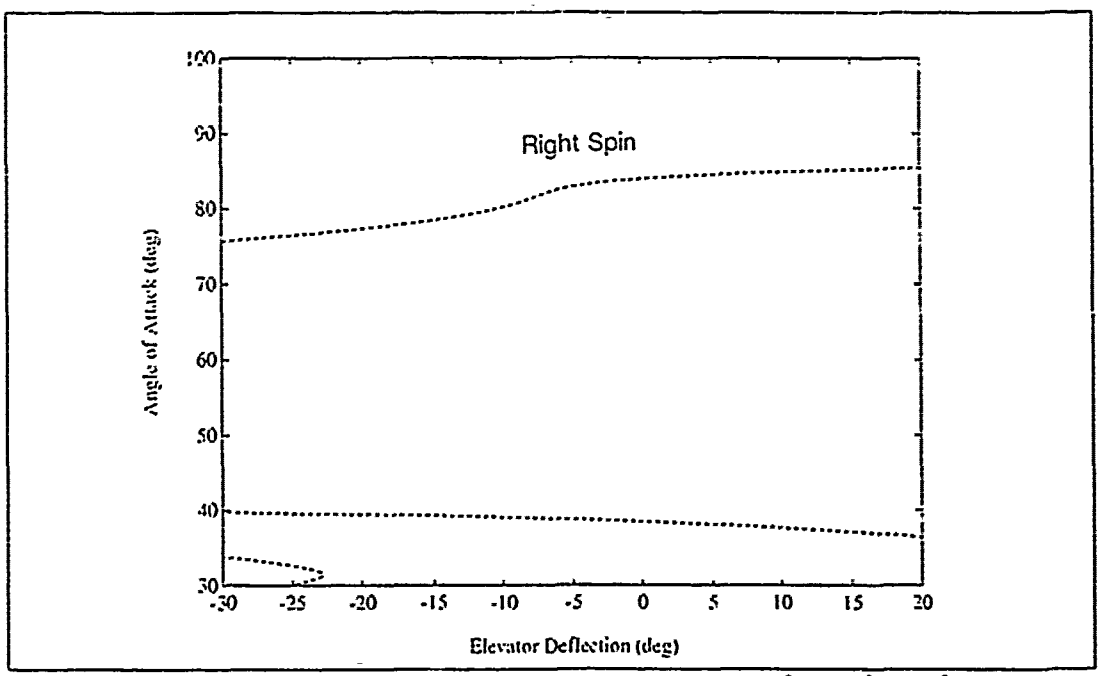

Figure 5.2 Elevator Sweep Bifurcation Diagram (δ_a=0°,δ_e=0°,δ_r=0°)
(d) Modified Hybrid Model.

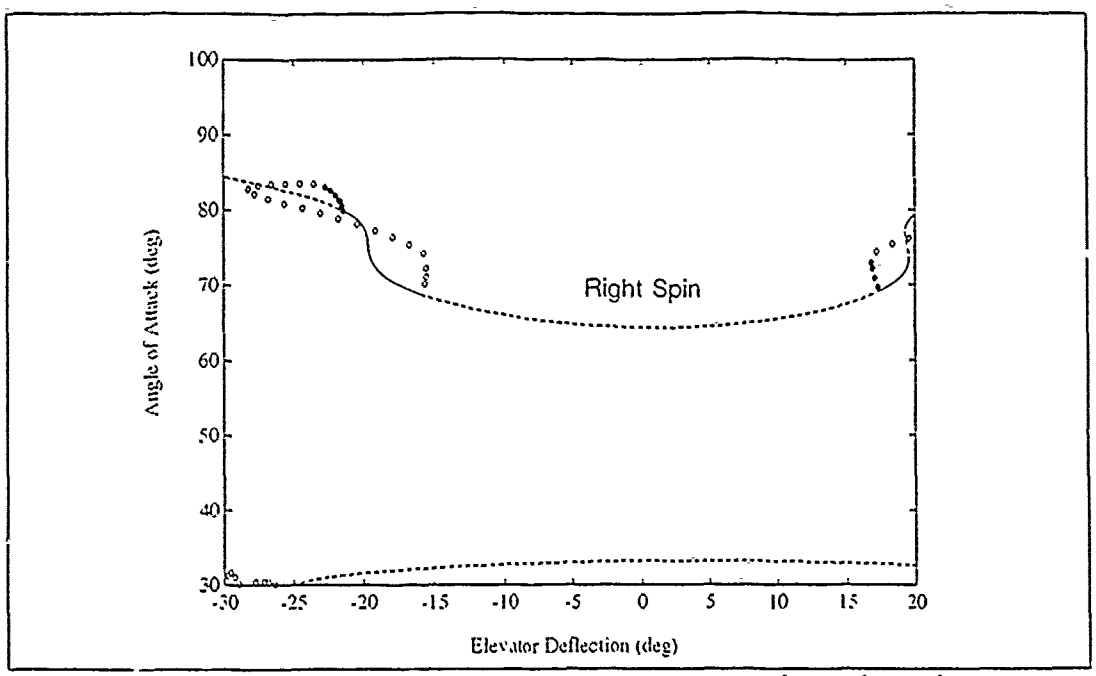

Figure 5.2 Elevator Sweep Bifurcation Diagram (δ_a=0°,δ_e=0°,δ_r=0°) (e) McDonnell Model.

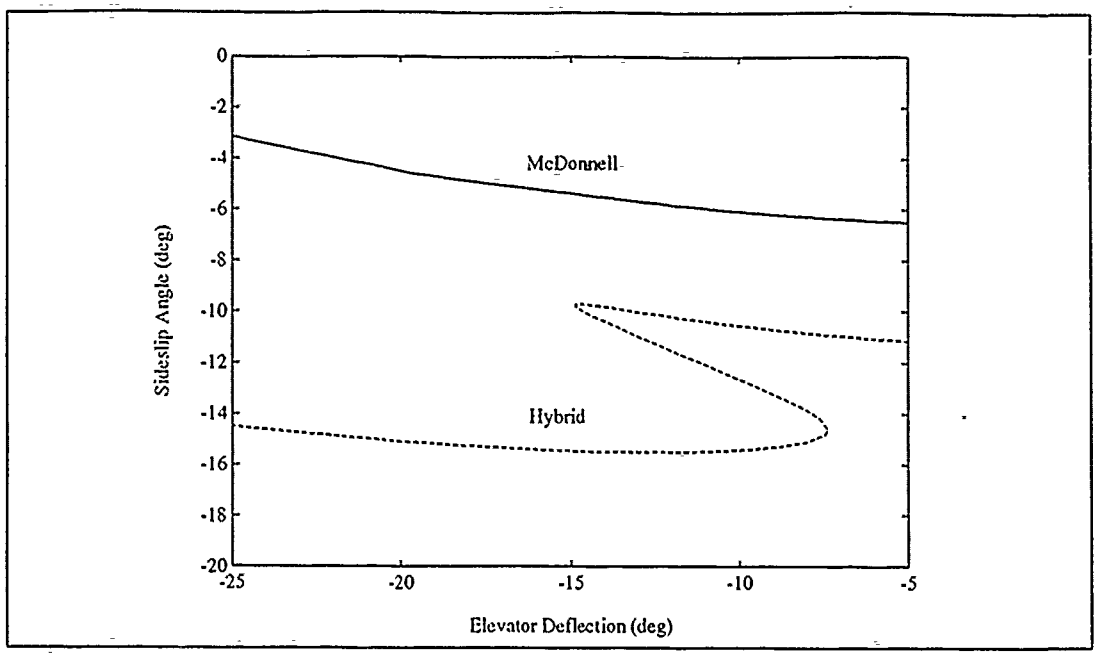

Figure 5.3 Comparison of Hybrid and McDonnell Model Aircraft States as δ_e is Varied (δ_a=0°,δ_d=0°,δ_f=0°). (a) Sideslip, β.

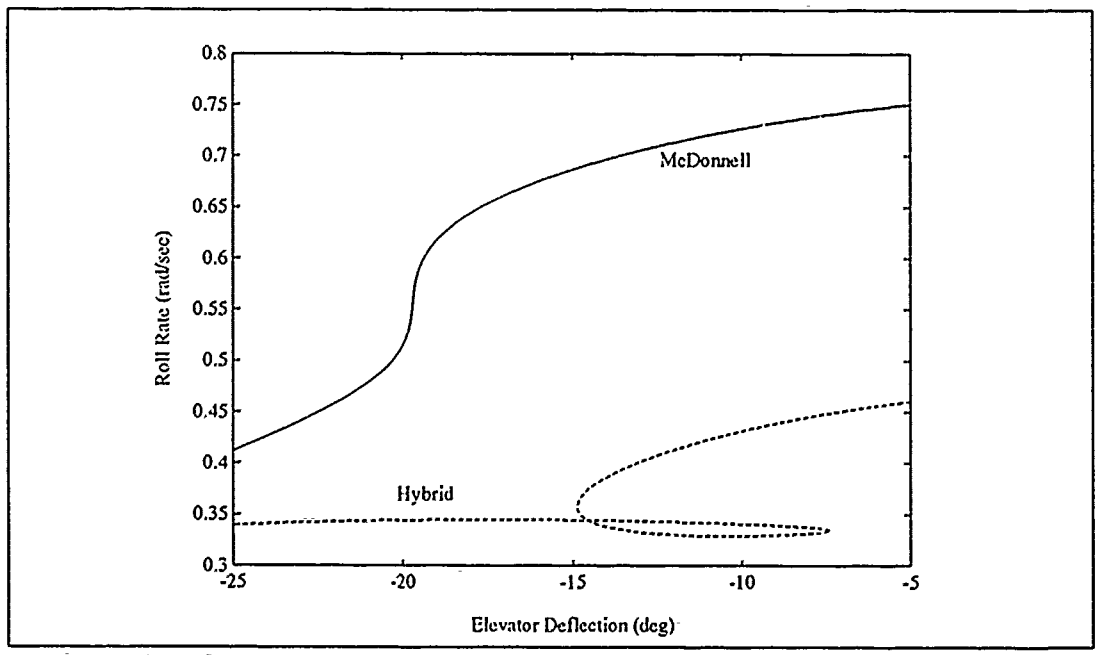

Figure 5.3 Comparison of Hybrid and McDonnell Model Aircraft States as δ_e is Varied (δ_a=0°,δ_d=0°,δ_f=0°). (b) Roll Rate, p.

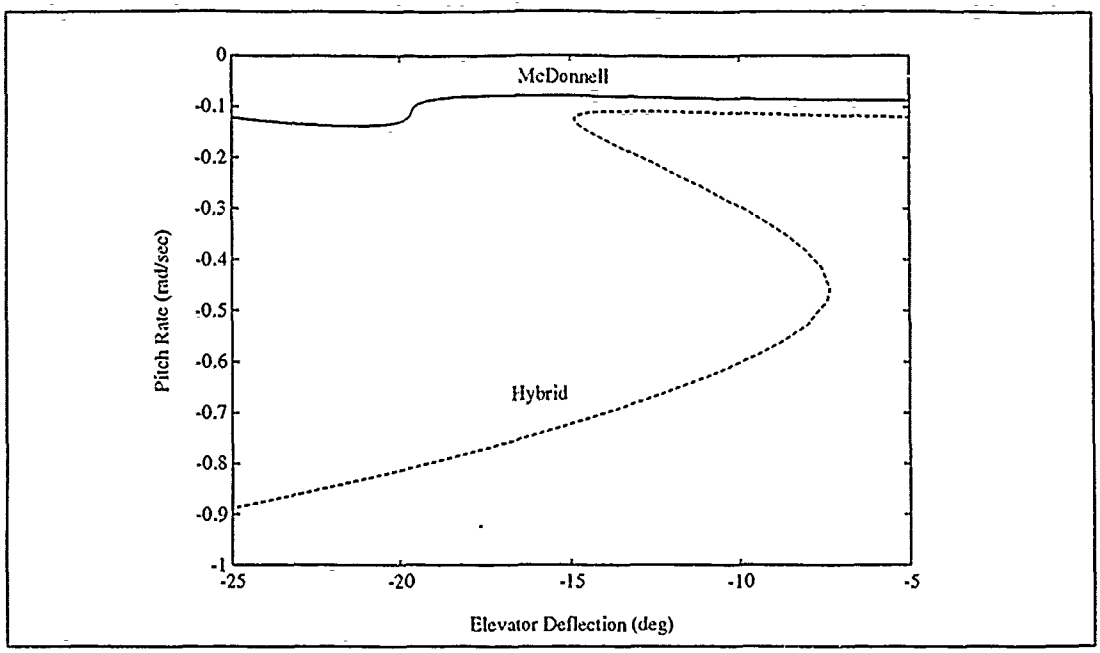

Figure 5.3 Comparison of Hybrid and McDonnell Model Aircraft States as δ_e is Varied (δ_a=0°,δ_d=0°,δ_r=0°). (c) Pitch Rate, q.

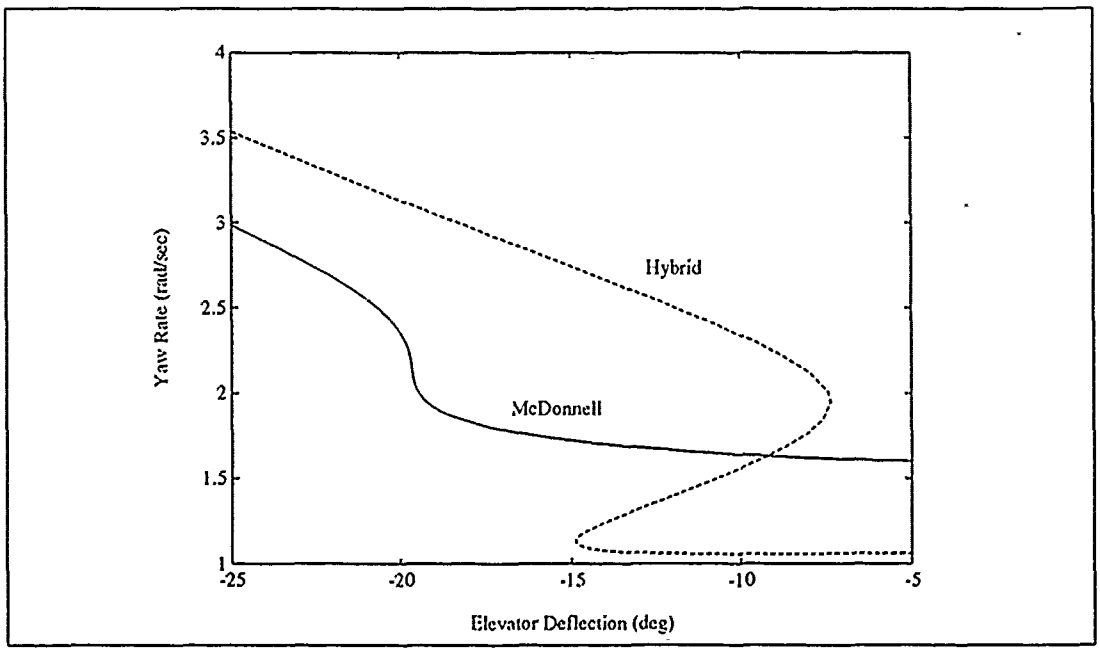

Figure 5.3 Comparison of Hybrid and McDonnell Model Aircraft States as δ_e is Varied (δ_a=0°,δ_d=0°,δ_r=0°). (d) Yaw Rate, r.

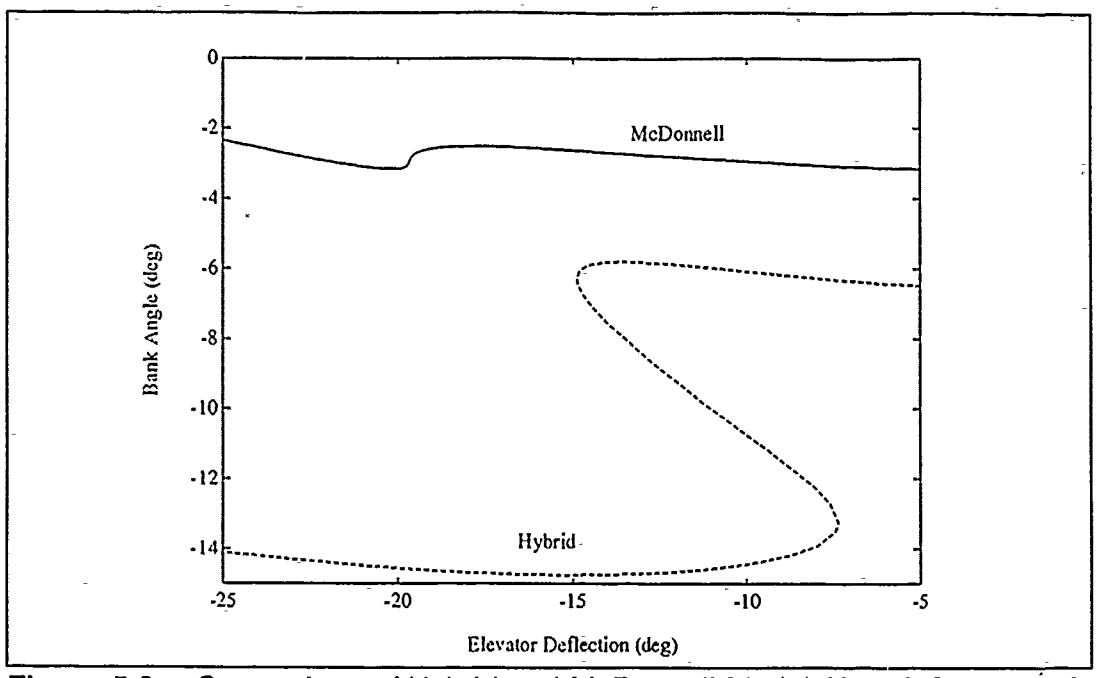

Figure 5.3 Comparison of Hybrid and McDonnell Model Aircraft States as δ_e is Varied (δ_a=0°,δ_d=0°,δ_r=0°). (e) Bank Angle, ϕ.

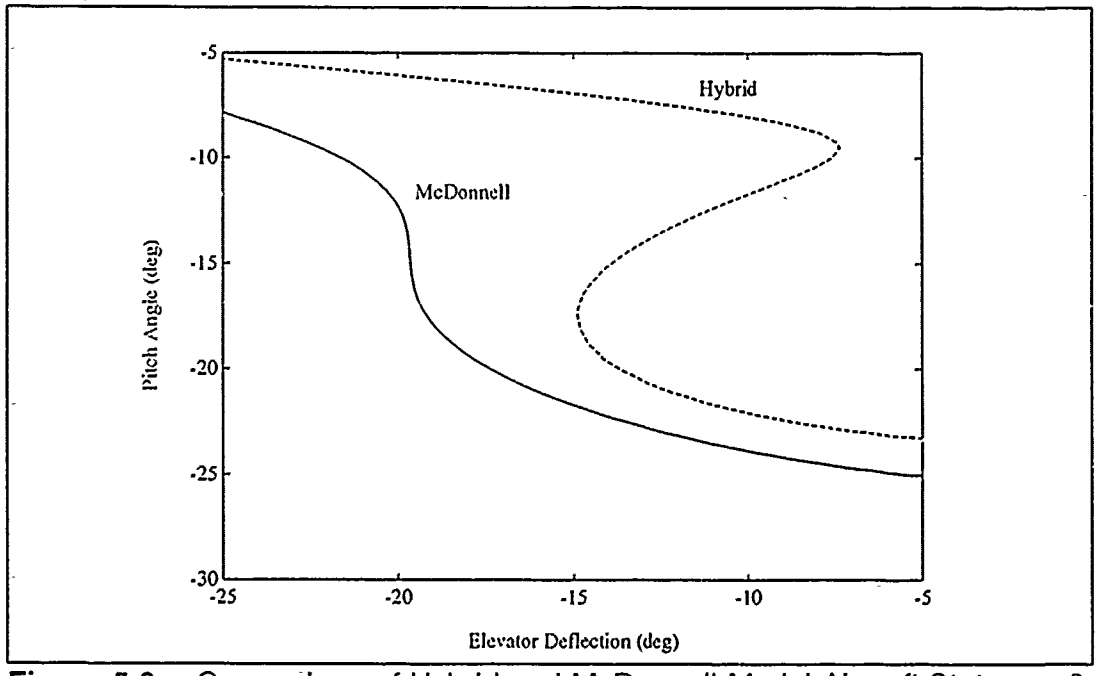

Figure 5.3 Comparison of Hybrid and McDonnell Model Aircraft States as δ_e is Varied (δ_a=0°,δ_d=0°,δ_r=0°). (f) Pitch Angle, θ.

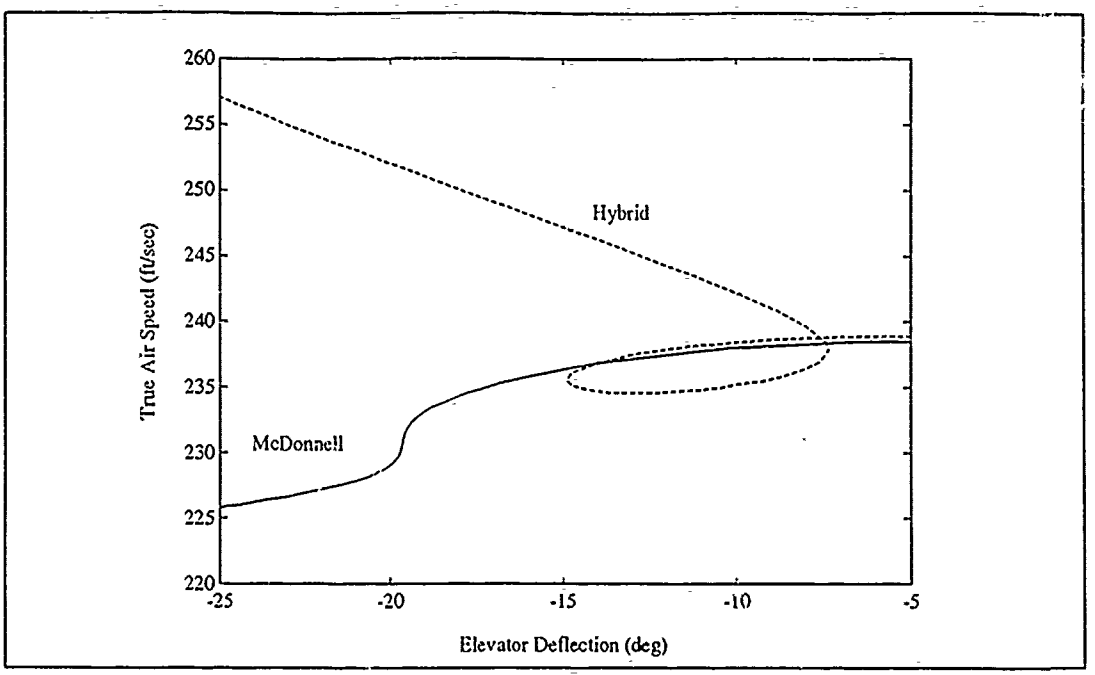

Figure 5.3 Comparison of Hybrid and McDonnell Model Aircraft States as δ_e is Varied (δ_a=0°,δ_d=0°,δ_r=0°). (g) True Velocity, V_{tr}.

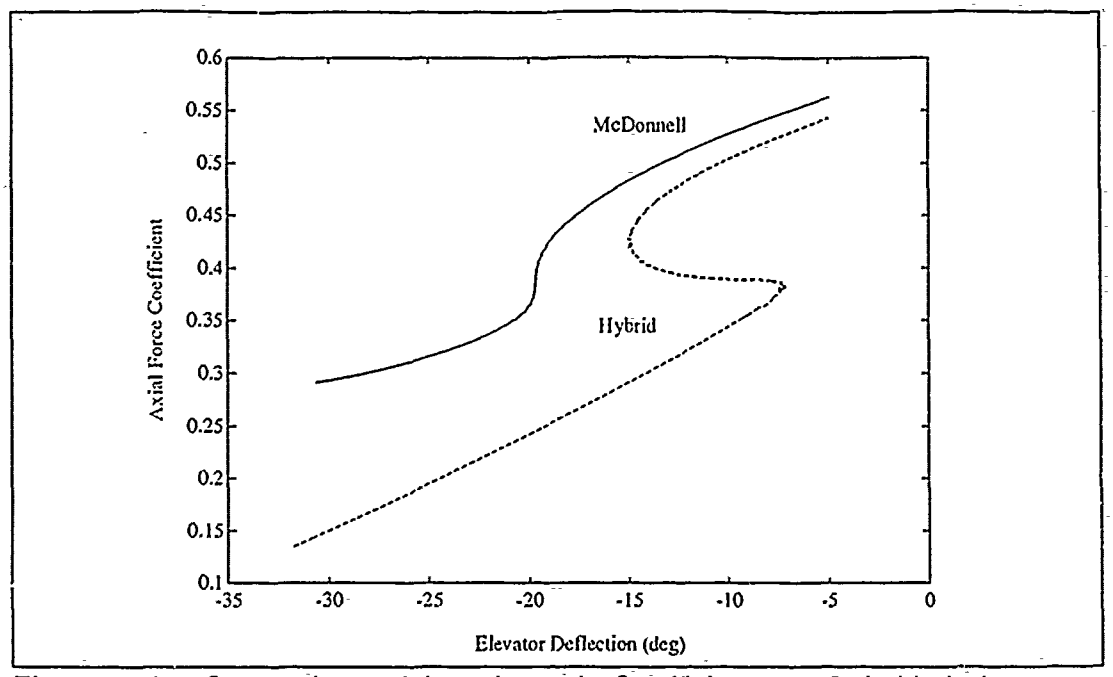

Figure 5.4 Comparison of Aerodynamic Coefficients as δ_e is Varied (δ_a=0°,δ_d=0°,δ_r=0°). (a) Axial Force C_x.

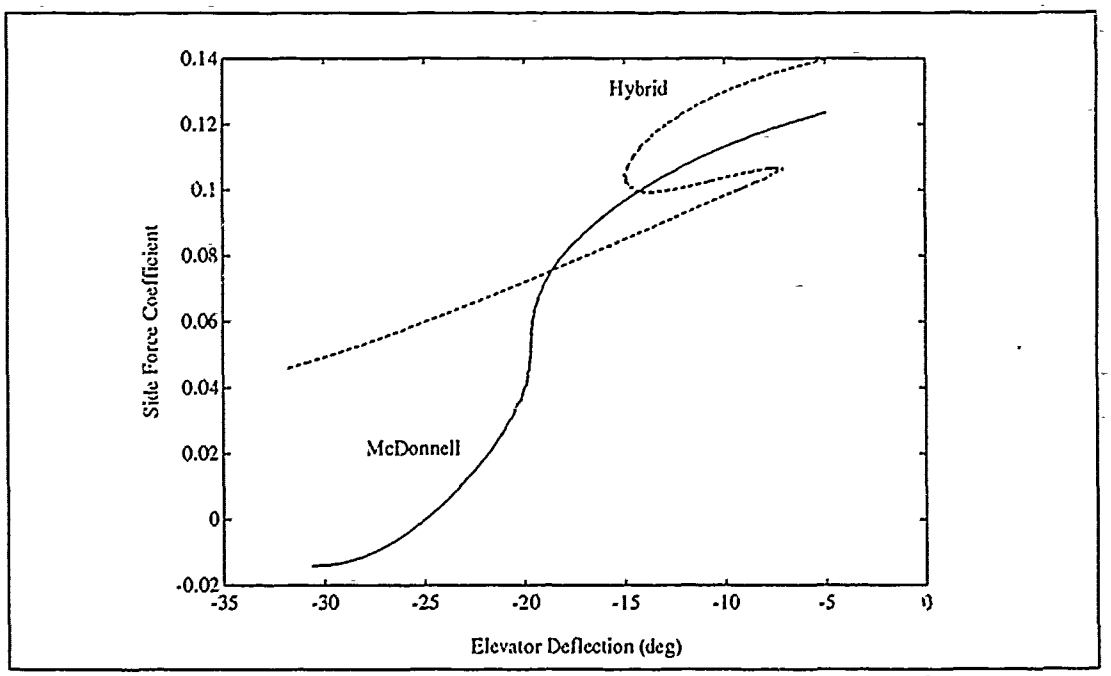

Figure 5.4 Comparison of Aerodynamic Coefficients as δ_e is Varied (δ_a=0°,δ_d=0°,δ_r=0°). (b) Side Force C_y.

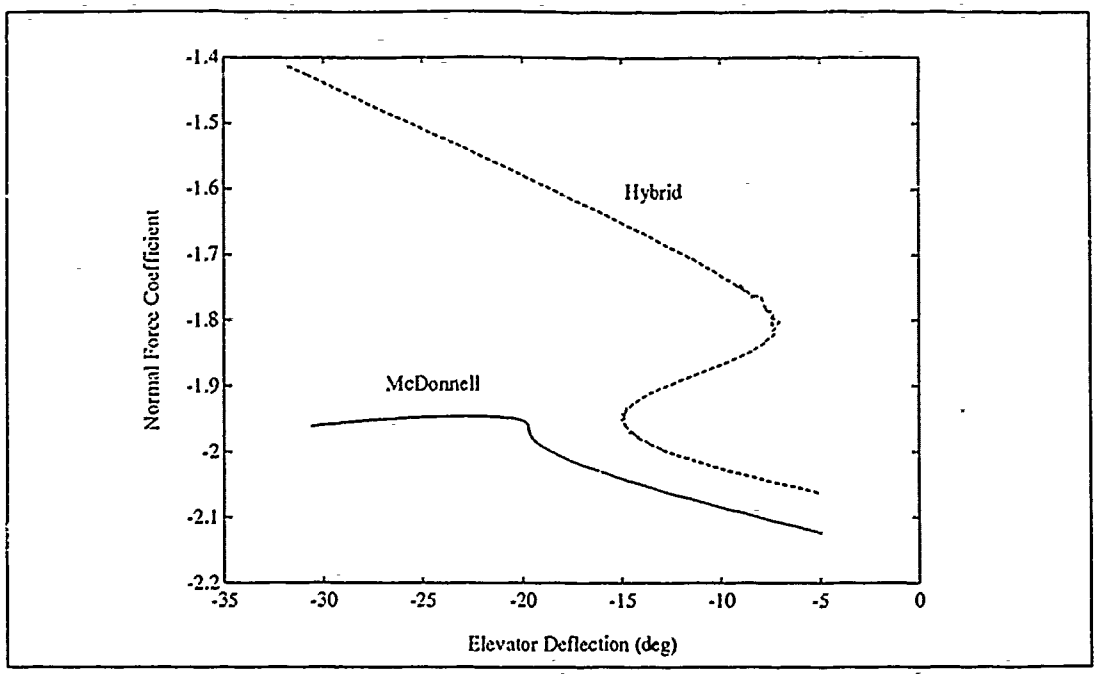

Figure 5.4 Comparison of Aerodynamic Coefficients as δ_e is Varied (δ_a=0°,δ_d=0°,δ_r=0°). (c) Normal Force C_z.

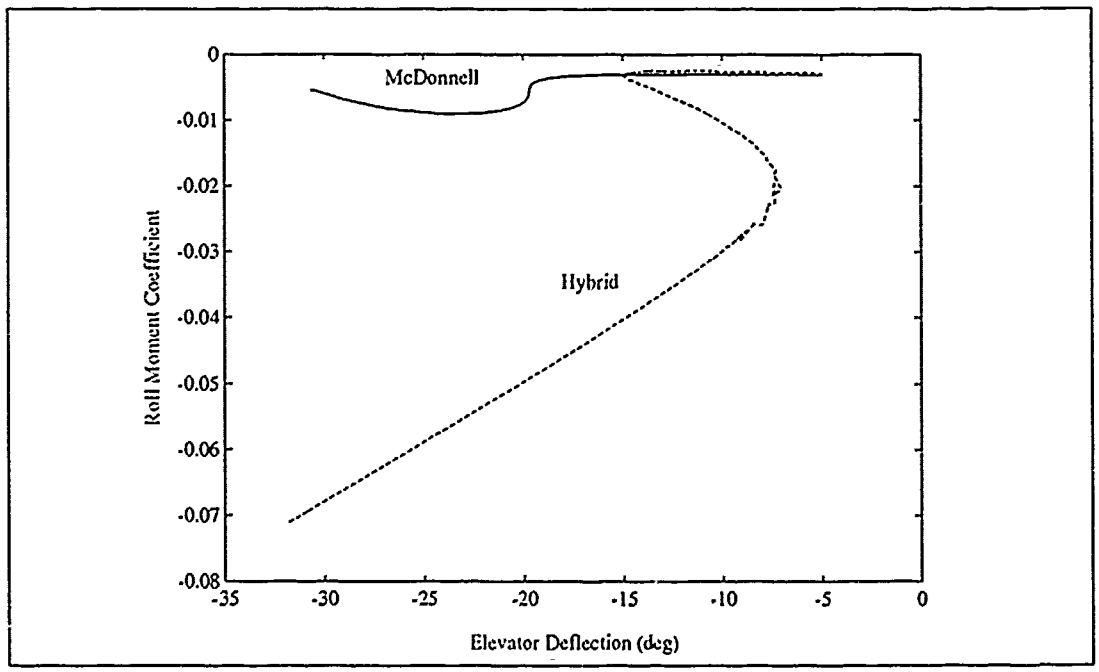

Figure 5.4 Comparison of Aerodynamic Coefficients as δ_e is Varied (δ_a=0°,δ_d=0°,δ_r=0°). (d) Roll Moment C_l.

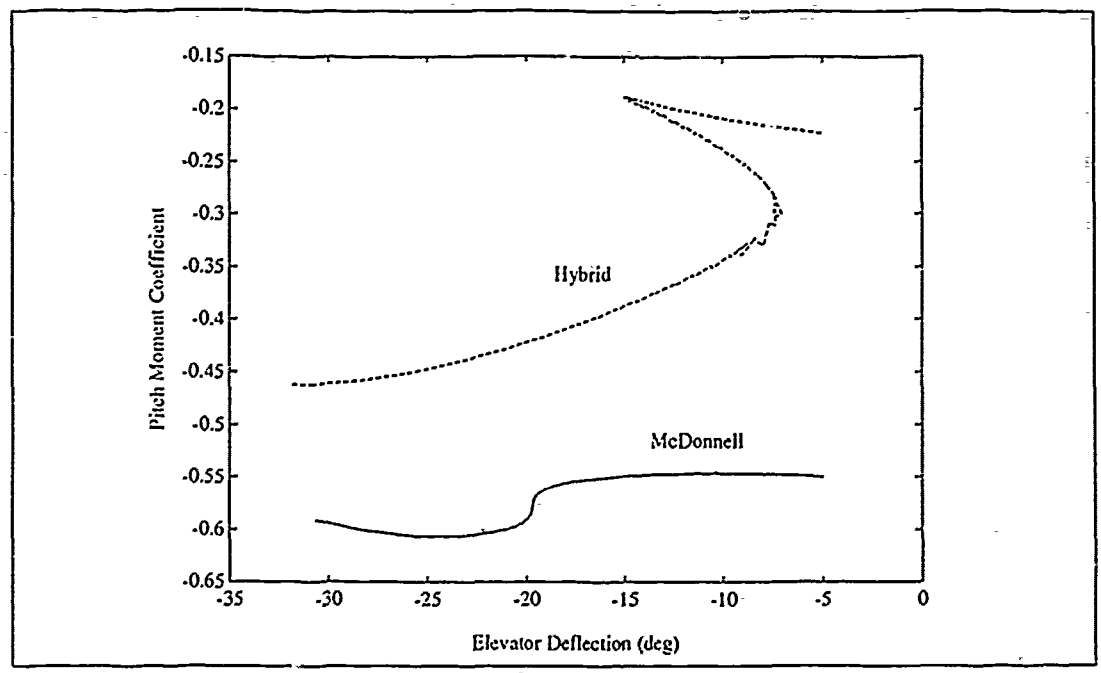

Figure 5.4 Comparison of Aerodynamic Coefficients as δ_e is Varied (δ_a=0°,δ_d=0°,δ_r=0°). (e) Pitch Moment C_m.

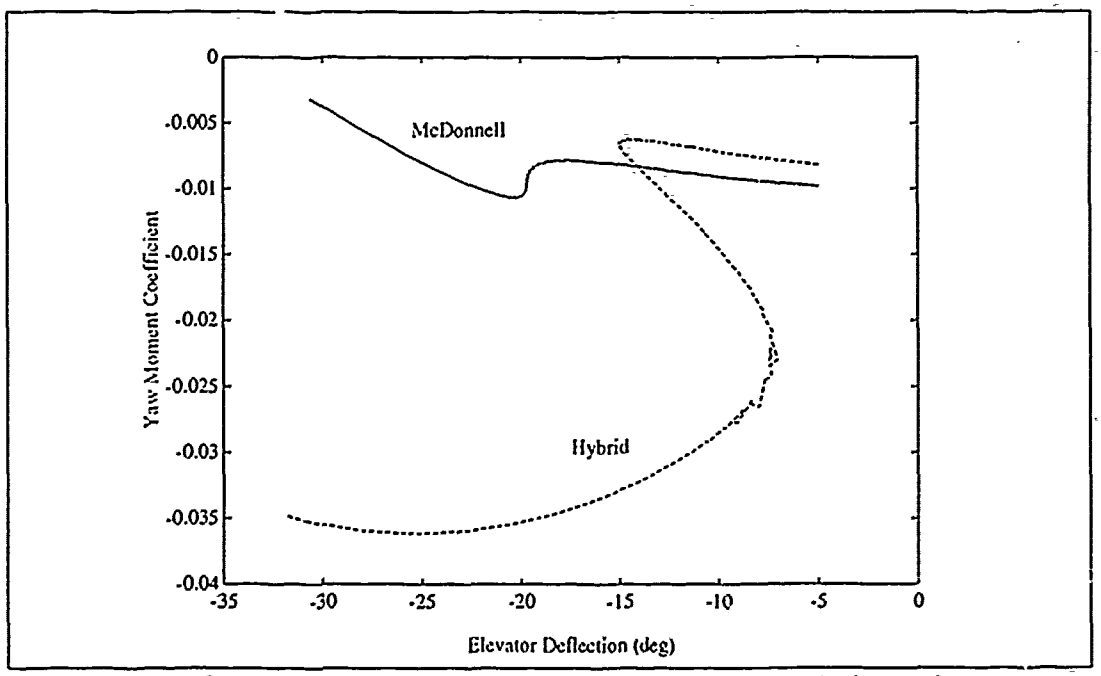

Figure 5.4 Comparison of Aerodynamic Coefficients as δ_e is Varied (δ_a=0°,δ_d=0°,δ_r=0°). (f) Yaw Moment C_n.

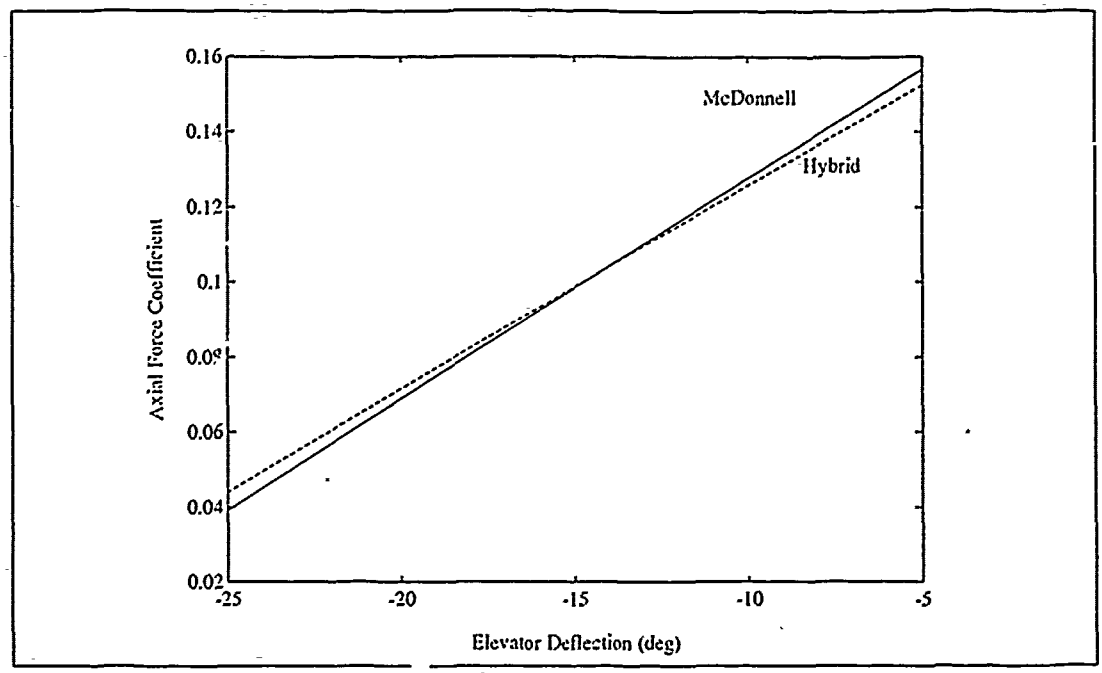

Figure 5.5 Comparison of the Aerodynamic Coefficients as δ_e is Varied for the state defined in Table V. (a) Axial Force C_x.

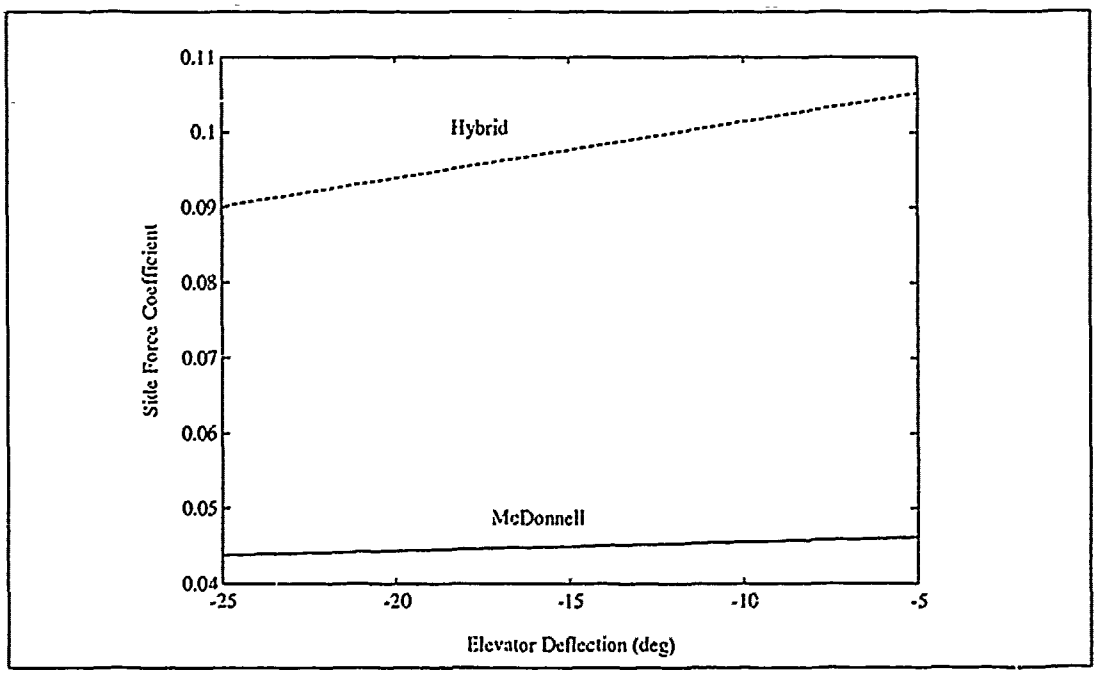

Figure 5.5 Comparison of the Aerodynamic Coefficients as δ_e is Varied for the state defined in Table V. (b) Side Force C_y.

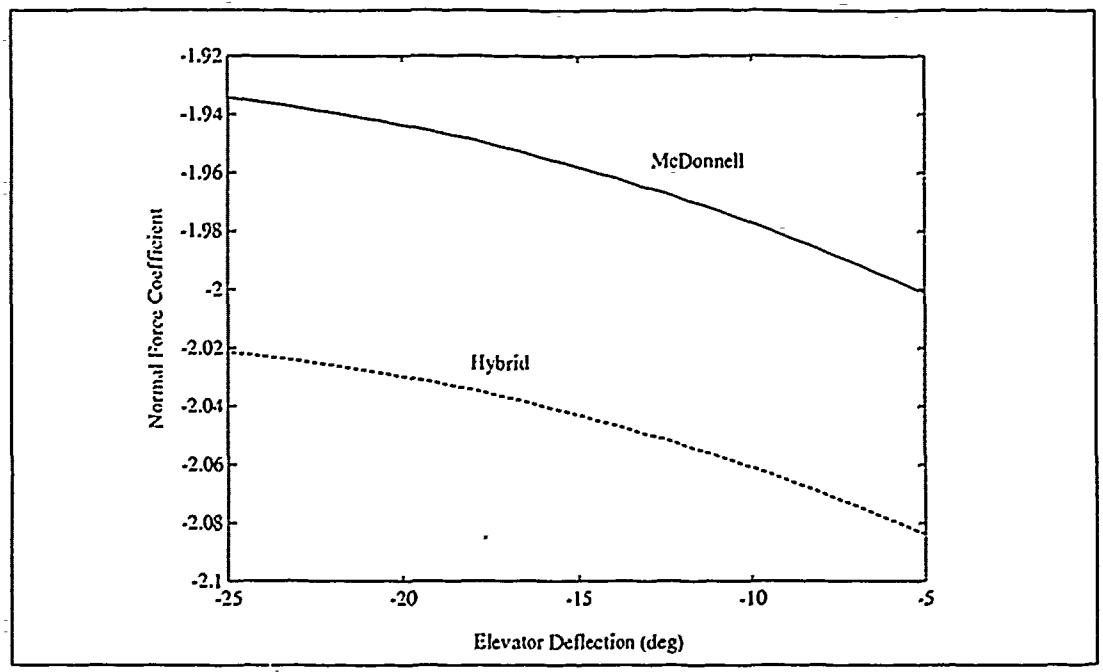

Figure 5.5 Comparison of the Aerodynamic Coefficients as δ_e is Varied for the state defined in Table V. (c) Normal Force C_z.

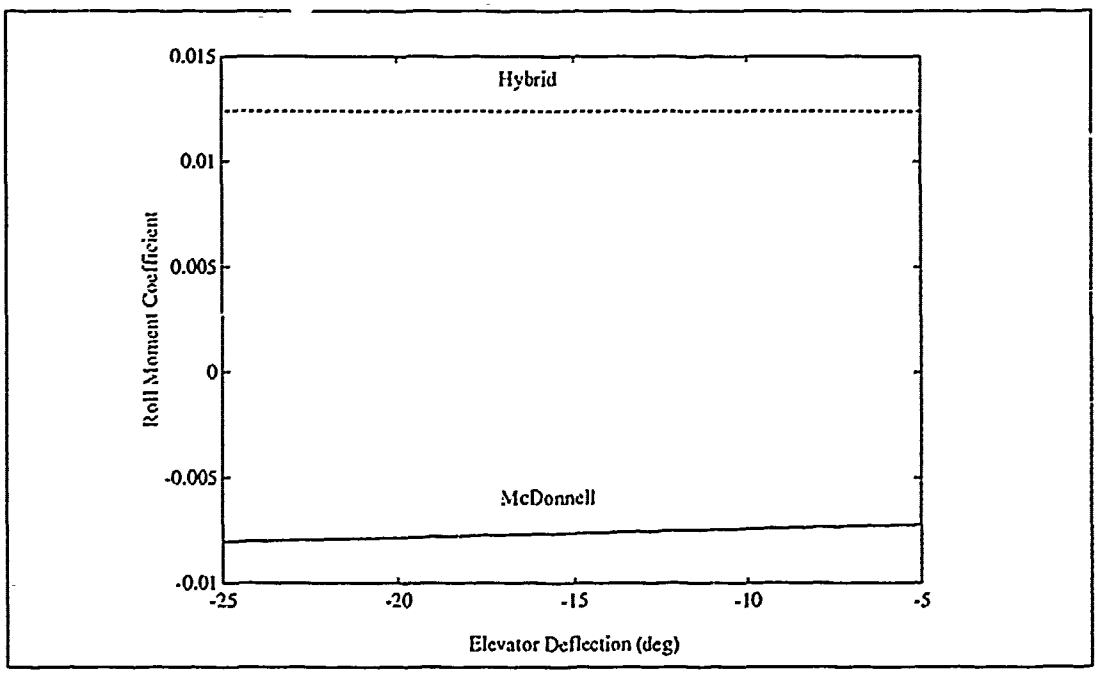

Figure 5.5 Comparison of the Aerodynamic Coefficients as δ_e is Varied for the state defined in Table V. (d) Roll Moment C_l.

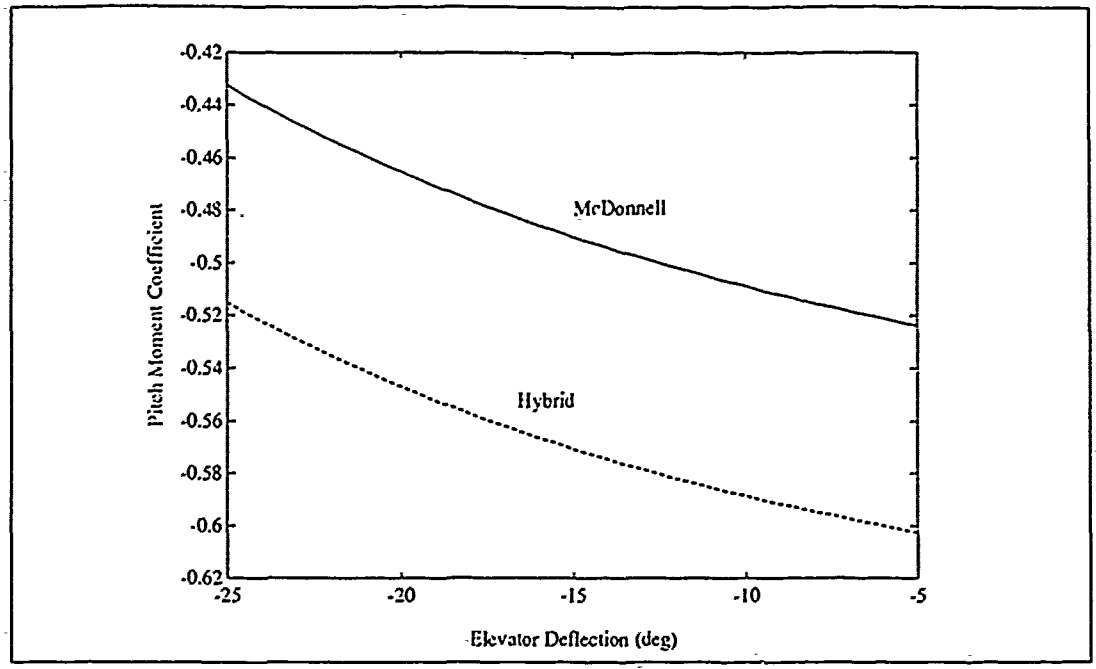

Figure 5.5 Comparison of the Aerodynamic Coefficients as δ_e is Varied for the state defined in Table V. (e) Pitch Moment C_m.

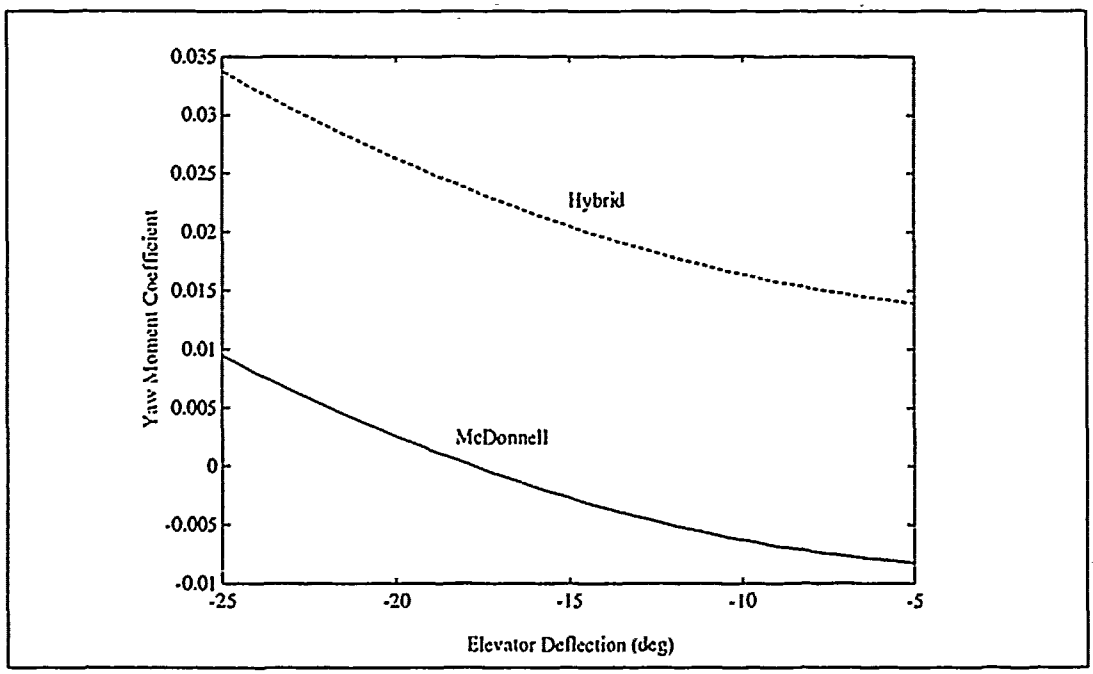

Figure 5.5 Comparison of the Aerodynamic Coefficients as δ_e is Varied for the state defined in Table V. (f) Yaw Moment C_n.

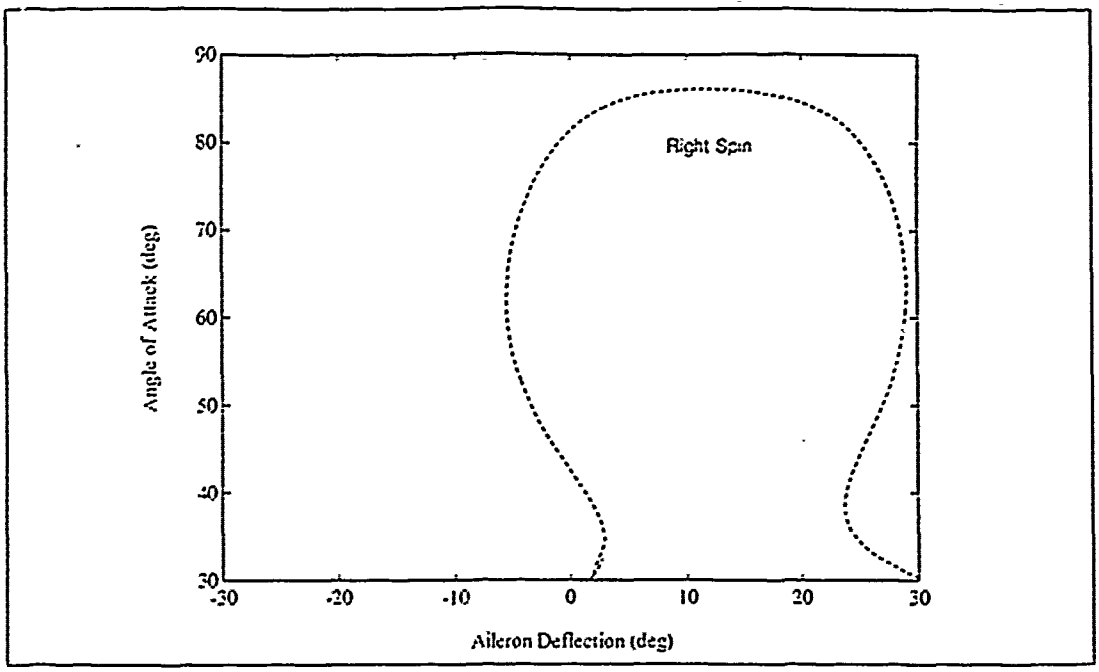

Figure 5.6 Aileron Sweep Bifurcation Diagram With Pro-spin Controls ($\delta_c=0.3\delta_a,\delta_e=0°,\delta_r=-15°$) (a) Rotary Balance Model.

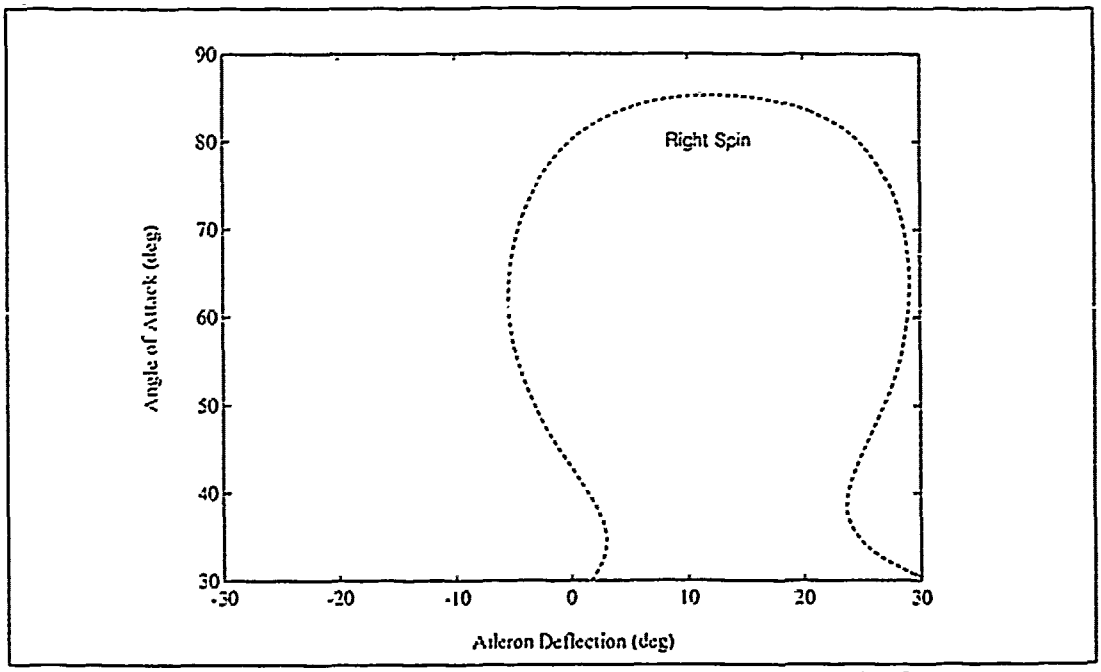

Figure 5.6 Aileron Sweep Bifurcation Diagram With Pro-spin Controls ($\delta_c=0.3\delta_a,\delta_e=0°,\delta_r=-15°$) (b) Modified Rotary Balance Model.

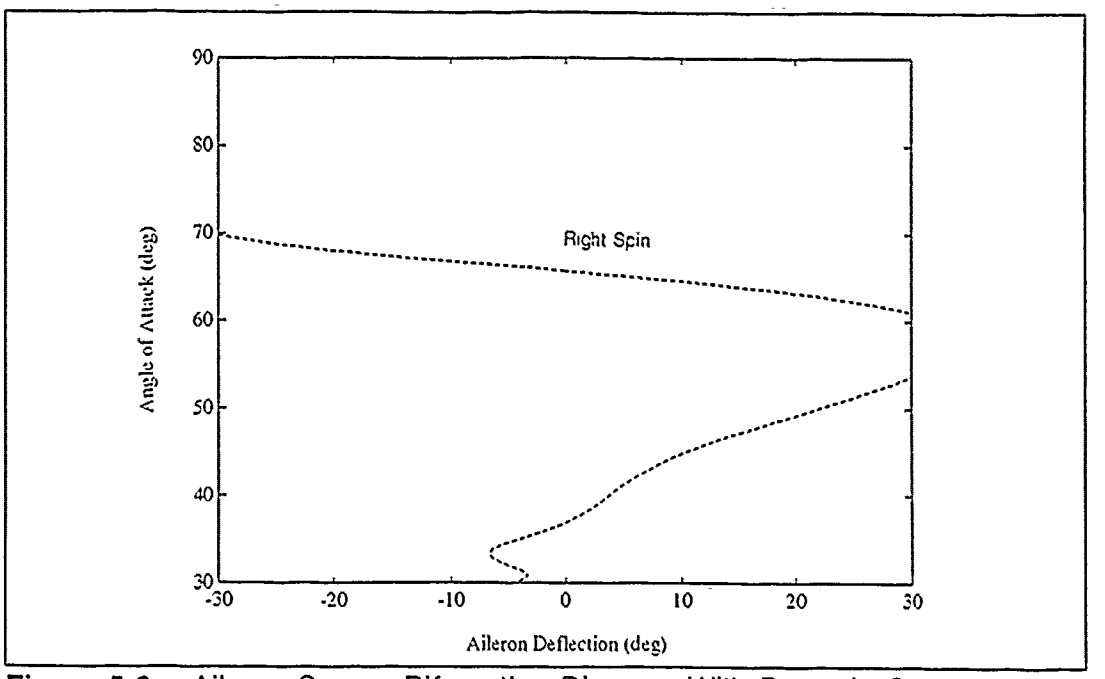

Figure 5.6 Aileron Sweep Bifurcation Diagram With Pro-spin Controls ($\delta_d=0.3\delta_a,\delta_e=0°,\delta_f=-15°$) (c) Hybrid Model.

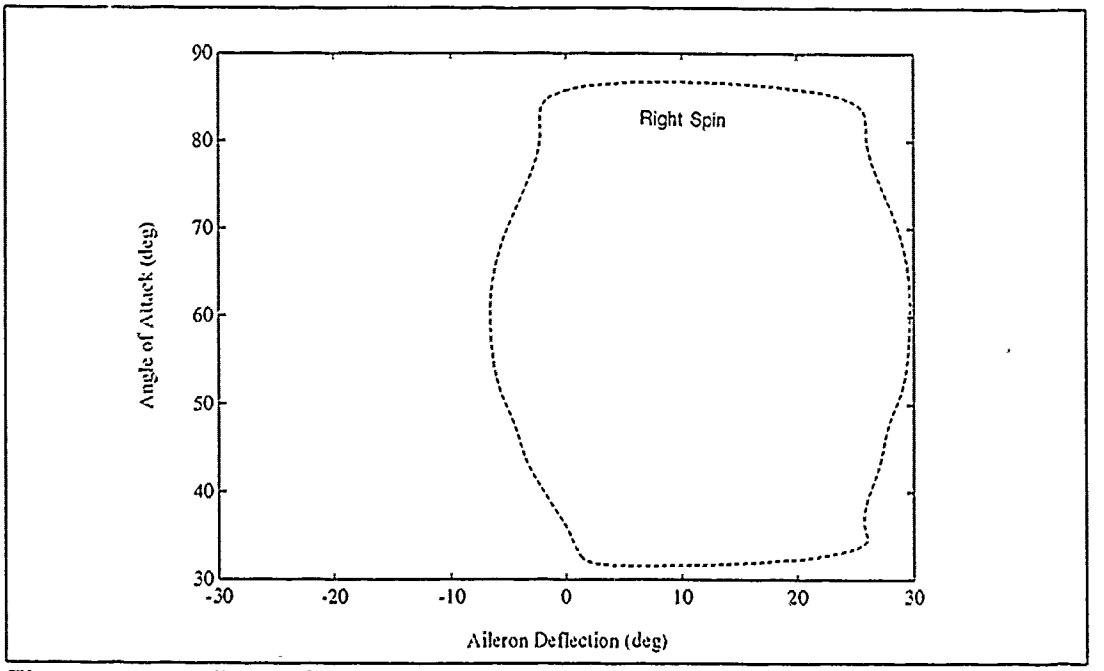

Figure 5.6 Aileron Sweep Bifurcation Diagram With Pro-spin Controls ($\delta_d=0.3\delta_a,\delta_e=0°,\delta_f=-15°$) (d) Modified Hybrid Model.

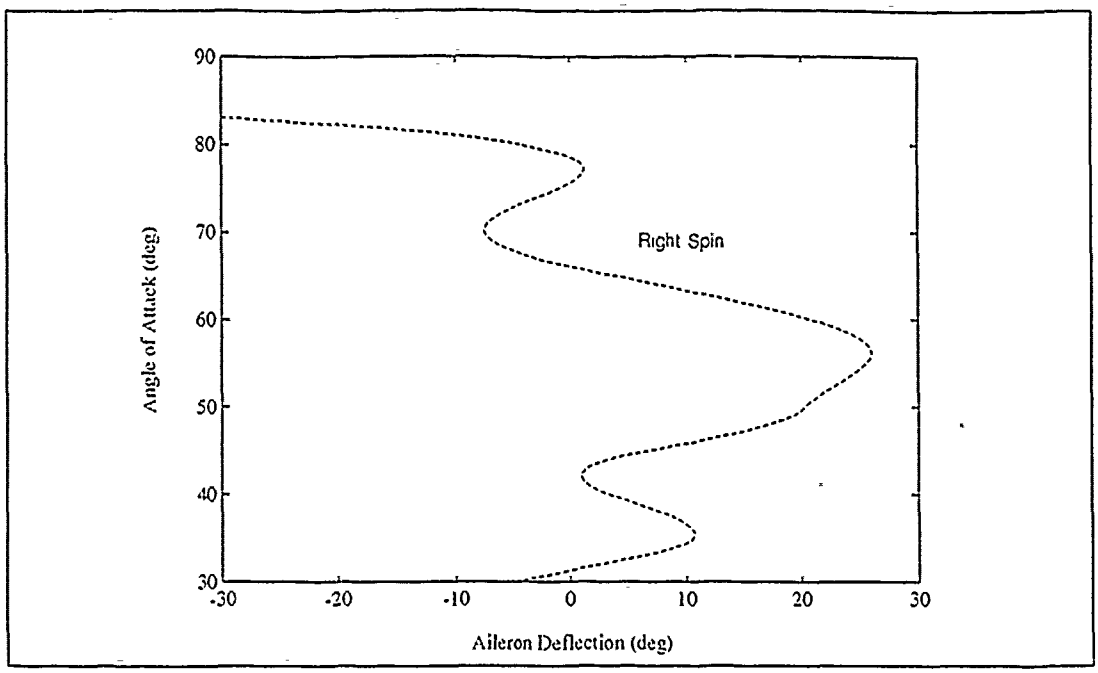

Figure 5.6 Aileron Sweep Bifurcation Diagram With Pro-spin Controls ($\delta_d=0.3\delta_a,\delta_e=0^\circ,\delta_r=-15^\circ$) (e) McDonnell Model.

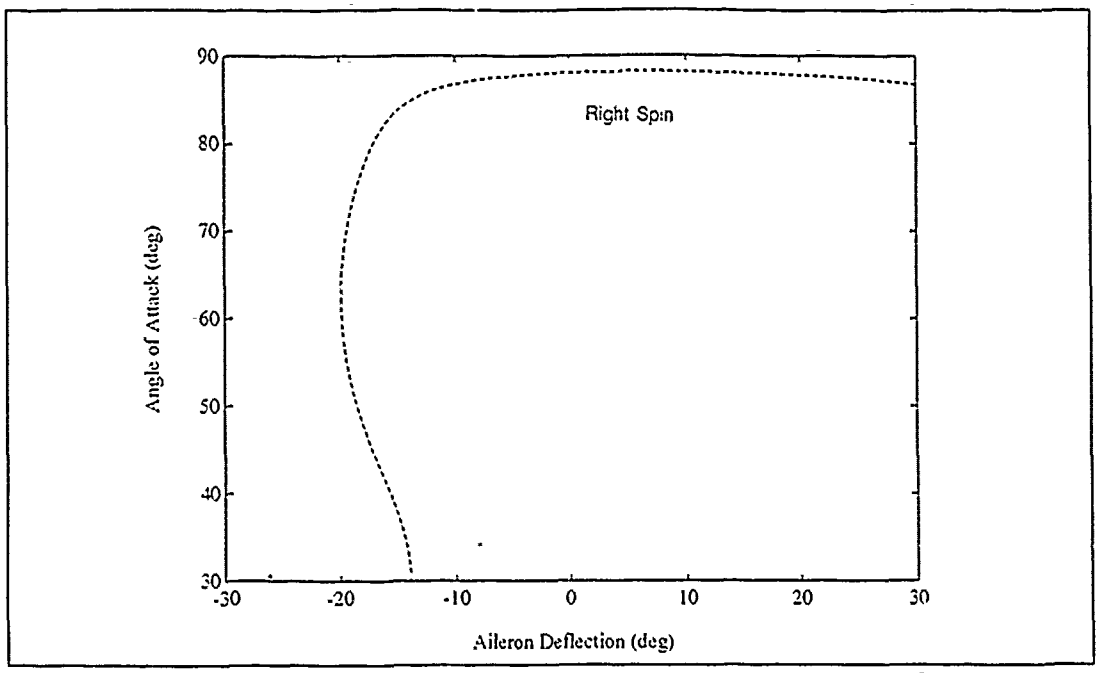

Figure 5.7 Aileron Sweep Bifurcation Diagram With Recovery Controls ($\delta_d=0.3\delta_a,\delta_e=0^\circ,\delta_r=30^\circ$) (a) Rotary Balance Model.

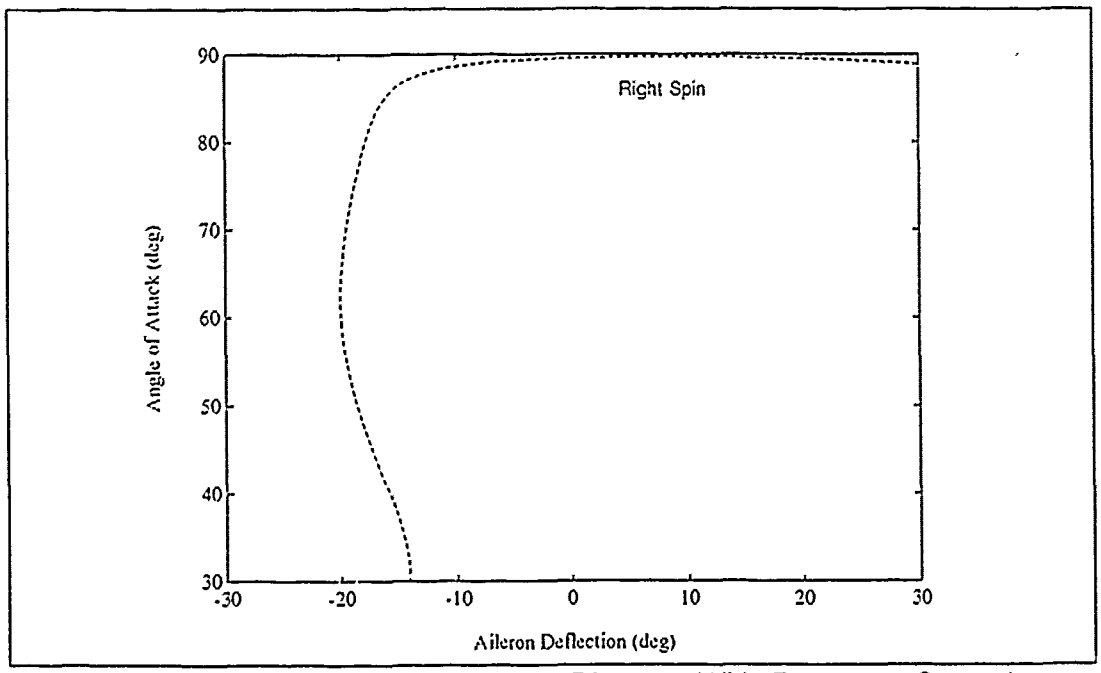

Figure 5.7 Aileron Sweep Bifurcation Diagram With Recovery Controls ($\delta_d=0.3\delta_a,\delta_e=0^\circ,\delta_r=30^\circ$) (b) Modified Balance Model.

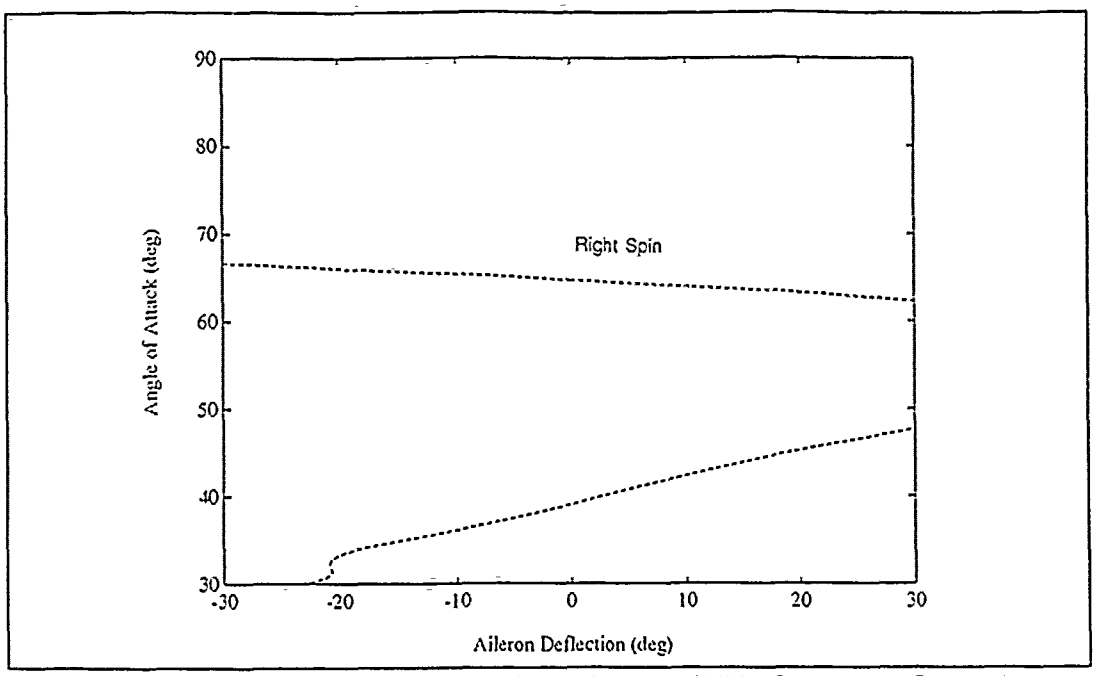

Figure 5.7 Aileron Sweep Bifurcation Diagram With Recovery Controls (δ_d=0.3δ_a,δ_e=0°,δ_r=30°) (c) Hybrid Model.

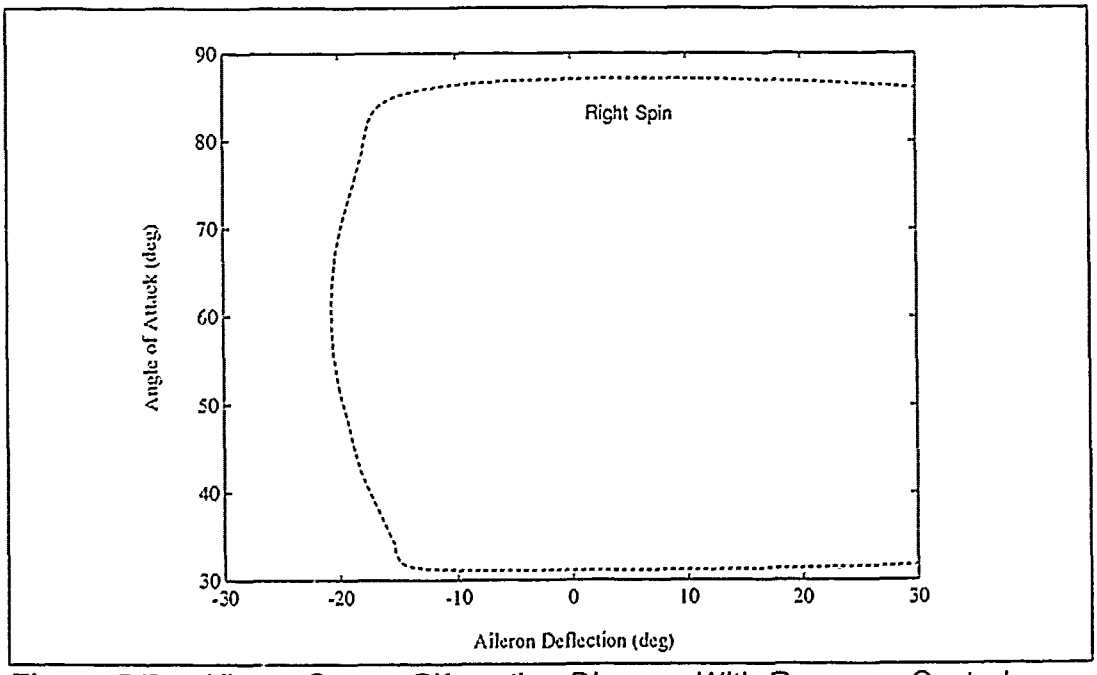

Figure 5.7 Aileron Sweep Bifurcation Diagram With Recovery Controls (δ_d=0.3δ_a,δ_e=0°,δ_r=30°) (d) Modified Hybrid Model.

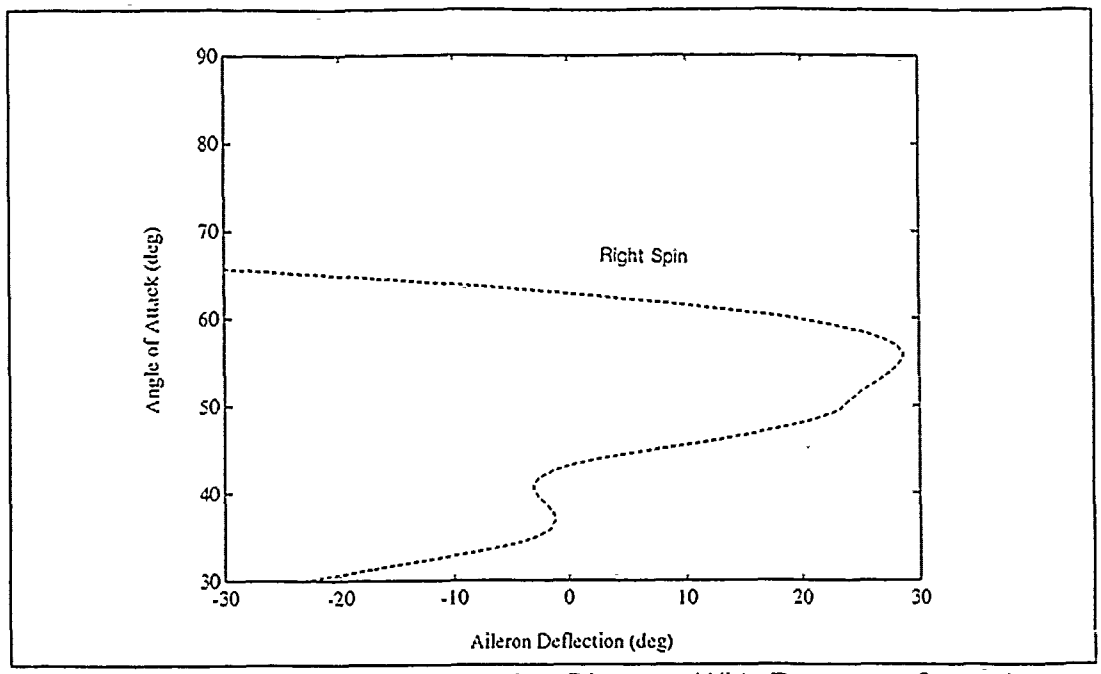

Figure 5.7 Aileron Sweep Bifurcation Diagram With Recovery Controls ($\delta_d=0.3\delta_a,\delta_e=0^\circ,\delta_r=30^\circ$) (e) McDonnell Model.

VI. Conclusions

As evidenced from this investigation, one of the distinctive differences and sources of difficulty in models of aircraft dynamics is the representation of the aerodynamic forces and moments. It is difficult to accept any research results that apply experimental data for modeling without a validation of the integrity of the data upon which the research was based. This investigation presented an opportunity to compare three models based on three very different aerodynamic coefficient databases. The results have given evidence of the caution that needs to be exercised when models are compared as well as the possible error that is introduced when two different sets of data are combined.

Both the McDonnell and RB model have the ability to predict high AOA behavior of the F-15B. The fundamental difficulty is that the qualitative and quantitative outlay of equilibria is very different. There is still the question of which model is better. The McDonnell model, representing static and forced oscillation data, has demonstrated wing rock behavior indicative of full scale flight test results as identified in reference (3). It does however have problems with the consequences of aileron and rudder deflection at high α which is probably more evident of the modelling of the stability derivatives than with the capability of static and forced oscillation data. With the possible problems with the McDonnell/Baumann coefficient modelling in δ_a and δ_r it is difficult to draw any conclusions concerning

its relative merits when compared to the RB model. The McDonnell model would however provide initial indication of high α spin behavior to initiate further investigations with the RB model. Moreover, the McDonnell model was used at $\delta_a=\delta_r=0$ with thrust vectoring producing quality results, so it is not always limited by this problem (24).

The results of Chapter V have shown that rotary balance data does enable prediction of aircraft spin motion with good correlation to full scale flight test results.

In particular:

(1) The RB model properly represented rudder motion as not being optimum for spin recovery as demonstrated by full scale flight tests.

(2) The RB model properly represented recovery control behavior with ailerons in a representative flight test recovery configuration.

(3) In pro-spin control configuration representative of full scale flight test behavior, the RB model showed no immediate spin recovery.

In addition:

(4) The rotary balance model was unable to identify stable equilibrium branches. as predicted by Mehra and Carroll for fighter aircraft and shown in their research results for the F-4 fighter (26).

The results from the RB model does demonstrate rotary balance data has strength in representing spinning motions of the aircraft however there is not enough

evidence to declare supremacy over the McDonnell model.

These results were determined with a single polynomial representation of each of the aerodynamic force and moment coefficients. It should be evident that the modeling of the RB data has smoothed much of the character of the original database. However, even with a "smoothed" representation of the RB data, it was able to provide good correlation to experimental flight test results. The promising results shown by the RB data as a stand alone representation of the aerodynamic coefficients in high AOA dynamics analysis yields further investigation of the effects of the static errors. With the RB data more effectively modelled it may provide more character in the bifurcation diagrams.

The problems encountered with the blending of two databases acquired from different testing facilities was evident in the Hybrid model. Because of the different sources of the data, inherent errors may conflict or even amplify. It needs to be assured that the data being blended is representative of the same testing condition. The error evident in the RB coefficient static configuration had a definite influence on the results found with the Hybrid model. The problems with aileron and rudder deflection in the McDonnell/Baumann model introduced error with the Hybrid model. Any research intending to use a hybrid model needs to develop three models. The RB, hybrid and static and forced oscillation model, need to be examined to ensure each is representing basic behavior such as rudder ineffectiveness or anticipated recovery results before the hybrid is used. If the databases were blended without concern, the Hybrid model may be presenting

false information which is based on conflicting databases.

Results from the Modified RB model showed that perturbation in the Axial and Side Force coefficients had a minor influence on the equilibrium solution branches when investigating the spin regime of the F-15B. The Modified Hybrid model gave indication that the static contributions to the aerodynamic coefficients was most influential in the character of equilibrium solutions.

Recommendations

1. An investigation of the evident static contribution problem of the rotary balance data and its effects on the Hybrid model could be made. A filtering process could be developed to adjust the removal of the rotary balance static contribution at small increments, artificially reducing its contribution to the model. A homotopy variable could be defined to adjust the proportions of the rotary balance static contributions removed and then a continuation on this variable could be performed to see what features of the bifurcation diagrams are most effected.

2. The static and forced oscillation contributions of the McDonnell model coefficients could be isolated and analyzed using bifurcation analysis to provide insight into which features of the equilibrium solutions are driven by static and forced oscillation information separately. The results from the analysis of the McDonnell model static contributions may provide assistance in determining the level of adjustments that could be made on the rotary balance data in

recommendation (1).

3. As demonstrated by the Modified RB model, analysis of the influence of each force and moment coefficient on the equilibrium solutions should be investigated. Before bifurcation analysis can be used confidently for analysis of aircraft dynamics its tolerance to perturbations in each of the force and moment coefficients needs to be determined. In addition, the analysis may provide insight into the behavicral differences between the models. Using the McDonnell,Rotary balance or an artificial database, each coefficient could be perturbed separately with either a static bias or a selected function. The results could assist in identification of which coefficients are driving the gross differences. The data could be adjusted to develop certain phenomena and then by adjusting the coefficient data until the phenomena distorts or disappears, the tolerance in accuracy of the coefficients could be determined.

Appendix A: F-15B Specification Data

The F-15 specifications for the F-15 are contained in Table IX. The data was obtained from Beck (8) and (23).

Table IX. Physical Characteristics of the F-15B

Wing	
Area (theoretical)	608 sq ft
Aspect Ratio	3.01
Airfoil	
Root	NACA64006.6
Xw 155	NACA64A(x)04.6 (a = 0.8 MOD)
Tip	NACA64A203 (a = 0.8 MOD)
Span	42.8 ft
Taper Ratio	0.25
Root Chord (Theoretical)	273.3 in
Tip Chord	68.3 in
Mean Aerodynamic Chord	191.3 in
Leading Edge Sweep Angle	45°
25% Chord Sweep Angle	38.6°
Dihedral	-1°
Incidence	None
Twist at Tip	None
Aileron Area	26.5 Sq ft
Flap Area	35.8 sq ft
Speed Brake Area	31.5 sq ft
Control Surface Movement	
Aileron	±20°
Speedbrake	45° up
Flap	30° down
Horizontal Tail	29° down, 15° up
Rudder	±30°

Vertical Tail

Area (Theoretical Each)	62.6 sq ft
Rudder Area (Each)	10.0 sq ft
Span	10.3 ft
Root Chord	115.0 in
Tip Chord	30.6 in
Airfoil - Root	NACA0005-64
- Tip	NACA0003.5-64
Taper Ratio	0.27
Leading Edge Sweep Angle	36.6°
25% Chord Sweep Angle	29.7°
Mean Aerodynamic Chord	81.0 in
Cant	2° out
Length ($.25c_w$ to $.25c_v$)	212.4 in

Horizontal Tail

Area (Theoretical)	120.0 sq ft
Area (Actual)	111.4 sq ft
Span	15.7 ft
Aspect Ratio	2.05
Taper Ratio	0.34
Root Chord	137.2 in
Tip Chord	46.5 in
Airfoil - Root	NACA0005.5-64
- Tip	NACA0002.5-64
Leading Edge sweep Angle	50°
25% Chord Sweep Angle	43.6°
Mean Aerodynamic chord	99.3 in
Dihedral	0°
Length ($.25c_w$ to $.25c_h$)	241.0 in

Wetted Area

Fuselage	1405 sq ft
Nozzles	53 sq ft
Horizontal Tail	216 sq ft
Vertical tail	257 sq ft
Wing	698 sq ft
Total Area	2629 sq ft

Miscellaneous Data

Aircraft Length	63.8 ft
Aircraft Height	18.6 ft
Aircraft Volume	1996 cu ft
Aircraft Gross Weight	37000 lbs
C.G. Station X Direction	557.173
Y Direction	0.0
Z Direction	116.173

Inertia Data is for a basic F-15 with 4 AIM-7F missiles, ammo, 50% fuel and gear up.

I_x	25480 slug-ft^2
I_y	166620 slug-ft^2
I_z	186930 slug-ft^2
I_{xz}	-1000 slug-ft^2

Appendix B: Sign Conventions

The airplane is considered in an upright attitude with all directions with respect to the pilot seated in the cockpit. Refer to figure B-1. The sign convention data for the F-15 was obtained from (23).

Airplane

Forces - Positive up, aft or to the right

Moments - Positive when the nose pitches up, to the right, or the left wing rises.

Angular Velocity - Positive when the nose rotates up, to the right, or the left wing rises.

Control Surfaces

Aileron - Positive when right aileron is down.

Differential Horizontal Tail - Positive when right panel is down.

Symmetrical Horizontal tail - Positive when trailing edge is down.

Rudder - Positive when trailing edge is to the left.

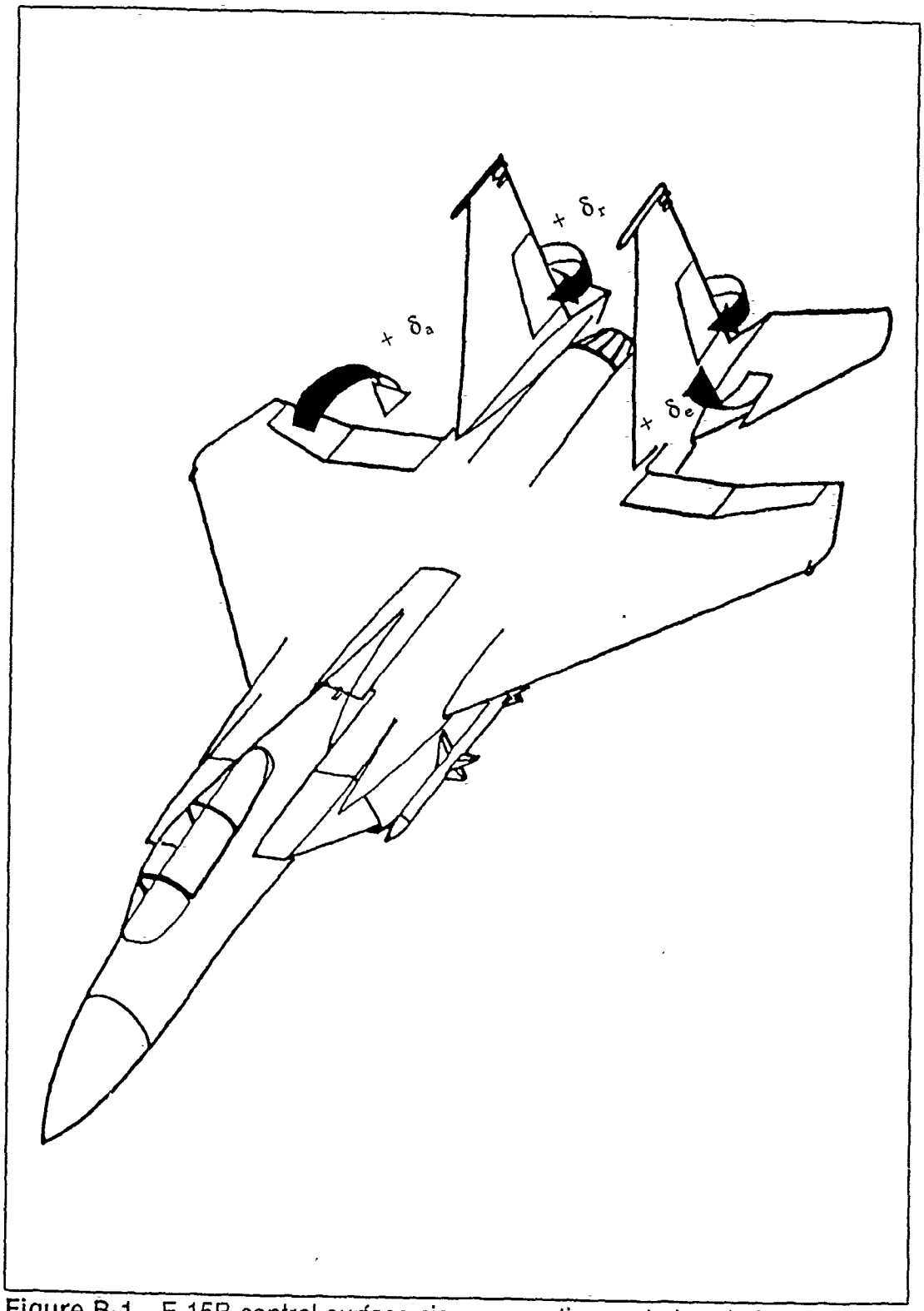

Figure B-1 F-15B control surface sign convention and aircraft drawing.

Appendix C: AUTO Driver Program

```
C
C    CAPTAIN RALPH D. FERO  AFIT GA-91D
C    MASTERS THESIS
C
C    THE FOLLOWING DRIVER PROGRAM IS A MODIFIED VERSION OF
C    CAPT ROBERT MCDONNELL'S 1990 THESIS.  THE ADDITIONS IN
C    THIS VERSION OF THE PROGRAM INVOLVE INTEGRATION OF
C    F-15 ROTARY AERODYNAMIC DATA.  THIS PROGRAM SOLVES THE
C    NONLINEAR DIFFERENTIAL EQUATIONS OF MOTION FOR THE
C    F-15B AIRCRAFT. FOR THIS RESEARCH EFFORT, THIS PROGRAM
C    WILL BE USED TO INVESTIGATE THE EFFECTS OF ROTARY
C    BALANCE DATA ON THE ANALYSIS OF HIGH ANGLE OF ATTACK
C    PHENOMENA.  THE PROGRAM IS CAPABLE OF VARYING
C    ELEVATOR, AILERON, RUDDER DEFLECTIONS, ENGINE
C    THRUST VECTOR (PITCH AND YAW), PORT AND  STARBOARD
C    ENGINE THRUST, AND TOTAL THRUST.  IN ADDITION, THE
C    PROGRAM HAS BEEN MODIFIED TO VARY DIFFERENTIAL
C    ELEVATOR  AND A HOMOTOPY BLENDING PARAMETER FOR
C    TRANSITION FROM  THE 1988 F-15 AEROBASE DATA TO ROTARY
C    AERODYNAMIC DATA.
C
C    LAST EDITED ON 14 OCTOBER 1991
C
     IMPLICIT DOUBLE PRECISION(A-H,O-Z)
     COMMON /RBPOLY/ PC, OMEGA
     DIMENSION W(300000), IW(1000),PC(6,79)

C
C
     OPEN(UNIT=3,FILE='fort.3')
     OPEN(UNIT=4,FILE='fort.4')
     OPEN(UNIT=7,FILE='fort.7')
     OPEN(UNIT=8,FILE='fort.8')
     OPEN(UNIT=9,FILE='fort.9')
     OPEN(UNIT=10,FILE='fort.10')
     OPEN(UNIT=12,FILE='seize')
     OPEN(UNIT=13,FILE='seizet')
C
     REWIND 7
     REWIND 8
     REWIND 9
     REWIND 10
     REWIND 3
     REWIND 4
     REWIND 12
     REWIND 13
C
C  ADDED 15 AUG 91
```

```
C
      CALL RBPOLYCOEF
C
C     CALL AUTO - CONTINUATION & BIFURCATION LOCATION
C     SUBROUTINE
C
      CALL AUTO(W,IW)
C
      STOP
      END
C
C
      SUBROUTINE FUNC(NDIM,NPAR,U,ICP,PAR,IJAC,F,DFDU,DFDP)
C     --------- ---------------------------------------
C
      IMPLICIT DOUBLE PRECISION (A-H,O-Z)
      COMMON /KS/ K1,K5,K7,K8,K9,K10,K12,K13,K14,K15,K16,K17
      COMMON /ACDATA/ BWING,CWING,SREF,RHO,RMASS
      DOUBLE PRECISION K1,K5,K7,K8,K9,K10,K12,K13,K14,K15,K16,K17
      COMMON /SEIZE/ CX,CY,CZ,CLM,CMM,CNM
      COMMON /SEIZET/ CXT,CYT,CZT,CLMT,CMMT,CNMT
      COMMON /SEIZER/ CXR,CYR,CZR,CLMR,CMMR,CNMR
      COMMON /RBPOLY/ PC, OMEGA
C
C
      DIMENSION DFDU(NDIM,NDIM),DFDP(NDIM,NPAR),DELF1(8),
     + DELF2(8),U(NDIM),PAR(10),F(NDIM),DX(8),PC(6,79)
C
C
C
C     INITIALIZE SOME CONSTANTS THAT ARE PASSED THROUGH
C     THE COMMON BLOCK ACDATA
C
C     DATA IS FROM MCAIR REPORT# A4172 AND AFFTC-TR-75-32
C     F-15A APPROACH-TO-STALL/STALL/POST-STALL EVALUATION
C
C     BWING  - A/C WINGSPAN, FT
C     CWING  - A/C MEAN AERODYNAMIC CHORD, FT
C     SREF   - A/C WING REFERENCE AREA, SQ FT
C     RHO    - AIR DENSITY AT 20000 FT ALTITUDE, SLUG/FT^3
C     RMASS  - A/C MASS, SLUGS
C
      BWING=42.8
      CWING=15.94
      SREF=608.
      RHO=.0012673
      RMASS=37000./32.174
C
C
C     DETERMINE CONSTANTS K1 THROUGH K17.  SOME ARE MADE
```

```
C     COMMON AND PASSED TO SUBROUTINE FUNX AND USED IN THE
C     EQUATIONS OF MOTION THERE
C
C     INERTIAS HAVE UNITS OF SLUG-FT^2
C
C     K1 HAS UNITS OF 1/FT
C
C     K6, K8, K11, K14, AND K17 HAVE UNITS OF 1/FT^2
C
C
C     IX=  25480.0d0
C     IY= 166620.0d0
C     IZ= 186930.0d0
C     IXZ= -1000.0d0
C     K1=0.5d0*RHO*SREF/RMASS
C     K2=(IZ-IY)/IX
C     K3=IXZ*IXZ/(IX*IZ)
C     K4=(IY-IX)/IZ
C     K5=IXZ/IX
C     K6=0.5d0*RHO*BWING*SREF/IX
C     K7=IXZ/IZ
C     K8=0.5d0*RHO*SREF*CWING/IY
C     K9=(IZ-IX)/IY
C     K10=IXZ/IY
C     K11=0.5d0*RHO*SREF*BWING/IZ
C     K12=(K2+K3)/(1.0d0-K3)
C     K13=(1.0d0-K4)*K5/(1.0d0-K3)
C     K14=K6/(1.0d0-K3)
C     K15=(K3-K4)/(1.0d0-K3)
C     K16=(1.0d0+K2)*K7/(1.0d0-K3)
C     K17=K11/(1.0d0-K3)
C
C
      K1  = 3.350088890D-04
      K5  =-3.924646781D-02
      K7  =-5.349596105D-03
      K8  = 3.685650971D-05
      K9  = .96897131196
      K10 =-6.001680471D-03
      K12 = .79747314581
      K13 =-9.615755341D-03
      K14 = 6.472745847D-04
      K15 =-.754990553922
      K16 =  K13
      K17 = 8.822851558D-05
C
C
C
C     FIND THE VALUES OF F(1) THROUGH F(NDIM).  SUBROUTINES
C     COEFF AND FUNX ARE CALLED ONCE.
```

```
C
C
      CALL COEFF(U,PAR,NDIM,ICP)
C
C     THE FOLLOWING ADDED 15 AUG 91
C
C     THE SUBROUTINE RBPOLYCOEF AND RBCOEF DETERMINE THE
C     ASSOCIATED COEFICIENTS USING ROTARY BALANCE DATA
C     OBTAINED FROM THE NASA LANGLEY SPIN TUNNEL.  THE DATA
C     WAS OBTAINED ON FLOPPY DISKS.  THE DATA IS DOCUMENTED
C     IN NASA CR 3478. THE DATA IS ONLY CODED FOR  AOA ABOVE
C     30 DEGREES THEREFORE WILL BE BLENDED AT THIS VALUE.
C
      IF (U(1) .GT. 30) THEN
C
       CALL RBCOEF(U,PAR,NDIM)

C     SUBROUTINE BLEND PERFORMS THREE FUNCTIONS. USING THE
C     PARAMETER BLEND, (1) IDENTIFY A UNIQUE EQUILIBRIUM
C     STATE SOLUTION FOR PURE ROTARY BALANCE DATA BASED
C     MODEL,(2) PERFORM THE ADDITION THRUST CONTRIBUTIONS TO
C     THE PURE ROTARY BALANCE DATA BASED MODEL, (3) PERFORM
C     THE BLEND   TRANSITION FROM MCDONNELL'S MODEL TO THE
C     HYBRID ROTARY BALANCE DATABASE MIXED MODEL (HYBRID
C     MODEL).
C
       CALL RBBLEND(U,PAR,NDIM,ICP)
C
      ENDIF
C
      CALL FUNX(NDIM,U,F)
C
C
      IF(IJAC.EQ.0) RETURN
C
C  SET THE VALUES OF DX
C  MODIFIED TO SCALE DX ACCORDING TO VARIABLE
C  13 JUN 88
C
C
      DX0=1.0D-9
      DX(1)=DX0*50.0d0
      DX(2)=DX0*10.0d0
      DX(3)=DX0*0.5d0
      DX(4)=DX0*0.25d0
      DX(5)=DX0*0.5d0
      DX(6)=DX0*50.0d0
      DX(7)=DX0*50.0d0
      DX(8)=DX0*0.5d0
C
```

```
C
C     NEXT THE PARTIAL OF F W.R.T. A GIVEN PARAMETER ARE
C     FINITE  DIFFERENCED
C
      PTEMP=PAR(ICP)
      PAR(ICP)=PTEMP+DX(1)
C
C
      CALL COEFF(U,PAR,NDIM,ICP)
C
C
C     FOLLOWING ADDED 15 AUG 91
C
      IF (U(1) .GT. 30) THEN
        CALL RBCOEF(U,PAR,NDIM)
        CALL RBBLEND(U,PAR,NDIM,ICP)
      ENDIF
C
      CALL FUNX(NDIM,U,DELF1)
C
      PAR(ICP)=PTEMP-DX(1)
C
C
      CALL COEFF(U,PAR,NDIM,ICP)
C
C
C     FOLLOWING ADDED 15 AUG 91
C
      IF (U(1) .GT. 30) THEN
        CALL RBCOEF(U,PAR,NDIM)
        CALL RBBLEND(U,PAR,NDIM,ICP)
      ENDIF
C

      CALL FUNX(NDIM,U,DELF2)
C
        DO 13 I=1,NDIM
C
          DFDP(I,ICP)=(DELF1(I)-DELF2(I))/(2.0d0*DX(1))
C
C
 13     CONTINUE
      PAR(ICP)=PTEMP
C
C     THE NEXT DO LOOP CALCULATES THE PARTIAL DERIVATIVE OF
C     F W.R.T. TO U USING FINITE DIFFERENCES.
C
C     SET U(J) EQUAL TO U+DU, THEN CALL COEFF WITH THIS
C     UPDATED STATE VECTOR.  THIS IS DONE SIMILARLY WITH
C     U-DU
```

```
C
      DO 20 J=1,NDIM
C
        UTEMP=U(J)
C
        U(J)=UTEMP+DX(J)
C
C
        CALL COEFF(U,PAR,NDIM,ICP)
C
C
C     FOLLOWING ADDED 15 AUG 91
C
      IF (U(1) .GT. 30) THEN
        CALL RBCOEF(U,PAR,NDIM)
        CALL RBBLEND(U,PAR,NDIM,ICP)
      ENDIF
C
        CALL FUNX(NDIM,U,DELF1)
C
        U(J)=UTEMP-DX(J)
C
C
        CALL COEFF(U,PAR,NDIM,ICP)
C
C     FOLLOWING ADDED 15 AUG 91
C
      IF (U(1) .GT. 30) THEN
        CALL RBCOEF(U,PAR,NDIM)
        CALL RBBLEND(U,PAR,NDIM,ICP)
      ENDIF
C
        CALL FUNX(NDIM,U,DELF2)
C
C
        DO 16 I=1,NDIM
          DFDU(I,J)=(DELF1(I)-DELF2(I))/(2.0d0*DX(J))
16        CONTINUE
C
        U(J)=UTEMP
C
 20   CONTINUE

      RETURN
      END
```

```
      SUBROUTINE FUNX(NDIM,U,F)
C     --------- -----------
C
C     SUBROUTINE FUNX EVALUATES THE NDIM EQUATIONS GIVEN THE
C     STATE VECTOR U.
C
C     NDIM- THE DIMENSION OF THE PROBLEM
C     U   - THE VECTOR OF STATES ALPHA, BETA, ... (INPUT)
C     F   - THE VECTOR RESULT OF FUNCTION EVALUATIONS
C           (OUTPUT)
C
      IMPLICIT DOUBLE PRECISION (A-H,O-Z)
      COMMON /SEIZE/ CX,CY,CZ,CLM,CMM,CNM
      COMMON /SEIZET/ CXT,CYT,CZT,CLMT,CMMT,CNMT
      COMMON /KS/ K1,K5,K7.K8,K9,K10,K12,K13,K14,K15,K16,K17
      DOUBLE PRECISION K1,K5,K7,K8,K9,K10,K12,K13,K14,K15,K16,K17
      DIMENSION U(NDIM),F(NDIM)
C
C     SET TRIGONOMETRIC RELATIONSHIPS OF THE STATES ALPHA,
C     BETA, THETA, AND PHI AND THEN SET P, Q, R, AND VTRFPS
C
      IWRITE=1
C
C
      DEGRAD=57.29577951D0
C
      CA=COS(U(1)/DEGRAD)
      SA=SIN(U(1)/DEGRAD)
      CB=COS(U(2)/DEGRAD)
      SB=SIN(U(2)/DEGRAD)
      CTHE=COS(U(6)/DEGRAD)
      STHE=SIN(U(6)/DEGRAD)
      CPHI=COS(U(7)/DEGRAD)
      SPHI=SIN(U(7)/DEGRAD)
C
      P=U(3)
      Q=U(4)
      R=U(5)
      VTRFPS=1000.0d0*U(8)
C
C     SET THE GRAVITATIONAL CONSTANT, FT/SEC
C
      G=32.1740d0
C
C     THE FOLLOWING SYSTEM OF NONLINEAR DIFFERENTIAL
C     EQUATIONS GOVERN AIRCRAFT MOTION
C
C     UPDATED FOR PROPER DEGREE-RADIAN UNITS AND PROPERLY
C     SCALED VELOCITY EQUATION:  7 JUN 88
C
```

```
C   F(1)=ALPHA-DOT
C
 1  F(1)=Q+(-(K1*VTRFPS*CX-G*STHE/VTRFPS+R*SB)*SA+(K1*VTRFPS
   + *CZ+(G*CTHE*CPHI/VTRFPS)-P*SB)*CA)/CB
    F(1)=F(1)*DEGRAD
C
C
C  F(2)=BETA-DOT
C
 2  F(2)=-((K1*VTRFPS*CX-G*STHE/VTRFPS)*SB+R)*CA+(K1*VTRFPS*CY
   +  +G*CTHE*SPHI/VTRFPS)*CB-((K1*VTRFPS*CZ+G*CTHE*CPHI/VTRFPS)
   +  *SB-P)*SA

   F(2)=F(2)*DEGRAD
C
C
C  F(3)=P-DOT
C
 3  F(3)=-K12*Q*R+K13*P*Q+K14*(CLM+K7*CNM)*VTRFPS*VTRFPS
C
C
C  F(4)=Q-DOT
C
 4  F(4)=K8*VTRFPS*VTRFPS*CMM+K9*P*R+K10*(R*R-P*P)
C
C
C  F(5)=R-DOT
C
 5  F(5)=K15*P*Q-K16*Q*R+K17*VTRFPS*VTRFPS*(K5*CLM+CNM)
C
C
C  F(6)=THETA-DOT
C
 6  F(6)=Q*CPHI-R*SPHI
    F(6)=F(6)*DEGRAD
C
C
C  F(7)=PHI-DOT
C
 7  F(7)=P+Q*(STHE/CTHE)*SPHI+R*(STHE/CTHE)*CPHI
    F(7)=F(7)*DEGRAD
C
C
C  F(8)=VTRFPS-DOT  (SCALED BY A FACTOR OF 1000)
C
 8  F(8)=U(8)*((K1*VTRFPS*CX-G*STHE/VTRFPS)*CA*CB+(K1*VTRFPS*CY
   + +G*CTHE*SPHI/VTRFPS)*SB
   + +(K1*VTRFPS*CZ+G*CTHE*CPHI/VTRFPS)*SA*CB)
C
C
```

```
      RETURN
      END
C
      SUBROUTINE STPNT(NDIM,U,NPAR,ICP,PAR)
C     --------- ----------------------
C
C     THIS SUBROUTINE SETS THE VALUES OF THE STATES AND
C     PARAMETERS AT THE START OF THE ANALYSIS.  THE STATES
C     AND CONTROL SURFACE SETTINGS REPRESENT AN EQUILIBRIUM
C     STATE OF THE AIRCRAFT
C
      IMPLICIT DOUBLE PRECISION (A-H,O-Z)
C
      DIMENSION U(NDIM),PAR(10)
C     U(1) - ALPHA, DEG
C     U(2) - BETA, DEG
C     U(3) - P, RAD/SEC
C     U(4) - Q, RAD/SEC
C     U(5) - R, RAD/SEC
C     U(6) - THETA, DEG
C     U(7) - PHI, DEG
C     U(8) - TRUE VELOCITY, IN THOUSANDS OF FT/SEC
C
C     THE STARTING POINT (VECTOR)
C
      OPEN(UNIT=15,FILE='fort.15')
      REWIND (15)
C
      READ(15,*) U(1)
      READ(15,*) U(2)
      READ(15,*) U(3)
      READ(15,*) U(4)
      READ(15,*) U(5)
      READ(15,*) U(6)
      READ(15,*) U(7)
      READ(15,*) VTRFPS
      U(8)=VTRFPS/1000.0d0

C
C     PAR(1)=DELESD
C     PAR(2)=DRUDD      THE PARAMETERS, IN DEGREES
C     PAR(3)=DDA
C     PAR(4)=ENGPA  PORT ENGINE THRUST, POUNDS/1000
C     PAR(5)=ENGSA  STARBORD ENGINE THRUST, POUNDS/1000
C     PAR(6)=TPTAL  PITCH THRUST VECTOR, DEG
C     PAR(7)=TYTAL  YAW THRUST VECTOR, DEG
C     PAR(8)=TTHRST  TOTAL THRUST, POUNDS/1000

C     MODIFIED 13 AUG 91
```

```
C     PAR(9)=DELEDD  DIFFERENTIAL ELEVATOR, IN DEGREES
C     PAR(10)=BLEND  TRANSITION PARAMETER FROM STATIC TO
C                    ROTARY BALANCE COEFICIENT DATA

C
      READ(15,*) PAR(1)
      READ(15,*) PAR(2)
      READ(15,*) PAR(3)
      READ(15,*) PAR(4)
      READ(15,*) PAR(5)
      READ(15,*) PAR(6)
      READ(15,*) PAR(7)
      READ(15,*) PAR(8)

C     MODIFIED 13 AUG 91

      READ(15,*) PAR(9)
      READ(15,*) PAR(10)

C
C
      RETURN
      END
C
C
      SUBROUTINE INIT
C     ---------- ----
C
      IMPLICIT DOUBLE PRECISION(A-H,O-Z)
C

      COMMON /BLCSS/ NDIM,ITMX,NPAR,ICP,IID,NMX,IPS,IRS
      COMMON /BLCPS/ NTST,NCOL,IANCH,NMXPS,IAD,NPR,NWTN,ISP,ISW1
      COMMON /BLDLS/ DS,DSMIN,DSMAX,IADS
      COMMON /BLLIM/ RL0,RL1,A0,A1,PAR(10)
      COMMON /BLOPT/ ITNW,MXBF,IPLT,ICP2,ILP
      COMMON /BLEPS/ EPSU,EPSL,EPSS,EPSR
C
C
C IN THIS SUBROUTINE THE USER SHOULD SET THOSE CONSTANTS
C THAT REQUIRE VALUES DIFFERENT FROM THE DEFAULT VALUES
C ASSIGNED IN THE LIBRARY SUBROUTINE DFINIT.  FOR A
C DESCRIPTION OF THESE CONSTANTS SEE THE DOCUMENTATION
C CONTAINED IN THE LIBRARY.  COMMON BLOCKS CORRESPONDING TO
C CONSTANTS THAT THE USER WANTS TO CHANGE MUST BE INSERTED
C ABOVE.  THESE COMMON BLOCKS SHOULD OF COURSE BE IDENTICAL
C TO THOSE IN DFINIT.
C
C
      DSMAX = 10.0d0
```

```
      DSMIN =0.00000010d0
      EPSU  = 1.0D-07
      EPSL  = 1.0D-07
      EPSS  = 1.0D-05
      EPSR  = 1.0D-07
      IAD   = 1
      ILP   = 1
      ITMX  = 40
      ITNW  = 20
      MXBF  = 5
      NDIM  = 8
      NPAR  = 10
C
      OPEN(UNIT=25,FILE='fort.25')
      REWIND (25)
C
      READ(25,*) RL0,RL1
      READ(25,*) A0,A1
      READ(25,*) DS
      READ(25,*) NMX
      READ(25,*) NTST,NCOL,NMXPS,NPR
      READ(25,*) ISP,IRS,ICP,ICP2,IPLT,IPS
      READ(25,*) ISW1
      RETURN
      END
      SUBROUTINE BCND
C     --------- ----
C
      RETURN
      END
C
      SUBROUTINE ICND
C     --------- ----
C
      RETURN
      END
C
C
      SUBROUTINE COEFF(U,PAR,NDIM,ICP)
C
C
      IMPLICIT DOUBLE PRECISION (A-H,O-Z)
      COMMON /ACDATA/ BWING,CWING,SREF,RHO,RMASS
      COMMON /SEIZE/ CX,CY,CZ,CLM,CMM,CNM
      COMMON /SEIZET/CXT,CYT,CZT,CLMT,CMMT,CNMT
      DIMENSION U(NDIM),PAR(10)
C
C
C  THE PRIMARY SOURCE OF THESE COEFFICIENT EQUATIONS IS
C  SUBROUTINE ARO10 FROM MCAIR CODE USED IN THE F15
```

```
C  BASELINE SIMULATOR.
C
C  MOST OF THE COEFFICIENTS USED IN THE EQUATIONS WERE
C  COMPUTED  USING SAS WITH RAW DATA FROM THE F15 SIMULATOR
C  DATA TABLES.
C
C  THIS SUBROUTINE IS CALLED BY THE DRIVER PROGRAM FOR THE
C  AUTO  SOFTWARE.  IT MERELY TAKES INPUTS ON THE A/C
C  STATE, CONTROL  SURFACE POSITIONS, AND THRUST VALUES
C  AND RETURNS THE APPROPRIATE AERO COEFFICIENTS CX, CY,
C  CZ, CL, CM, AND CN.
C
C  INPUTS TO THIS SUBROUTINE
C
C  AL     - ANGLE OF ATTACK, DEG
C  BETA   - SIDESLIP ANGLE, DEG
C  DDA    - AILERON DEFLECTION ANGLE, DEG
C  DELEDD - DIFFERENTIAL TAIL DEFLECTION ANGLE, DEG
C  DELESD - SYMMETRICAL TAIL DEFLECTION ANGLE, DEG
C  DRUDD  - RUDDER DEFLECTION, POSITIVE TRAILING EDGE
C           LEFT, DEG
C  P      - ROLL RATE, RAD/SEC
C  Q      - PITCH RATE, RAD/SEC
C  R      - YAW RATE, RAD/SEC
C  ENGPA  - PORT ENGINE THRUST, POUNDS/1000
C  ENGSA  - STARBOARD ENGINE THRUST, POUNDS/1000
C  TYTAL  - YAW THRUST ANGLE, DEG
C  TPTAL  - PITCH THRUST ANGLE, DEG
C  TTHRST - TOTAL THRUST, POUNDS/1000
C  VTRFPS - TRUE AIRSPEED, FT/SEC
C
C  INTERMEDIATE VARIABLES USED IN THIS SUBROUTINE
C
C  ABET   - ABSOLUTE VALUE OF BETA, DEG
C  ARUD   - ABSOLUTE VALUE OF RUDDER DEFLECTION, DEG
C  BWING  - WING SPAN, FEET
C  CA     - COSINE RAL (RAL IN RADIANS)
C  CD     - COEFFICIENT OF DRAG
C  CL     - BASIC LIFT COEFFICIENT
C  CWING  - MEAN AERODYNAMIC CHORD, FEET
C  DAHD   - DIFFERENTIAL ELEVATOR DEFLECTION, DEG
C  DAHLD  - LEFT AILERON DEFLECTION, DEG
C  DAHRD  - RIGHT AILERON DELFECTION, DEG
C  DELEDR - DIFFERENTIAL TAIL DEFLECTION ANGLE, RAD
C  DELESR - SYMMETRIC TAIL DEFLECTION ANGLE, RAD
C  ENGP   - PORT ENGINE THRUST, POUNDS
C  ENGS   - STARBOARD ENGINE THRUST, POUNDS
C  PTAL   - PITCH THRUST VECTOR, RAD
C  QBARS  - DYNAMIC PRESSURE TIMES WING REFERENCE AREA,
C           LBF
```

```
C  RABET   - ABSOLUTE VALUE OF BETA, RADIANS
C  RAL     - ABSOLUTE VALUE OF ALPHA, RADIANS
C  RARUD   - ABSOLUTE VALUE OF RUDDER, RADIANS
C  SA      - SINE RAL (RAL IN RADIANS)
C  YTAL    - YAW THRUST VECTOR, RAD
C
C
C

C  OUTPUTS FROM THIS SUBROUTINE
C
C  CX      - BASIC AXIAL FORCE COEFFICIENT, BODY AXIS,
C            + FORWARD
C  CY      - BASIC SIDE FORCE COEFFICIENT, BODY AXIS,
C            + RIGHT
C  CZ      - BASIC NORMAL FORCE COEFFICIENT, BODY AXIS,
C            + DOWN
C  CLM     - BASIC ROLLING MOMENT COEFFICIENT, BODY AXIS,
C            + R WING DOWN
C  CMM     - BASIC PITCHING MOMENT COEFFICIENT, BODY AXIS,
C            + NOSE UP
C  CNM     - BASIC YAWING MOMENT COEFFICIENT, BODY AXIS,
C            + NOSE RIGHT
C
C   ANGLES USED IN CALCULATING CL, CLLDB, ..., ARE IN
C   RADIANS. THIS IS BECAUSE RADIANS WERE USED IN THE CURVE
C   FITTING PROGRAM TO OBTAIN THE COEFFICIENTS OF THE
C   ALPHA, BETA, ..., TERMS IN THE
C   FOLLOWING EQUATIONS.
C
C
C  MOMENT REFERENCE CENTER WAS SET IN ARO10 PROGRAM AS:
C
C    DATA CMCGR /.2565/, CNCGR /.2565/
C
C  THE AERO STABILITY DATA WAS TAKEN REFERENCED TO THESE CG
C  LOCATIONS.  THE MOMENTS OF INERTIA AND OTHER AIRCRAFT
C  DATA  ARE FOR A CLEAN CONFIGURATION TEST AIRCRAFT WITH A
C  CG AT THE SAME CG.  AS A RESULT, THERE IS NO 'CG OFFSET'
C  TO BE COMPUTED.
C
      IWRITE=0
C
      AL=U(1)
      BETA=U(2)
      P=U(3)
      Q=U(4)
      R=U(5)
      THETA=U(6)
      PHI=U(7)
```

```
      VTRFPS=U(8)*1000.
C
      DELESD=PAR(1)
      DRUDD=PAR(2)
      DDA=PAR(3)
      ENGPA=PAR(4)
      ENGSA=PAR(5)
      TPTAL=PAR(6)
      TYTAL=PAR(7)
      TTHRST=PAR(8)
C
      DEGRAD=57.29577951
      DELESR=DELESD/DEGRAD
      YTAL=TYTAL/DEGRAD
      PTAL=TPTAL/DEGRAD
C
C     IF BLOCK TO CHANGE TOTAL THRUST
C
      IF(ICP.EQ.8)THEN
        DIFT=PAR(4)-PAR(5)
        THALF=TTHRST/2.0d0
        ENGPA=THALf+DIFT/2.0d0
        ENGSA=THALF-DIFT/2.0d0
      ENDIF
C
      ENGP=ENGPA*1000.0
      ENGS=ENGSA*1000.0
C
      QBARS=0.5d0*RHO*VTRFPS*VTRFPS*SREF
      CO2V=CWING/(2.0d0*VTRFPS)
      BO2V=BWING/(2.0d0*VTRFPS)
      QSB=BWING*QBARS
      ARUD=ABS(DRUDD)
      RARUD=ARUD/DEGRAD
      RAL=AL/DEGRAD
      ABET=ABS(BETA)
      RABET=ABET/DEGRAD
C
C
C

C*************************************************************
C
C
C
C                    1) ALL THE AERODYNAMIC COEFFICIENTS IN
C                      THIS VERSION OF THE DRIVER PROGRAM
C                      ARE TAKEN DIRECTLY FROM THE 1988
C                      F15 AEROBASE (0.6 MACH, 20000 FEET)
C
```

```
C                    2) THIS SECTION SUMMARIZES THE
C                      AERODYNAMIC COEFFICIENTS AS TO WHAT
C                      THEY ARE AND HOW THEY ARE USED.
C                      THE FIRST ACCRONYM IS THE JOVIAL
C                      NAME OF THE AERODYNAMIC COEFFICIENT
C                      (CFX1, ETC), THE SECOND ACCRONYM IS
C                      THE F15 AEROBASE CODE OR CTAB NAME
C                      (ATAB15, ETC).  A BRIEF DEFINITION
C                      OF THE AERODYNAMIC COEFFICIENT IS
C                      ALSO PROVIDED.
C
C                    3) THERE IS ALSO A SECTION THAT
C                      PROVIDES A TABLE OF CONVERSIONS
C                      BETWEEN WHAT THE VARIABLE IS CALLED
C                      IN THE OR SECTION OF THIS PROGRAM
C                      AND ITS NAME IN THE 1988 F15
C                      AEROBASE.  FOR THE SAKE OF
C                      CONTINUITY THE ORIGINAL PROGRAM NAME
C                      IS USED AND THE 1988 F15 AEROBASE
C                      NAME IS PROVIDED AS BOOK KEEPING
C                      INFORMATION.
C
C
C*****************************************************************
C
C
C  CFX = FORCE IN STABILITY AXIS X DIRECTION (CD IN BODY AXIS)
C       (FUNCTION OF CL OR CFZ1)
C  CFX = CFX1 + CXRB + STORE INCREMENTS + CXDSPD + DCXLG + DCD
C
C  CFX1 = ATAB15 = PERFORMANCE DRAG COEFFICIENT - CD
C  CXRB = ATAB22 = DELTA CD DUE TO CG (=0.0)
C  CXDSPD = ATAB27 = DELTA CD DUE TO SPEEDBRAKE (NORMALLY = 0.0436)
C                SET TO 0 SINCE THIS STUDY IS CONCERNED
C                WITH HIGH ANGLES
C                OF ATTACK PHENOMENON (>40 DEGREES) AND BECAUSE
C                THE SPEEDBRAKE WILL NOT DEPLOY AT ANGLES OF
C                ATTACK GREATER THAN 15 DEGREES.
C  DCXLG = ATAB19 = DELTA CD DUE TO REYNOLD'S NUMBER  (=-0.0005)
C  DCD = BTAB03 = DELTA CD DUE TO 2-PLACE CANOPY (F15B) (=0.0005)
C       ******* NOTE THAT DCXLG AND DCD CANCEL EACH OTHER *******
C
C
C*****************************************************************
C
C
C  CFY = FORCE IN BODY AXIS Y DIRECTION
C  CFY = CFY1*EPA02 + CYDAD*DAILD + [CYDRD*DRUDD*DRFLX5]*EPA43
C       +[CYDTD*DTFLX5 + DTFLX6]*DTALD + CFYP*PB + CFYR*RB
C       +CYRB + STORE INCREMENTS + DCYB*BETA
```

```
C
C  CFY1  = ATAB16 = BASIC SIDE FORCE COEFFICIENT - CY(BETA)
C  EPA02 = ATAB21 = BETA MULTIPLIER TABLE
C  CYDAD = ATAB75 = SIDE FORCE COEFFICIENT DUE TO AILERON
C                   DEFLECTION
C  DAILD          = AILERON DEFLECTION (DEG)
C  CYDRD = ATAB69 = SIDE FORCE COEFFICIENT DUE TO RUDDER DEFLECTION
C  DRUDD          = RUDDER DEFLECTION  (DEG)
C  DRFLX5 = ATAB88 = FLEX MULTIPLIER ON CYDRD (=0.89)
C  EPA43 = ATAB30 = MULTIPLIER ON CNDR, CLDR, CYDR DUE TO
C                   SPEEDBRAKE
C                   (=1.0)
C  CYDTD = ATAB72 = SIDE FORCE COEFFICIENT DUE TO DIFFERENTIAL TAIL
C                   DEFLECTION - CYDDT
C  DTFLX5 = ATAB10 = FLEX MULTIPLIER ON CYDTD (=0.975)
C  DTFLX6 = ATAB77 = FLEX INCREMENT TO CYDTD (=0.0)
C  DTALD          = DIFFERENTIAL TAIL DEFLECTION (DEG) WHICH IS
C                   DIRECTLY PROPORTIONAL TO AILERON DEFLECTION
C                   AND IS PRIMARILY USED TO ASSIST IN ROLLING THE
C                   F-15B (DTALD=0.3*DAILD)
C  CFYP = ATAB13 = SIDE FORCE COEFFICIENT DUE TO ROLL RATE (CYP)
C  PB             = (PEOBB*SPAN)/(2*VILWF)
C                   PEOBB = ROLL RATE IN RAD/SEC = P
C                   SPAN = WING SPAN = 42.8 FEET = BWING
C                   VILWF = VELOCITY IN FT/SEC = VTRFPS
C  CFYR = ATAB07 = SIDE FORCE COEFFICIENT DUE TO YAW RATE (CYR)
C  RB             = (REOBB*SPAN)/(2*VILWF)
C                   REOBB = YAW RATE IN RAD/SEC = R
C  CYRB = ATAB93 = ASSYMETRIC CY AT HIGH ALPHA (ANGLE OF ATTACK)
C  DCYB           = 0.0  THERE IS NO INCREMENT DELTA CYB (SIDE
C                     FORCE)
C                  DUE TO A 2-PLACE CANOPY ON THE F15B.  THIS IS
C                  BECAUSE THE SAME CANOPY IS USED ON BOTH THE
C                  BASELINE F15A AND THE F15B.  THE SIDEFORCE IS
C                  THE SAME FOR BOTH VERSIONS OF THE F15 AND
C                  ALREADY INCLUDED IN THE BASIC SIDE FORCE (CFY1).
C                  THE TWO PLACE CANOPY IS MOUNTED DIFFERENTLY
C                  HOWEVER, SO  THERE IS A DIFFERENCE IN YAWING AND
C                  ROLLING MOMENT.
C                  (SEE DCNB AND DCLB)
C
C
C*****************************************************************
C
C
C  CFZ = FORCE IN STABILITY AXIS Z DIRECTION (CL IN BODY AXIS)
C  CFZ = CFZ1 + CZDSPD + STORE INCREMENTS + DCL*BETA
C
C
C  CFZ1 = ATAB17 = BASIC LIFT COEFFICIENT - CL
```

```
C  CZDSPD = ATAB26 = DELTA CL DUE TO SPEEDBRAKE
C                SET TO 0 DUE TO THE REASONS GIVEN ABOVE IN
C                CXDSPD
C  DCL = BTAB01 = DELTA CL DUE TO 2-PLACE CANOPY (F15B) (=0.0)
C
C
C*****************************************************************
C
C
C  CML = TOTAL ROLLING MOMENT COEFFICIENT IN BODY AXIS
C  CML = CML1*EPA02 + CLDAD*DAILD + [CLDRD*DRUDD*DRFLX1]*EPA43 +
C       [CLDTD*DTFLX1 + DTFLX2]*DTALD + CMLP*PB + CMLR*RB +
C       STORE INCREMENTS + CLDSPD + DCLB*BETA
C
C
C  CML1 = ATAB01 = BASIC ROLLING MOMENT COEFFICIENT - CL(BETA)
C  EPA02 = ATAB21 = BETA MULTIPLIER TABLE
C  CLDAD = ATAB73 = ROLL MOMENT COEFFICIENT DUE TO AILERON
C                DEFLECTION
C                -(CLDA)
C  DAILD          = AILERON DEFLECTION (DEG)
C  CLDRD = ATAB67 = ROLLING MOMENT COEFFICIENT DUE TO RUDDER
C                DEFLECTION  -(CLD)
C  DRUDD          = RUDDER DEFLECTION (DEG)
C  DRFLX1 = ATAB80 = FLEX MULTIPLIER ON CLDRD (=0.85)
C  EPA43 = ATAB30 = MULTIPLIER ON CNDR, CLDR, CYDR DUE TO
C                SPEEDBRAKE
C                (=1.0)
C  CLDTD = ATAB70 = ROLL MOMENT COEFFICIENT DUE TO DIFFERENTIAL
C                TAIL
C                DEFLECTION - CLDD
C  DTFLX1 = ATAB04 = FLEX MULTIPLIER ON CLDTD (=0.975)
C  DTFLX2 = ATAB84 = FLEX INCREMENT TO CLDTD (=0.0)
C  DTALD          = DIFFERENTIAL TAIL DEFLECTION (DEG) WHICH IS
C                 DIRECTLY PROPORTIONAL TO AILERON DEFLECTION
C                 AND IS PRIMARILY USED TO ASSIST IN ROLLING THE
C                 F-15B
C                 (DTALD = 0.3*DAILD)
C  CMLP = ATAB02 = ROLL DAMPING DERIVATIVE -CLP
C  PB           = (PEOBB*SPAN)/(2*VILWF)
C                PEOBB = ROLL RATE IN RAD/SEC = P
C                SPAN = WING SPAN = 42.8 FEET = BWING
C                VILWF = VELOCITY IN FT/SEC = VTRFPS
C  CMLR = ATAB11 = ROLLING MOMENT COEFFICIENT DUE TO YAW RATE - CLR
C  RB           = (REOBB*SPAN)/(2*VILWF)
C                REOBB = YAW RATE IN RAD/SEC = R
C  CLDSPD = ATAB29 = DELTA CL DUE TO SPEEDBRAKE
C                 SET TO 0 DUE TO THE REASONS GIVEN ABOVE IN
C                 CXDSPD
C  DCLB = BTAB04 = INCREMENT DELTA CLB (ROLLING MOMENT) DUE TO
```

```
C              2-PLACE
C              CANOPY FROM PSWT 499
C
C
C*****************************************************************
C
C
C  CMM = TOTAL PITCHING MOMENT COEFFICIENT IN STABILITY AXIS
C       (BODY AXIS - AS WELL)
C  CMM = CMM1 + CMMQ*QB + STORE INCREMENTS + CMDSPD + DCM
C
C  CMM1 = ATAB03 = BASIC PITCHING MOMENT COEFFICIENT - CM
C  CMMQ = ATAB05 = PITCH DAMPING DERIVATIVE - CMQ
C  QB           = (QEOBB*MAC)/(2*VILWF)
C               QEOBB = PITCH RATE IN RAD/SEC = Q
C               MAC = MEAN AERODYNAMIC CHORD = 15.94 FEET = CWING
C               VILWF = VELOCITY IN FT/SEC = VTRFPS
C  CMDSPD = ATAB25 = DELTA CM DUE TO SPEEDBRAKE
C                 SET TO 0 DUE THE REASONS GIVEN ABOVE IN CXDSPD
C  DCM = BTAB02 = DELTA CM DUE TO 2-PLACE CANOPY (F15B) (=0.0)
C
C
C*****************************************************************
C
C
C
C  CMN = TOTAL YAWING MOMENT COEFFICIENT IN BODY AXIS
C  CMN = CMN1*EPA02 + CNDAD*DAILD + [CNDRD*DRUDD*DRFLX3]*EPA43
C       +[CNDTD*DTLX3 + DTFLX4]*DTALD + CMNP*PB + CMNR*RB + CNRB
C       +DCNB2*EPA36 + STORE INCREMENTS + CNDSPD + DCNB*BETA
C
C
C  CMN1 = ATAB12 = BASIC YAWING MOMENT COEFFICIENT  - CN (BETA)
C  EPA02 = ATAB21 = BETA MULTIPLIER TABLE
C  CNDAD = ATAB74 = YAW MOMENT COEFFICIENT DUE TO AILERON
C                DEFLECTION -CNDA
C  DAILD =        = AILERON DEFLECTION (DEG)
C  CNDRD = ATAB68 = YAWING MOMENT COEFFICIENT DUE TO RUDDER
C                DEFLECTION -CNDR
C  DRUDD          = RUDDER DEFLECTION (DEG)
C  DRFLX3 = ATAB85 = FLEX MULTIPLIER ON CNDRD
C  EPA43 = ATAB30 =  MULTIPLIER ON CNDR, CLDR, CYDR DUE TO SPEEDBRAKE
C  CNDTD = ATAB71 = YAWING MOMENT COEFFICIENT DUE TO DIFFERENTIAL TAIL
C                DEFLECTION - CNDDT
C  DTFLX3 = ATAB08 = FLEX MULTIPLIER ON CNDTD
C  DTFLX4 = ATAB09 = FLEX INCREMENT ON CNDTD  (=0.0)
C  DTALD =         = DIFFERENTIAL TAIL DEFLECTION (DEG) WHICH IS
C                DIRECTLY PROPORTIONAL TO AILERON DEFLECTION
C                AND IS PRIMARILY USED TO ASSIST IN ROLLING
C                THE F-15B (DTALD = 0.3*DAILD)
```

```
C  CMNP = ATAB06 = YAWING MOMENT COEFFICIENT DUE TO ROLL RATE - CNP
C  PB          = (PEOBB*SPAN)/(2*VILWF)
C               PEOBB=ROLL RATE IN RAD/SEC = P
C               SPAN = WING SPAN = 42.8 FT = BWING
C               VILWF = VELOCITY IN FT/SEC = VTRFPS
C  CMNR = ATAB14 = YAW DAMPING DERIVATIVE - CNR
C  RB          = (REOBB*SPAN)/(2*VILWF)
C               REOBB = YAW RATE IN RAD/SEC = R
C  CNRB = ATAB86 = ASSYMETRIC CN AT HIGH ALPHA
C  DCNB2 = ATAB44 = DELTA CNB WITH STABILATOR EFFECT - DELCNB (=0.0)
C  EPA36 = ATAB94 = MULTIPLIER ON DCNB2  (=BETA)
C  CNDSPD = ATAB28 = DELTA CN DUE TO SPEEDBRAKE
C                SET TO 0 DUE TO THE REASONS GIVEN ABOVE IN CXDSPD
C  DCNB = BTAB05 = INCREMENT DELTA CNB (YAWING MOMENT) DUE TO
C               2-PLACE CANOPY (F15B)
C
C
C*********************************************************************
C
C
C
C  MISCELLANEOUS COEFFICIENTS AND NAME CONVERSION TABLE
C
C
C     1988 F15            ORIGINAL
C     AEROBASE NAME       PROGRAM NAME      DEFINITION
C     *************       ************      **********
C
C     AL77D               AL                ANGLE OF ATTACK
C                                           (DEG)
C     BE77D               BETA              SIDESLIP ANGLE
C                                           (DEG)
C     BE77D               RBETA             SIDESLIP ANGLE
C                                           (RAD)
C     BO77D               ABET              ABSOLUTE VALUE OF
C                                           SIDESLIP ANGLE
C                                           (DEG)
C     DAILA               DAILA             ABSOLUTE VALUE OF
C                                           AILERON DEFLEC-
C                                           TION (DEG)
C     DAILD               DDA               AILERON DEFLEC-
C                                           TION (DEG)
C     DRUABS              ARUD              ABSOLUTE VALUE OF
C                                           RUDDER DEFLEC-
C                                           TION (DEG)
C     DRUABS              RARUD             ABSOLUTE VALUE OF
C                                           RUDDER DEFLEC-
C                                           TION (RAD)
C     DRUDD               DRUDD             RUDDER DEFLECTION
C                                           (DEG)
```

```
C     DSTBD              DELESD(R)          AVERAGE
C                                         STABILATOR
C                                         DEFLECTION
C                                         DEG (RAD)
C     DTALD              DELEDD(R)          DIFFERENTIAL TAIL
C                                         DEFLECTION
C                                         DEG (RAD)
C
      RBETA=BETA/DEGRAD
      DAILA=ABS(DDA)
C
C
C
C
C
      PB=(P*BWING)/(2.0d0*VTRFPS)
      QB=(Q*CWING)/(2.0d0*VTRFPS)
      RB=(R*BWING)/(2.0d0*VTRFPS)
C
C     THE F-15B AERO DATA TABLES DO NOT CONTAIN STABILITY COEFFICIENT
C     DATA FOR BETA AND RUDDER DEFLECTION ,DRUDD, LESS THAN 0
C     DEGREES.  THE ABSOLUTE VALUE OF BETA, ABET, AND THE ABSOLUTE
C     VALUE OF RUDDER DEFLECTION, ARUDD, ARE USED IN THE FOLLOWING
C     EQ' ATIONS.  IN RADIANS THESE PARAMETERS ARE RABET AND RARUD,
C     RESPECTIVELY.  IN SOME CASES THE COEFFICIENT IS MULTIPLIED BY A
C     -1 FOR PARAMETER VALUES LESS THAN ZERO.
C
C     EPA02 IS A MULTIPLIER THAT ADJUSTS THE PARTICULAR COEFFICIENT
C     IT IS WORKING ON (CFY1,CML1,CMN1) BY CHANGING THAT PARTICULAR
C     COEFFICIENTS SIGN (POSITIVE OR NEGATIVE) DEPENDENT ON THE SIGN
C     OF THE SIDESLIP ANGLE (BETA).  IF BETA IS NEGATIVE THEN
C     EPA02=-1.0.  IF BETA IS POSITIVE THEN EPA02=1.0.  SINCE THIS
C     FUNCTION IS DISCONTINUOUS AT THE ORIGIN A CUBIC SPLINE HAS
C     BEEN EMPLOYED TO REPRESENT THIS FUNCTION IN ORDER THAT
C     AUTO CAN RUN.
C
C
      IF (BETA .LT. -1.0) THEN
      EPA02S= -1.0d0
      ENDIF
C
      IF ((BETA .GE. -1.0) .AND. (BETA .LE. 1.0)) THEN
      EPA02S=-1.0d0+(1.50d0*((BETA+1.0d0)**2.0d0))-
     1 (0.50d0*((BETA+1.0d0)**3.0d0))
      ENDIF
C
      IF (BETA .GT. 1.0) THEN
      EPA02S=1.0d0
      ENDIF
C
```

```
      IF (BETA .LT. -5.0) THEN
      EPA02L= -1.0d0
      ENDIF
C
      IF ((BETA .GE. -5.0) .AND. (BETA .LE. 5.0)) THEN
      EPA02L=-1.0d0+(0.060d0*((BETA+5.0d0)**2.0d0))-
     1 (0.0040d0*((BETA+5.0d0)**3.0d0))
      ENDIF
C
      IF (BETA .GT. 5.0) THEN
      EPA02L=1.0d0
      ENDIF
C
C
C       DTALD=0.30d0*DAILD
      DELEDD=0.30d0*DDA
      DELEDR=0.30d0*(DDA/DEGRAD)
C
C
C
C*****************************************************************
C
C
C
C
      CFZ1=-0.00369376+(3.78028702*RAL)+(0.6921459*RAL*RAL)-(5.0005867
     +*(RAL**3))+(1.94478199*(RAL**4))+(0.40781955*DELESR)+(0.10114579
     +*(DELESR*DELESR))
C
      CFZ=CFZ1
C
C
C*****************************************************************
C
C
C
C
C
      CL=CFZ1/57.29578
C
C     THIS CONVERSION OF CFZ1 TO CL IS AN ARTIFACT FROM THE
C     CURVE FITTING PROCESS WHERE ALL THE INDEPENDENT VARIABLES
C     WERE ANGLES THAT WERE CONVERTED FROM DEGREES TO RADIANS.
C     IT JUST SO HAPPENED THAT FOR CFX1 ONE OF THE VARIABLES
C     WAS NOT AN ANGLE BUT A DIMENSIONLESS COEFFICIENT.
C
C
      CFX1=0.01806821+(0.01556573*CL)+(498.96208868*CL*CL)
     +-(14451.56518396*(CL**3))+(2132344.6184755*(CL**4))
C
```

```
C     TRANSITIONING FROM LOW AOA DRAG TABLE TO HIGH AOA DRAG TABLE
C
      CFX2=0.0267297-(0.10646919*RAL)+(5.39836337*RAL*RAL)
     +-(5.0086893*(RAL**3))+(1.34148193*(RAL**4))+
     +(0.20978902*DELESR)+(0.30604211*(DELESR**2))+0.09833617
C
      A1=20.0d0/DEGRAD
      A2=30.0d0/DEGRAD
      A12=A1+A2
      BA=2.0/(-A1**3+3.*A1*A2*(A1-A2)+A2**3)
      BB=-3.0d0*BA*(A1+A2)/2.0d0
      BC=3.0d0*BA*A1*A2
      BD=BA*A2**2*(A2-3.0d0*A1)/2.0d0
      F1=BA*RAL**3+BB*RAL**2+BC*RAL+BD
      F2=-BA*RAL**3+(3.0d0*A12*BA+BB)*RAL**2.0d0-
     +   (BC+2.0d0*A12*BB+3.0d0*A12**2*BA)*RAL+
     +   BD+A12*BC+A12**2*BB+A12**3*BA
C
      IF (RAL .LT. A1) THEN
C
        CFX=CFX1
C
      ELSEIF (RAL .GT. A2) THEN
C
        CFX=CFX2
C
      ELSE
C
        CFX=CFX1*F1+CFX2*F2
C
      ENDIF
C
C
C*****************************************************************
C
C
      DTFLX5=0.975d0
      DRFLX5=0.89d0
C
      CFY1=-0.05060386-(0.12342073*RAL)+(1.04501136*RAL*RAL)
     +-(0.17239516*(RAL**3))-(2.90979277*(RAL**4))
     ++(3.06782935*(RAL**5))-(0.88422116*(RAL**6))
     +-(0.06578812*RAL*RABET)-(0.71521988*RABET)-(0.00000475273
     +*(RABET**2))-(0.04856168*RAL*DELESR)-(0.05943607*RABET*DELESR)+
     +(0.02018534*DELESR)
C
      IF (RAL .LT. .52359998) THEN
C
      CFYP=0.014606188+(2.52405055*RAL)-(5.02687473*(RAL**2))
     +-(106.43222962*(RAL**3))+(256.80215423*(RAL**4))
```

```
     ++(1256.39636248*(RAL**5))
     +-(3887.92878173*(RAL**6))-(2863.16083460*(RAL**7))+
     +(17382.72226362*(RAL**8))-(13731.65408408*(RAL**9))
      ENDIF
C
      IF ((RAL .GE. .52359998) .AND. (RAL .LE. .610865)) THEN
C
      CFYP=0.00236511+(0.52044678*(RAL-0.52359998))-(12.8597002*(RAL-
     +0.52359998)**2)+(75.46138*(RAL-0.52359998)**3)
      ENDIF
C
      IF (RAL .GT. 0.610865) THEN
C
      CFYP=0.0d0
      ENDIF
C
      IF (RAL .LT. -0.06981) THEN
C
      CFYR=0.35d0
      ENDIF
C
      IF ((RAL .GE. -0.06981) .AND. (RAL .LT. 0.0)) THEN
C
      CFYR=0.34999999+(35.4012413*(RAL+0.06981)**2)-(493.33441162*
     +(RAL+0.06981)**3)
      ENDIF
C
      IF ((RAL .GE. 0.0) .AND. (RAL .LE. 0.523599)) THEN
C
      CFYR=0.35468605-(2.26998141*RAL)+(51.82178387*RAL*RAL)
     +-(718.55069823*(RAL**3))
     ++(4570.00492172*(RAL**4))-(14471.88028351*(RAL**5))+
     +(22026.58930662*(RAL**6))-(12795.99029404*(RAL**7))
      ENDIF
C
      IF ((RAL .GT. 0.523599) .AND. (RAL .LE. 0.61087)) THEN
C
      CFYR=0.00193787+(1.78332496*(RAL-0.52359903))-(41.63198853*(RAL-
     +0.52359903)**2)+(239.97909546*(RAL-0.52359903)**3)
      ENDIF
C
      IF (RAL .GT. 0.61087) THEN
C
      CFYR=0.0d0
      ENDIF
C
      IF (RAL .LT. 0.55851) THEN
C
      CYDAD=-0.00020812+(0.00062122*RAL)+(0.00260729*RAL*RAL)
     ++(0.00745739*(RAL**3))-(0.0365611*(RAL**4))
```

```
     +-(0.04532683*(RAL**5))+(0.20674845*(RAL**6))
     +-(0.13264434*(RAL**7))-(0.00193383*(RAL**8))
      ENDIF
C
      IF ((RAL .GE. 0.55851) .AND. (RAL .LT. 0.61087)) THEN
C
      CYDAD=0.00023894+(0.00195121*(RAL-0.55851001))+(0.02459273
     +*(RAL-0.55851001)**2)-(0.1202244*((RAL-0.55851001)**3))
      ENDIF
C
      IF (RAL .GE. 0.61087) THEN
C
      CYDAD=0.27681285-(2.02305395*RAL)+(6.01180715*RAL*RAL)
     +-(9.24292188*(RAL**3))+(7.59857819*(RAL**4))
     +-(2.8565527*(RAL**5))+(0.25460503*(RAL**7))
     +-(0.01819815*(RAL**9))
      ENDIF
C
C
C     IF (RAL .LE. 0.0) THEN
C     EPA43=1.0d0
C     ENDIF
C     IF (RAL .GT. 0.0 AND .LE. 0.6283185) THEN
C     0.6283185 RADIANS = 36 DEGREES
C     EPA43=0.9584809+(4.13369452*RAL)-(18.31288396*RAL*RAL)+
C     +(19.5511466*(RAL**3))-(1.09295946*RAL*DSPBD)+(0.17441033*
C     +DSPBD*DSPBD)
C     ENDIF
C     IF (RAL .GT. 0.6283185) THEN
      EPA43=1.0d0
C     ENDIF
C          ************************************************************
C          * NOTE - THE PARAMETER EPA43 IS A MULTIPLIER ON RUDDER
C          * EFFECTIVENESS DUE TO SPEEDBRAKE.  THIS TABLE IS ALSO
C          * LIMITED TO 36 DEG AOA.  HOWEVER, THERE IS NO AERODY
C          * NAMIC EFFECT FOR ANGLES OF ATTACK LESS THAN 16 DEG,
C          * AND THE SPEEDBRAKE IS AUTOMATICALLY RETRACTED AT AOA
C          * GREATER THAN 15 DEG.  THEREFORE, THIS TABLE SHOULD
C          * NOT BE NECESSARY FOR THE ORDINARY OPERATION OF THE
C          * AIRCRAFT
C          ************************************************************
C
      CYDRD=0.00310199+(0.00119963*RAL)+(0.02806933*RAL*RAL)
     +-(0.12408447*(RAL**3))-(0.12032121*(RAL**4))
     ++(0.79150279*(RAL**5))-(0.86544347*(RAL**6))
     ++(0.27845115*(RAL**7))+(0.00122999*RAL*RARUD)+(0.00145943
     +*RARUD)-(0.01211427*RARUD*RARUD)+(0.00977937*(RARUD**3))
C
      CYDTD=-0.00157745-(0.0020881*RAL)+(0.00557239*RAL*RAL)
     +-(0.00139886*(RAL**3))+(0.04956247*(RAL**4))
```

```
     +-(0.0135353*(RAL**5))-(0.11552397*(RAL**6))
     ++(0.11443452*(RAL**7))-(0.03072189*(RAL**8))-(0.01061113*
     +(RAL**3)*DELESR)-(0.00010529*RAL*RAL*DELESR*DELESR)
     +-(0.00572463*RAL*DELESR*DELESR)
     ++(0.01885361*RAL*RAL*DELESR)-(0.01412258*RAL*(DELESR**3))
     +-(0.00081776*DELESR)+(0.00404354*(DELESR**2))-
     +(0.00212189*(DELESR**3))+(0.00655063*(DELESR**4))
     ++(0.03341584*(DELESR**5))
C
      RALY1=0.6108652
      RALY2=90.0d0/DEGRAD
      RBETY1=-0.0872665
      RBETY2=0.1745329
C
      AY=0.1640d0
      ASTARY=0.95993
      BSTARY=0.087266
C
      ZETAY=(2.0D0*ASTARY-(RALY1+RALY2))/(RALY2-RALY1)
      ETAY=(2.0D0*BSTARY-(RBETY1+RBETY2))/(RBETY2-RBETY1)
C
      X=(2.0D0*RAL-(RALY1+RALY2))/(RALY2-RALY1)
      Y=(2.0D0*RBETA-(RBETY1+RBETY2))/(RBETY2-RBETY1)
C
      FY=((5.0D0*(ZETAY**2))-(4.0D0*ZETAY*X)-1.0D0)*(((X**2)-1.0D0)
     +**2)*(1.0D0/(((ZETAY**2)-1.0D0)**3))
C
      GY=((5.0D0*(ETAY**2))-(4.0D0*ETAY*Y)-1.0D0)*(((Y**2)-1.0D0)**2)
     +*(1.0D0/(((ETAY**2)-1.0D0)**3))
C
      CYRB=AY*FY*GY
C
      IF (RAL .LT. 0.6108652) THEN
C
      CYRB=0.0d0
      GOTO 500
      ENDIF
C
      IF ((RBETA .LT. -0.0872665) .OR. (RBETA .GT. 0.1745329)) THEN
C
      CYRB=0.0d0
      GOTO 500
      ENDIF
C
 500  CFY=(CFY1*EPA02L)+(CYDAD*DDA)+(CYDRD*DRUDD*DRFLX5*EPA43)+
     +((CYDTD*DTFLX5)*DELEDD)+(CFYP*PB)+(CFYR*RB)
     ++CYRB
C
C
C*****************************************************************
```

```
C
C
C
      DTFLX1=0.9750d0
      DRFLX1=0.850d0
C
      CML1=-0.00238235-(0.04616235*RAL)+(0.10553168*RAL*RAL)
     ++(0.10541585*(RAL**3))-(0.40254765*(RAL**4))
     ++(0.32530491*(RAL**5))-(0.08496121*(RAL**6))
     ++(0.00112288*(RAL**7))-(0.05940477*RABET*RAL)-
     +(0.07356236*RABET)-(0.00550119*RABET*RABET)+(0.00326191
     +*(RABET**3))
C
      IF (RAL .LT. 0.29671) THEN
C
      CMLP=-0.24963201-(0.03106297*RAL)+(0.12430631*RAL*RAL)
     +-(8.95274618*(RAL**3))+(100.33109929*(RAL**4))
     ++(275.70069578*(RAL**5))-(1178.83425699*(RAL**6))
     +-(2102.66811522*(RAL**7))+(2274.89785551*(RAL**8))
      ENDIF
C
      IF ((RAL .GE. 0.29671) .AND. (RAL .LT. 0.34907)) THEN
C
      CMLP=-0.1635261-(3.77847099*(RAL-0.29671001))+(147.47639465
     +*(RAL-0.29671001)**2)-(1295.94799805*(RAL-0.29671001)**3)
      ENDIF
C
      IF (RAL .GE. 0.34907) THEN
C
      CMLP=-1.37120291+(7.06112181*RAL)-(13.57010422*RAL*RAL)
     ++(11.21323850*(RAL**3))
     +-(4.26789425*(RAL**4))+(0.6237381*(RAL**5))
      ENDIF
C
      IF (RAL .LT. 0.7854) THEN
C
      CMLR=0.03515391+(0.59296381*RAL)+(2.27456302*RAL*RAL)
     +-(3.8097803*(RAL**3))
     +-(45.83162842*(RAL**4))+(55.31669213*(RAL**5))+
     +(194.29237485*(RAL**6))-(393.22969953*(RAL**7))+(192.20860739*
     +(RAL**8))
      ENDIF
C
      IF ((RAL .GE. 0.7854) .AND. (RAL .LE. 0.87266)) THEN
C
      CMLR=0.0925579071-(0.6000000238*(RAL-0.7853999734))
     ++(1.3515939713*((RAL-0.7853999734)**2))
     ++(29.0733299255*((RAL-0.7853999734)**3))
      ENDIF
C
```

```
      IF (RAL .GT. 0.87266) THEN
C
      CMLR=-311.126041+(1457.23391042*RAL)-(2680.19461944*RAL*RAL)+
     +(2361.44914738*(RAL**3))-(893.83567263*(RAL**4))+(68.23501924*
     +(RAL**6))-(1.72572994*(RAL**9))
      ENDIF
C
      CLDAD=0.00057626+(0.00038479*RAL)-(0.00502091*RAL*RAL)
     ++(0.00161407*(RAL**3))+(0.02268829*(RAL**4))
     +-(0.03935269*(RAL**5))+(0.02472827*(RAL**6))
     +-(0.00543345*(RAL**7))+(0.0000007520348*DELESR*RAL)+
     +(0.000000390773*DELESR)
C
      CLDRD=0.00013713-(0.00035439*RAL)-(0.00227912*RAL*RAL)
     ++(0.00742636*(RAL**3))+(0.00991839*(RAL**4))
     +-(0.04711846*(RAL**5))+(0.046124*(RAL**6))
     +-(0.01379021*(RAL**7))+(0.00003678685*RARUD*RAL)+
     +(0.00001043751*RARUD)-(0.00015866*RARUD*RARUD)+(0.00016133
     +*(RARUD**3))
C
      CLDTD=0.00066663+(0.00074174*RAL)+(0.00285735*RAL*RAL)
     +-(0.02030692*(RAL**3))-(0.00352997*(RAL**4))
     ++(0.0997962*(RAL**5))-(0.14591227*
     +(RAL**6))+(0.08282004*(RAL**7))
     +-(0.0168667*(RAL**8))+(0.00306142*(RAL**3)*DELESR)
     +-(0.00110266*RAL*RAL*(DELESR**2))+(0.00088031*RAL*
     +(DELESR**2))-(0.00432594*RAL*RAL*DELESR)-
     +(0.00720141*RAL*(DELESR**3))
     +-(0.00034325*DELESR)+(0.00033433*(DELESR**2))+(0.00800183
     +*(DELESR**3))-(0.00555986*(DELESR**4))-(0.01841172*(DELESR**5))
C
      IF (RAL .LT. 0.0) THEN
C
      DCLB=-0.000060d0
      ENDIF
C
      IF ((RAL .GE. 0.0) .AND. (RAL .LE. 0.209434)) THEN
C
      DCLB=-0.000060d0+(0.0041035078*RAL*RAL)-(0.0130618699*(RAL**3))
      ENDIF
C
      IF (RAL .GT. 0.209434) THEN
C
      DCLB=0.0d0
      ENDIF
C
C
      CML=(CML1*EPA02S)+(CLDAD*DDA)+(CLDRD*DRUDD*DRFLX1*EPA43)+
     +((CLDTD*DTFLX1)*DELEDD)+(CMLP*PB)+(CMLR*RB)+(DCLB*BETA)
C
```

```
C
C*********************************************************************C
C
C
      CMM1=0.00501496-(0.08004901*RAL)-(1.03486675*RAL*RAL)
     +-(0.68580677*(RAL**3))+(6.46858488*(RAL**4))
     +-(10.15574108*(RAL**5))+
     +(6.44350808*(RAL**6))-(1.46175188*(RAL**7))
     ++(0.24050902*RAL*DELESR)
     +-(0.42629958*DELESR)-(0.03337449*DELESR*DELESR)
     +-(0.53951733*(DELESR**3))
C
C     modified 25 Jul 90 to use new curve fit for CMQ
C
C          OLD EQUATION
C
C     IF (RAL .LE. 0.25307) THEN
C
C     CMMQ=-3.8386262+(13.54661297*RAL)+(402.53011559*RAL*RAL)
C    +-(6660.95327122*(RAL**3))-(62257.89908743*(RAL**4))
C    ++(261526.10242329*(RAL**5))
C    ++(2177190.33155227*(RAL**6))-(703575.13709062*(RAL**7))-
C    +(20725000.34643054*(RAL**8))-(27829700.53333649*(RAL**9))
C     ENDIF
C
C     IF ((RAL .GT. 0.25307) .AND. (RAL .LT. 0.29671)) THEN
C
C     CMMQ=-8.4926528931-(2705.3000488281*(RAL-0.2530699968))
C    ++(123801.5*(RAL-0.2530699968)**2)
C    +-(1414377*(RAL-0.2530699968)**3)
C     ENDIF
C
C     IF (RAL .GE. .29671) THEN
C
C     CMMQ=47.24676075-(709.60757056*RAL)+(3359.08807193*RAL*RAL)-
C    +(7565.32017266*(RAL**3))+(8695.1858091*(RAL**4))
C    +-(4891.77183313*(RAL**5))+(1061.55915089*(RAL**6))
C     ENDIF
C
C     CMMQ vs. alpha n degrees
C
C
C          NEW EQUATION
C
C     convert alpha to degrees
C
      A=RAL*DEGRAD
C
      F1=-4.33509d0+A*(-0.141624d0+A*(0.0946448d0+A*(-0.00798481d0
     + +A*(-0.00168344d0+A*(0.000260037d0+A*(6.64054d-6+A*(
```

```
     + -2.20055d-6+A*(-2.74413d-8+A*(7.14476d-9+A*
     + 2.07046d-10)))))))))
C
      F2=-302.567+a*(106.288+a*(-14.7034+A*(1.02524+A*(-0.0393491
     + +A*(0.00084082+A*(-9.365e-6+A*4.2355e-8))))))
C
      F3=1724.99+A*(-158.944+A*(5.59729+A*(-0.0949624+A*(
     + 0.000779066+A*(-2.47982e-6)))))
C
C    ramp functions
C
      R1=1.0-0.75*(A-10.0)**2+0.25*(A-10.0)**3
      R2=1.0-R1
      R3=1.0-7.5*(A-40.0)**2/62.5+(A-40.0)**3/62.5
      R4=1.0-R3
C
      IF(A.LT.10.0)THEN
        CMMQ=F1
      ELSEIF(A.LT.12.0)THEN
        CMMQ=F1*R1+F2*R2
      ELSEIF(A.LT.40.0)THEN
        CMMQ=F2
      ELSEIF(A.LT.45.0)THEN
        CMMQ=F2*R3+F3*R4
      ELSE
        CMMQ=F3
      ENDIF
C
      CMM=CMM1+(CMMQ*QB)
C
C
C*********************************************************************C
C
C
      DTFLX3=0.9750d0
      DRFLX3=0.890d0
C
C
      CMN1=0.01441512+(0.02242944*RAL)-(0.30472558*(RAL**2))
     ++(0.14475549*(RAL**3))
     ++(0.93140112*(RAL**4))-(1.52168677*(RAL**5))+
     +(0.90743413*(RAL**6))-(0.16510989*(RAL**7))
     +-(0.0461968*(RAL**8))
     ++(0.01754292*(RAL**9))-(0.17553807*RAL*RABET)+
     +(0.15415649*RAL*RABET*DELESR)
     ++(0.14829547*(RAL**2)*(RABET**2))
     +-(0.11605031*(RAL**2)*RABET*DELESR)
     +-(0.06290678*(RAL**2)*(DELESR**2))
     +-(0.01404857*(RAL**2)*(DELESR**2))
     ++(0.07225609*RABET)-(0.08567087*(RABET**2))
```

```
     ++(0.01184674*(RABET**3))
     +-(0.00519152*RAL*DELESR)+(0.03865177*RABET*DELESR)
     ++(0.00062918*DELESR)
C
      CNDRD=-0.00153402+(0.00184982*RAL)-(0.0068693*RAL*RAL)
     ++(0.01772037*(RAL**3))
     ++(0.03263787*(RAL**4))-(0.15157163*(RAL**5))+(0.18562888
     +*(RAL**6))-(0.0966163*(RAL**7))+(0.01859168*(RAL**8))+(0.0002587
     +*RAL*DELESR)-(0.00018546*RAL*DELESR*RBETA)-(0.00000517304*RBETA)
     +-(0.00102718*RAL*RBETA)-(0.0000689379*RBETA*DELESR)-(0.00040536
     +*RBETA*RARUD)-(0.00000480484*DELESR*RARUD)
     +-(0.00041786*RAL*RARUD)
     ++(0.0000461872*RBETA)+(0.00434094*(RBETA**2))
     +-(0.00490777*(RBETA**3))
     ++(0.000005157867*RARUD)+(0.00225169*RARUD*RARUD)-(0.00208072
     +*(RARUD**3))
C
      IF (RAL .LT. 0.55851) THEN
C
      CMNP=-0.00635409-(1.14153932*RAL)+(2.82119027*(RAL**2))+
     +(54.4739579*(RAL**3))-(140.89527667*(RAL**4))-(676.73746128*
     +(RAL**5))+(2059.18263976*(RAL**6))+(1579.41664748*(RAL**7))
     +-(8933.08535712*(RAL**8))+(6806.54761267*(RAL**9))
      ENDIF
C
      IF ((RAL .GE. 0.55851001) .AND. (RAL .LE. 0.61087)) THEN
C
      CMNP=-.07023239+(1.085815*(RAL -0.55851))
     ++(8.852651*((RAL-.55851)**2))-(192.6093*((RAL-0.55851)**3))
      ENDIF
C
      IF (RAL .GT. 0.61087) THEN
C
      CMNP=-71.03693533+(491.32506715*RAL)
     +-(1388.11177979*(RAL**2))+
     +(2033.48621905*(RAL**3))
     +-(1590.91322362*(RAL**4))+(567.38432316*(RAL**5))
     +-(44.97702536*(RAL**7))+(2.8140669*(RAL**9))
      ENDIF
C
C
C
      IF (RAL .LE. -.069813) THEN
C
      CMNR= -0.28050d0
      ENDIF
C
      IF ((RAL .GT. -.069813) .AND. (RAL .LT. 0.0)) THEN
C
      CMNR=-0.2804999948+(35.9903717041*(RAL+.0698129982)**2)
```

```
     +-(516.1574707031*(RAL+.0698129982)**3)
      ENDIF
C
      IF ((RAL .GE. 0.0) .AND. (RAL .LE. 0.78539801)) THEN
C
      CMNR=-.28071511-(2.52183924*RAL)+(68.90860031*(RAL**2))
     +-(573.23100511*(RAL**3))+(2009.08725005*(RAL**4))
     +-(3385.15675307*(RAL**5))
     ++(2730.49473149*(RAL**6))-(848.12322034*(RAL**7))
      ENDIF
C
      IF ((RAL .GT. 0.78539801) .AND. (RAL .LT. 0.95993102)) THEN
C
      CMNR=-0.1096954+(0.52893072*(RAL-0.78539801))-(6.09109497*(RAL-
     +0.78539801)**2)+(17.47834015*(RAL-0.78539801)**3)
      ENDIF
C
      IF (RAL .GE. 0.95993102) THEN
C
      CMNR=-0.110d0
      ENDIF
C
      CNDTD=0.00058286+(0.0007341*RAL)-(0.00746113*RAL*RAL)
     +-(0.00685223*(RAL**3))
     ++(0.03277271*(RAL**4))-(0.02791456*(RAL**5))
     ++(0.00732915*(RAL**6))
     ++(0.00120456*RAL*DELESR)-(0.00168102*DELESR)+(0.0006462*
     +DELESR*DELESR)
C
      CNDAD=0.00008228887-(0.00014015*RAL)-(0.0013493*RAL*RAL)+
     +(0.00020487*(RAL**3))+(0.00561241*(RAL**4))
     +-(0.00634392*(RAL**5))
     ++(0.00193323*(RAL**6))-(2.05815E-17*(RAL*DAILA))+(3.794816E-17*
     +(DAILA**3))
C
      DCNB=-2.500E-4
C
      RALN1=0.69813
      RALN2=90.0d0/DEGRAD
      RBETN1=-0.174532
      RBETN2=0.34906
C
      AN=0.034d0
      ASTARN=1.0472d0
      BSTARN=0.087266
C
      ZETAN=(2.0D0*ASTARN-(RALN1+RALN2))/(RALN2-RALN1)
      ETAN=(2.0D0*BSTARN-(RBETN1+RBETN2))/(RBETN2-RBETN1)
C
      XN=(2.0D0*RAL-(RALN1+RALN2))/(RALN2-RALN1)
```

```
      YN=(2.0D0*RBETA-(RBETN1+RBETN2))/(RBETN2-RBETN1)
C
      FN=((5.0D0*(ZETAN**2))-(4.0D0*ZETAN*XN)-1.0D0)*
     +(((XN**2)-1.0D0)**2)/(((ZETAN**2)-1.0D0)**3)
C
      GN=((5.0D0*(ETAN**2))-(4.0D0*ETAN*YN)-1.0D0)*
     +(((YN**2)-1.0D0)**2)/(((ETAN**2)-1.0D0)**3)
C
      CNRB=AN*FN*GN
C
      IF (RAL .LT. 0.69813) THEN
C
      CNRB=0.0d0
      GOTO 1000
      ENDIF
C
      IF ((RBETA .LT. -0.174532) .OR. (RBETA .GT. 0.34906)) THEN
C
      CNRB=0.0d0
      GOTO 1000
      ENDIF
C
C
C
 1000 CMN=(CMN1*EPA02S)+(CNDAD*DDA)+((CNDRD*DRUDD*DRFLX3)*EPA43)+
     +((CNDTD*DTFLX3)*DELEDD)+(CMNP*PB)+(CMNR*RB)+(DCNB*BETA)
     ++CNRB
C
C
C*********************************************************************C
C
C     THIS SECTION DETERMINES THE EFFECT OF THE THRUST VALUES FOR
C     ADDITION TO CX, CY, CZ, CLM, CMM, AND CNM VALUES DETERMINED
C     ABOVE AND CONTAIN THE FOLLOWING VARIABLES:
C     CPTAL  - COSINE OF PITCH VECTOR ANGLE
C     SPTAL  - SINE OF PITCH VECTOR ANGLE
C     CYTAL  - COSINE OF YAW VECTOR ANGLE
C     SYTAL  - SINE OF YAW VECTOR ANGLE
C     ENGPQ  - PORT ENGINE THRUST/(QBAR*S)
C     ENGSQ  - STARBOARD ENGINE THRUST/(QBARS*S)
C     CXENGP - COEFFICIENT OF PORT ENGINE THRUST IN X DIRECTION
C     CXENGS - COEFFICIENT OF SBRD ENGINE THRUST IN X DIRECTION
C     CXT    - COEFFICIENT OF TOTAL THRUST IN X DIRECTION
C     CYENGP - COEFFICIENT OF PORT ENGINE THRUST IN Y DIRECTION
C     CYENGS - COEFFICIENT OF SRBD ENGINE THRUST IN Y DIRECTION
C     CYT    - COEFFICIENT OF TOTAL THRUST IN Y DIRECTION
C     CZENGP -
C     CZENGS -
C     CZT    -
C     CLMT   -
```

```
C    CMMT  -
C    CNMT  -
C
     CPTAL=COS(PTAL)
     SPTAL=SIN(PTAL)
     CYTAL=COS(YTAL)
     SYTAL=SIN(YTAL)
     CRAL=COS(RAL)
     SRAL=SIN(RAL)
C
     ENGPQ=ENGP/QBARS
     ENGSQ=ENGS/QBARS
C
     CXENGP=ENGPQ*CPTAL*CYTAL
     CXENGS=ENGSQ*CPTAL*CYTAL
     CXT=CXENGP+CXENGS
C
     CYENGP=ENGPQ*CPTAL*SYTAL
     CYENGS=ENGSQ*CPTAL*SYTAL
     CYT=CYENGP+CYENGS
C
     CZENGP=ENGPQ*SPTAL
     CZENGS=ENGSQ*SPTAL
     CZT=CZENGS+CZENGP
C
     CLMT=(CZENGS-CZENGP)*(25.5d0/12.0d0)/BWING
C
     CMMT=CXT*(0.25d0/12.0d0)/CWING+
    +     CZT*20.219d0/CWING
C
     CNMT=(CXENGP-CXENGS)*(25.5d0/12.0d0)/BWING-
    +     CYT*20.219d0/BWING
C
     CX=CFZ*SRAL-CFX*CRAL+CXT
     CY=CFY+CYT
     CZ=-(CFZ*CRAL+CFX*SRAL)+CZT
     CLM=CML+CLMT
     CMM=CMM+CMMT
     CNM=CMN+CNMT
C
C
C    THE 0.25/12.0 IS THE OFFSET OF THE THRUST VECTOR FROM THE CG
C    THE 20.219 is the moment arm from the nozzle pivot to the cg
C    THE 25.5/12.0 is the moment arm of the engines from the cg
C
C    RETURN CX, CY, CZ, CLM, CMM, CNM TO CALLING PROGRAM.
C
C
     RETURN
     END
```

```
C
C
C  THE FOLLOWING SECTIONS ADDED 13 AUG 91
C
C

*****************************************************************
*  THIS SUBROUTINE EXECUTES THREE DIFFERENT BLENDS FROM
*  THE MCDONNELL MODEL COEFICIENT DATABASE TO THE ROTARY
*  BALANCE COEFICIENTS GIVEN THE VALUE OF PARAMETER (10);
*  BLEND.  THE FIRST MODE (PAR(10)<1.0) IS  INTENDED TO
*  BE USED TO DETERMINE AN EQUILIBRIUM STATE SET OF
*  PARAMETERS FOR THE ROTARY BALANCE DATA MODEL GIVEN A
*  SET OF KNOWN STATIC AERODYNAMIC EQUILIBRIA.  THE
*  SECOND MODE (PAR(10) = 2.0) SETS THE MODEL TO EXECUTE
*  PURE ROTARY BALANCE DATA ABOVE AOA 35 DEGREES.  THE
*  THIRD MODE (PAR(10) = 3.0) IS A HYBRID MODEL WHERE
*  BOTH THE STATIC AND ROTARY BLANCE DATABASES ARE
*        COMBINED  UTILIZING  UNIQUE     ASPECTS  OF  BOTH  DATABASES.
*****************************************************************
C
      SUBROUTINE RBBLEND(U,PAR,NDIM,ICP)
      IMPLICIT DOUBLE PRECISION (A-H,O-Z)
      COMMON /SEIZE/ CX,CY,CZ,CLM,CMM,CNM
      COMMON /SEIZET/ CXT,CYT,CZT,CLMT,CMMT,CNMT
      COMMON /SEIZER/ CXR,CYR,CZR,CLMR,CMMR,CNMR
      COMMON /RBPOLY/ PC, OMEGA
      DIMENSION PAR(10),PC(6,79),U(NDIM)
C
C
      IF (PAR(10) .LT. 2.0) THEN
C
C
        BLEND = PAR(10)
C
        CXS = CX-CXT
        CYS = CY-CYT
        CZS = CZ-CZT
        CLMS = CLM-CLMT
        CMMS = CMM-CMMT
        CNMS = CNM-CNMT
C
        CX = CX + (CXR-CXS)*BLEND
        CY = CY + (CYR-CYS)*BLEND
        CZ = CZ + (CZR-CZS)*BLEND
        CLM = CLM + (CLMR-CLMS)*BLEND
        CMM = CMM + (CMMR-CMMS)*BLEND
        CNM = CNM + (CNMR-CNMS)*BLEND
C
      ENDIF
```

```
C
      IF (PAR(10) .EQ. 3.0) THEN
C
         AL = U(1)
         BETA = U(2)
         DEGRAD = 57.2957795
         RAL = AL/DEGRAD
         RBETA = BETA/DEGRAD
C
         PTEMP = U(3)
         QTEMP = U(4)
         RTEMP = U(5)
C
         P = U(3) - OMEGA*DSIN(RBETA)
         Q = U(4) - OMEGA*DSIN(RAL)*DCOS(RBETA)
         R = U(5) - OMEGA*DCOS(RAL)*DCOS(RBETA)
C
         U(3) = P
         U(4) = Q
         U(5) = R
C
         CXRP = CXR
         CYRP = CYR
         CZRP = CZR
         CLMRP = CLMR
         CMMRP = CMMR
         CNMRP = CNMR
C
         CALL COEFF(U,PAR,NDIM,ICP)
C
         U(3) = 0
         U(4) = 0
         U(5) = 0
C
         CALL RBCOEF(U,PAR,NDIM)
C
         CXR0 = CXR
         CYR0 = CYR
         CZR0 = CZR
         CLMR0 = CLMR
         CMMR0 = CMMR
         CNMR0 = CNMR
C
         CXS = CX-CXT
         CYS = CY-CYT
         CZS = CZ-CZT
         CLMS = CLM-CLMT
         CMMS = CMM-CMMT
         CNMS = CNM-CNMT
C
```

```
      CXR = CXS + (CXRP-CXR0)
      CYR = CYS + (CYRP-CYR0)
      CZR = CZS + (CZRP-CZR0)
      CLMR = CLMS + (CLMRP-CLMR0)
      CMMR = CMMS + (CMMRP-CMMR0)
      CNMR = CNMS + (CNMRP-CNMR0)
C
      U(3) = PTEMP
      U(4) = QTEMP
      U(5) = RTEMP
C
      CALL COEFF(U,PAR,NDIM,ICP)
C
    ENDIF
C
C
    IF (PAR(10) .GE. 2.0) THEN
C

      DEGRAD = 57.2957795
      AL = U(1)
      RAL = AL/DEGRAD
      DELTA = 5/DEGRAD
      BLEND = (RAL - 0.523598776)/DELTA

      IF ((RAL .LE. 0.610865238) .AND.  (RAL .GE. 0.523598776))THEN
C
        CX = CX + (CXR-CX+CXT)*(3-2*BLEND)*BLEND*BLEND
        CY = CY + (CYR-CY+CYT)*(3-2*BLEND)*BLEND*BLEND
        CZ = CZ + (CZR-CZ+CZT)*(3-2*BLEND)*BLEND*BLEND
        CLM = CLM + (CLMR-CLM+CLMT)*(3-2*BLEND)*BLEND*BLEND
        CMM = CMM + (CMMR-CMM+CMMT)*(3-2*BLEND)*BLEND*BLEND
        CNM = CNM + (CNMR-CNM+CNMT)*(3-2*BLEND)*BLEND*BLEND
C
      ELSE
C
        CX = CXR + CXT
        CY = CYR + CYT
        CZ = CZR + CZT
        CLM = CLMR + CLMT
        CMM = CMMR + CMMT
        CNM = CNMR + CNMT

      ENDIF
    ENDIF
C
    RETURN
    END
C
C
```

```
**********************************************************************
*
*  THE FOLLOWING TWO SUBROUTINES, RBPOLYCOEF AND RBCOEF,
*  REPRESENT THE ROTARY BALANCE COEFICIENT DATA.  THE FIRST
*  ROUTINE READS IN THE COEFICIENTS OF THE POLYNOMIALS THAT
*  REPRESENT THE SIX COEFICIENTS AND THE SECOND ROUTINE IS THE
*  POLYNOMIAL THAT REPRESENTS THE POLYNOMIAL.
*
**********************************************************************
C
      SUBROUTINE RBPOLYCOEF
      IMPLICIT DOUBLE PRECISION  (A-H,O-Z)
      COMMON /RBPOLY/ PC, OMEGA
      DIMENSION  PC(6,79)
C
      OPEN(99,FILE='RBDATA.15O',STATUS='OLD')
      REWIND(99)
      DO 110 I=1,6
         DO 100 L=1,79
           READ(99,*) PC(I,L)
100        CONTINUE
110    CONTINUE
      RETURN
      END
C
      SUBROUTINE RBCOEF(U,PAR,NDIM)
      IMPLICIT DOUBLE PRECISION  (A-H,O-Z)
      COMMON /SEIZER/ CXR,CYR,CZR,CLMR,CMMR,CNMR
      COMMON /RBPOLY/ PC, OMEGA
      DIMENSION U(NDIM),PAR(10),PC(6,79)
C
      AL   = U(1)
      DEGRAD = 57.29577951
C
      RAL = AL/DEGRAD
C
      IF ((RAL .LE. 1.5708) .AND. (RAL .GE. 0.5235988)) THEN
C
       CALL RBDATA(U,PAR,NDIM,1,CXR)
       CALL RBDATA(U,PAR,NDIM,2,CYR)
       CALL RBDATA(U,PAR,NDIM,3,CZR)
       CALL RBDATA(U,PAR,NDIM,4,CLMR)
       CALL RBDATA(U,PAR,NDIM,5,CNMR)
       CALL RBDATA(U,PAR,NDIM,6,CMMR)
       CXR = -CXR
       CZR = -CZR
       ENDIF
       RETURN
       END
C
```

```
      SUBROUTINE RBDATA(U,PAR,NDIM,I,CF)
      IMPLICIT DOUBLE PRECISION  (A-H,O-Z)
      COMMON/ACDATA/BWING,CWING,SREF,RHO,RMASS
      COMMON /RBPOLY/ PC, OMEGA
      DIMENSION U(NDIM),PAR(10),PC(6,79)
C
      DEGRAD = 57.29577951
C
      A = U(1)/DEGRAD
      B = U(2)/DEGRAD
      P = U(3)
      Q = U(4)
      R = U(5)
C
      VTRFPS = U(8)*1000
C
      DE = PAR(1)/DEGRAD
      DR = PAR(2)/DEGRAD
      DA = PAR(3)/DEGRAD
      DD = PAR(9)/DEGRAD
C
C     FOR COMPARISON TO PREVIOUS MODELS, DIFFERENTIAL ELEVATOR
C     WILL BE VARIED AS A FUNCTION OF AILERON DEFLECTION.
C
      DD = 0.3*DA
C
      OMEGA = (P*DCOS(A) + R*DSIN(A))*DCOS(B) + Q*DSIN(B)
      OM = (BWING*OMEGA)/(2*VTRFPS)
C
C     79 TERM ROTARY BALANCE DATA POLYNOMIAL
C
C
      C1 = PC(I,1) + PC(I,2)*A + PC(I,3)*B
      C2 = PC(I,4)*DA + PC(I,5)*DD + PC(I,6)*DE
      C3 = PC(I,7)*OM + PC(I,8)*DR + PC(I,9)*A*A
      C4 = PC(I,10)*DA*B + PC(I,11)*B*B + PC(I,12)*B*DR
      C5 = PC(I,13)*A*OM + PC(I,14)*DA*DD + PC(I,15)*DR*DR
      C6 = PC(I,16)*OM*OM + PC(I,17)*DA*A  + PC(I,18)*B*OM
      C7 = PC(I,19)*DD*DD + PC(I,20)*OM*DE + PC(I,21)*DD*A
      C8 = PC(I,22)*A*DE + PC(I,23)*B*DE
      C9 = PC(I,24)*B*A + PC(I,25)*OM*DD + PC(I,26)*B*DD
      C10 = PC(I,27)*OM*DR + PC(I,28)*DA*OM*OM + PC(I,29)*DA*A*A
      C11 = PC(I,30)*DD*DD*B+PC(I,31)*OM*OM*A+PC(I,32)*OM*OM*OM
      C12 = PC(I,33)*A*B*B + PC(I,34)*B*A*OM
      C13 = PC(I,35)*B*A*DR + PC(I,36)*A*B*DD + PC(I,37)*B*B*OM
      C14 = PC(I,38)*DD*OM*OM + PC(I,39)*B*DA*OM
      C15 = PC(I,40)*B*OM*DR
      C16 = PC(I,41)*B*DA*A + PC(I,42)*DD*DD*A
      C17 = PC(I,43)*A*DR*DR
      C18 = PC(I,44)*DD*A*A + PC(I,45)*A*A*DE + PC(I,46)*B*A*A
```

```
      C19 = PC(I,47)*B*OM*DE+PC(I,48)*OM*DR*DR+PC(I,49)*B*OM*OM
      C20 = PC(I,50)*A*A*OM
      C21 = PC(I,51)*OM*OM*DE+PC(I,52)*A*OM*DR
      C22 = PC(I,53)*DD*DD*OM + PC(I,54)*A*A*A+PC(I,55)*A*DD*OM
      C23 = PC(I,56)*A*A*DR+PC(I,57)*OM*OM*DR+PC(I,58)*A*OM*DE
      C24 = PC(I,59)*A*A*OM*OM + PC(I,60)*B*B*OM*OM
      C25 = PC(I,61)*DD*DD*OM*OM
      C26 = PC(I,62)*DD*DD*DD*A + PC(I,63)*B*DD*DD*DD
      C27 = PC(I,64)*A*A*B*B  + PC(I,65)*B*OM*OM*OM
      C28 = PC(I,66)*OM*OM*OM*OM + PC(I,67)*OM*OM*OM*DE
      C29 = PC(I,68)*A*OM*OM*OM + PC(I,69)*DD*DD*A*A
      C30 = PC(I,70)*DE*A*A*A + PC(I,71)*DA*A*A*A
      C31 = PC(I,72)*B*A*A*A + PC(I,73)*A*A*A*A
      C32 = PC(I,74)*A*A*A*DD  + PC(I,75)*OM*DD*DD*DD
      C33 = PC(I,76)*A*A*A*DR + PC(I,77)*A*A*DR*DR
      C34 = PC(I,78)*OM*OM*DR*DR + PC(I,79)*OM*OM*OM*DR
C
      CF1 = C1+C2+ C3 + C4 + C5 + C6 + C7 + C8 + C9 + C10
      CF2 = C11 + C12 + C13 + C14 + C15 + C16 + C17 + C18
      CF3 = C19 + C20 + C21 + C22 + C23 + C24 + C25 + C26
      CF4 = C27 + C28 + C29 + C30 + C31 + C32 + C33 + C34
C
      CF  = CF1 + CF2 + CF3 + CF4
C
      RETURN
      END
```

Bibliography

1. Adams, W. M., Jr. "Analytic Prediction of Aircraft Equilibrium Spin Characteristics." NASA TN D-6926, 1972.

2. AGARD Advisory Report no. 265, *Report of the Fluid Dynamics Panel Working Group 11: Rotary-Balance Testing for Aircraft Dynamics.* Specialized Printing Services Limited, December 1990.

3. Arent, Lauren E.,D.B. Wilson and J.H. Taylor. "F-15A Approach-to-Stall/Stall/Post-Stall Evaluation, Final Report." U.S. Air Force, AFFTC-TR-75-32, Jan. 1976 (AD-B045-115L).

4. Barnhart, Billy. *Analysis of Rotary Balance Data for the F-15 Airplane Including the Effect of Conformal Fuel Tanks.* NASA Contractor Report CR-3479, April 1982.

5. Barnhart, Billy. *F-15 Rotary Balance Data for an Angle-of-Attack Range of 8 Degrees to 90 Degrees.* NASA Contractor Report CR-3478, May 1982.

6. Barth, Capt Thomas J. *Determination of High Angle-of-Attack Stability of the F-15B Aircraft Using Bifurcation Analysis.* MS Thesis, AFIT/GAE/AA/87D-1. School of Engineering, Air Force Institute of Technology (AU), Wright-Patterson AFB OH, December 1987.

7. Baumann, Capt Daniel D. *F-15B High Angle-of-Attack Phenomena and Spin Prediction Using Bifurcation Analysis.* MS Thesis, AFIT/GAE/ENY/89D-01. School of Engineering, Air Force Institute of Technology (AU), Wright-Patterson AFB OH, December 1989.

8. Beck, Capt Jeffery A. *Bifurcation Analysis of a Model Fighter Aircraft with Control Augmentation.* MS Thesis, AFIT/GAE/ENY/89D-02. School of Engineering, Air Force Institute of Technology (AU), Wright-Patterson AFB OH, December 1989.

9. Birhle, W. Jr. and B. Barnhart, "Spin Prediction Techniques," AIAA Paper 80-1564, August 1980.

10. Carroll, J.V. and R.K. Mehra, "Bifurcation Analysis of Nonlinear Aircraft Dynamics." *Journal of Guidance*, Vol 5 no 5 pp529-536, 1982.

11. Chambers, Bauman and Anglin. "Analysis of the Flat-Spin Characteristics of a Twin-Jet Swept-Wing Fighter Airplane." NASA TN D-5409, 1969.

12. Cuthbert, Daniel and Fred S. Wood. *Fitting Equations to Data.* New York: John Wiley and Sons, 1980.

13. Doedel, E. *AUTO: A Subroutine Package for the Bifurcation Analysis of Autonomous Systems of Ordinary Differential Equations,* Concordia University, Montreal, Canada.

14. Dornheim, Michael A., "X-31 Flight Tests to Explore Combat Agility to 70 Deg. AOA," *Aviation Week & Space Technology,* 134:38-41 Mar 11, 1991.

15. Guckenheimer, J. and Holmes, P. *Nonlinear Oscillations, Dynamical Systems, and Bifurcations of Vector Fields.* Springer-Verlag New York Inc, 1983.

16. Guicheteau, P. "Bifurcation Theory in Flight Dynamics; An Application to a Real Combat Aircraft. *CAS 90 Congress.* Paper no. 1990-116, Stockhlolm (Sweden): ONERA, September 9-14 1990.

17. Hawkins, Capt Carl A. *Application of Bifurcation and Catastrophe Theories to the Near Stall Flight Mechanics.* MS Thesis. Massachusetts Institute of Technology, December 1985 (AD-A167697).

18. Jahnke, Craig C. *Application of Dynamical Systems Theory to Nonlinear Aircraft Dynamics.* PhD Dissertation. Division of Engineering and Applied Sciences, California Institute of Technology, Pasadena Ca, January 1990.

19. Jahnke, Craig C. and Fred E.C. Culick. "Application of Dynamical Systems Theory to Nonlinear aircraft Dynamics," *AIAA Atmospheric Flight Mechanics Conference.* Paper no 88-4372. Washington D.C. : American Institute of Aeronautics and Astronautics, August 1988.

20. Jahnke, C. and F. Culick. "Application of Dynamical Systems Theory to the High Angle of Attack Dynamics of the F-14," *28th Aerospace Sciences Meeting.* Paper no 90-0221. Reno, NV: American Institute of Aeronautics and Astronautics, January 8-11, 1990.

21. Jordan, D.W. and P. Smith. *Nonlinear Ordinary Differential Equations.* New York: Oxford University Press, 1990.

22. Martin, C.A. and S.D. Hill "Prediction of Aircraft Spin Recovery," *AIAA Atmospheric Flight Mechanics Conference*. Paper no. 89-3363. Washington D.C. : American Institute of Aeronautics and Astronautics, August 1989.

23. McDonnell Aircraft Company. F/A-F-15 Stability Derivatives, Mass and Inertia Characteristics Flight Test Basis, Part II Aerodynamic Coefficients and Stability and Control Derivatives. Report No. MDC A4172.

24. McDonnell, Capt Robert J. *Investigation of the High Angle of Attack Dynamics of the F-15B Using Bifurcation Analysis.* MS Thesis, AFIT/GAE/ENY/90D-16. School of Engineering, Air Force Institute of Technology (AU), Wright-Patterson AFB OH, December 1990.

25. McRuer, D., A. Irving and D. Graham. *Aircraft Dynamics and Automatic Control.* Princeton University Press, Princeton, New Jersey, 1973.

26. Mehra, Raman K. and James V. Carroll, "Global Stability and Control Analysis of Aircraft at High Angles-of-Attack," Office of Naval Research Report ONR-CR215-248-3, 31 August 1979.

27. Ogburn, M.E., L.T. Nguyen and, K.D. Hoffler "Modeling of Large-Amplitude High-Angle-of-Attack Maneuvers," *AIAA Atmospheric Flight Mechanics Conference*. Paper no. 88-4357-CP. Washington D.C.:American Institute of Aeronautics and Astronautics, August 1988.

28. Planeaux, J.B. and T.J. Barth. "High Angle-of-Attack Dynamic Behavior of a Model High-Performance Fighter Aircraft," *AIAA Atmospheric Flight Conference*. Paper no 88-4368. Washington D.C.: American Institute of Aeronautics and Astronautics, August 1990.

29. Planeaux, J.B., J.A. Beck, and D.D. Baumann. "Bifurcation Analysis of a Model Fighter Aircraft with Control Augmentation." *AIAA Atmospheric Flight Mechanics Conference*. Paper no 88-4368. Washington, D.C. : American Institute of Aeronautics and Astronautics, August 1988.

30. Planeaux, J.B. and R.J. McDonnell. "Thrust Contributions to the Spin Characteristics of a Model Fighter Aircraft," *AIAA Atmospheric Flight Mechanics Conference*. Paper no 91-2887 Washington D.C.: American Institute of Aeronautics and Astronautics, August 1991.

31. *SAS User's Guide: Statistics, (Version 5 Edition).* Cary, North Carolina: SAS Institute Inc., 1985.

32. Scher, Stanley H. "An Analytical Investigation of Airplane Spin-Recovery by Use of Rotary-Balance Aerodynamic Data." NACA Technical Note 3188, June 1954.

33. Schy. A.A., and M.E. Hannah. "Prediction of Jump Phenomena in Roll-Coupled Maneuvers of Airplanes," *Journal of Aircraft*, 14: 375-382 (April 1977).

34. Seydel, Rüdiger. *From Equilibrium to Chaos: Practical Bifurcation and stability Analysis.* New York: Elsevier Press, 1988.

35. Seydel, Rüdiger. "Tutorial on Continuation." *International Journal of Bifurcation and Chaos.* Vol. 1, No. 1 3-11, 1991.

36. *Statistix Manual,* (Version 3.1). Analytical Software, December 1990.

37. Stone, Ralph W. Jr., S.M. Burk Jr., and W. Birhle Jr., "The Aerodynamic Forces and Moments on a 1/10 Scale Model of a Fighter Airplane in Spinning Attitudes as Measured on a Rotator in the Langley 20-foot Free-Spinning Tunnel." NACA TN 2181, 1950.

38. Tischler, M.B., and J.B. Barlow, "Determination of the Spin and Recovery Characteristics of a General Aviation Design." *Journal of Aircraft*, Vol 18 No 4 pp238-244,1981

39. Zgaynov, G.I. and M.G. Goman. "Bifurcation Analysis of Critical aircraft Flight Regimes," *International Council of Aeronautical Sciences*, 84: 217,223, 1984.

40. Ralston, Jack, Bihrle Applied Research, Inc. Telephone interview. NASA/Langley Spin Tunnel, Hampton, VA, 9 September 1991.